Shear Behaviour of Irregular Shaped Concrete Beams with and without Steel Fibres

by
Divan Visser

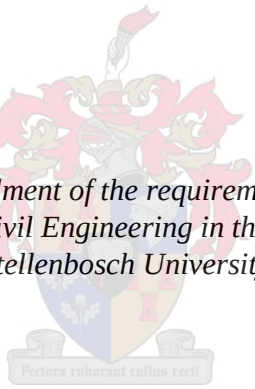

Thesis presented in fulfilment of the requirements for the degree of Master of Engineering in Civil Engineering in the Faculty of Engineering at Stellenbosch University

Supervisor: Prof. William Peter Boshoff
Co-supervisor: Prof. Celeste Viljoen

March 2020

Declaration

I have read and understand the Stellenbosch University Policy on Plagiarism and the definitions of plagiarism and self-plagiarism contained in the Policy [Plagiarism: The use of the ideas or material of others without acknowledgement, or the re-use of one's own previously evaluated or published material without acknowledgement or indication thereof (self-plagiarism or text-recycling)].

I also understand that direct translations are plagiarism.

Accordingly, all quotations and contributions from any source whatsoever (including the internet) have been cited fully. I understand that the reproduction of text without quotation marks (even when the source is cited) is plagiarism.

I declare that the work contained in this assignment is my own work and that I have not previously (in its entirety or in part) submitted it for grading in this module/assignment or another module/assignment.

Date: March 2020

Abstract

In a rapidly evolving world, the use of concrete for the development of infrastructure is steadily increasing and this trend is set to continue in the future. In order to decrease the environmental impact of the development of infrastructure, it is crucial to reduce the carbon footprint of cement production by reducing the amount of concrete used in structures. Through the application of fabric formwork, geometrically optimised structural members can be cast comprising up to 40% less concrete compared to prismatic members with equivalent strength formed with traditional formwork (Orr *et al.*, 2011). Such optimised members typically have irregular and varying cross-sections along its length, and codified methods that have been applied to these members provided inaccurate results (Orr *et al.*, 2014). This investigation serves as a preliminary study on the shear behaviour of fabric formed beams (FFB) and concentrates only on uniform beams with irregular sections. This investigation strives to augment the knowledge on the shear behaviour of irregular shaped beams inspired by fabric formed beams. Fabric formwork was not used in this investigation but it is suggested that fabric formwork is used in succeeding studies.

For this research, a steel fibre reinforced self-compacting concrete (SFR-SCC) mix was developed to cast irregular shaped beams (ISB). Steel fibres are used in the concrete to investigate their potential of replacing vertical reinforcement and self-compacting concrete (SCC) was used to avoid the challenge of external vibration in the complex moulds for proper compaction of the concrete. A total of 12 webbed beams, with four various irregular web shapes and fibres contents of either 0%, 0.6%, or 1%, were cast. Asymmetrical three-point bending tests were performed to investigate the shear behaviour of ISB and to investigate the effect of fibres on the shear behaviour of ISB. Furthermore, nine shear prediction models reported in literature were modified to accommodate the irregular sections of the beams and an analytical shear prediction model for ISB containing steel fibres is proposed. These models were evaluated on the accuracy of their predictions by comparing the predicted and experimental shear strengths.

The study showed that the cross-sectional area of the web significantly influences the shear capacity. Larger web cross-sectional areas result in remarkable increases in shear strength. The widely used assumption of calculating the cross-sectional area contributing to shear capacity as the width of the narrowest part of the web (b_w) multiplied by the effective depth (d), results

in over-conservative strength predictions and an inefficient use of concrete. It was found that the whole cross-sectional area of the web contributes to shear strength.

Furthermore, fibres significantly enhance the shear capacity of ISB and an average increase in normalised shear stresses of 49% and 74% was obtained for fibre volumes of 0.6% and 1%, respectively, compared to beams containing no fibres.

The comparison of the predicted values with the experimental values indicates that the proposed model predicts the shear capacity of ISB with reasonable accuracy with a mean shear strength ratio and standard deviation value of 0.95 and 0.10, respectively. However, a larger test database must be used to validate the proposed shear prediction model properly.

Opsomming

In ‘n vinnig ontwikkelende wêreld is die gebruik van beton baie algemeen om infrastruktuur te ontwikkel en word daar voorspel dat beton al hoe meer gebruik sal word. Om infrastruktuurontwikkeling se impak op die omgewing te verminder, is dit van kardinale belang om die inhoud van beton wat in strukture gebruik word, te verminder. Met die gebruik van gespande materiaal vormwerke, kan die geometrie van elemente geoptimeer word om tot en met 40% minder beton te gebruik in vergelyking met prismatiese elemente van ekwivalente sterkte (Orr *et al.*, 2011). Hierdie geoptimeerde elemente het onreëlmatige deursnitte wat varieër oor die lengte van die elemente. Bestaande metodes wat aangewend is op sulke balke het onakkurate resultate gelewer (Orr *et al.*, 2014). In hierdie studie is die skuifgedrag van balke wat in gespande materiaal vormwerke gegiet word, ondersoek en fokus meer op uniforme balke met onreëlmatige deursnitte. Die doel van die studie is om inligting rakende skuifgedrag van hierdie balke te ondersoek. Gespande materiaal vormwerke is nie gebruik in hierdie studie nie, maar dit word aanbeveel om gespande materiaal vormwerke in toekomstige studies te gebruik.

In hierdie navorsing is ‘n eie mengsel van selfkompakterende beton met staalvesels ontwikkel vir die balke met onreëlmatige deursnitte. Staalvesels is bygevoeg tot die beton om die moontlikheid te ondersoek om vertikale wapenstaal met hierdie vesels te vervang en selfkompakterende beton is gebruik om die eksterne vibrasie vir kompaksie in die komplekse bekisting uit te skakel. Daar is twaalf balke gebruik met vier verskillende webvorms met veselinhoud van 0%, 0.6% of 1%. Asimmetriese driepunt buigtoetse is uitgevoer om die skuifgedrag van balke met onreëlmatige deursnitte te ondersoek asook om die effek van vesels op die skuifgedrag te ondersoek. Daar is nege skuifmodele wat uit literatuur gekry is, aangepas om die onreëlmatige deursnitte van die balke in ag te neem. ‘n Analitiese skuifmodel vir balke met onreëlmatige deursnitte word ook voorgestel. Die akkuraatheid van hierdie modele is geëvalueer deur die voorspelde skuifsterktes te vergelyk met die eksperimentele skuifsterktes.

Hierdie studie het getoon dat die deursnitarea van die web ‘n groot invloed op die skuifkapasiteit het. Groter webdeursnitareas het ‘n aansienlike verhoging in skuifkapasiteit tot gevolg. ‘n Algemene aanname is om die deursnitarea wat bydrae tot skuifkapasiteit te bereken as die kleinste breedte van die web (b_w) vermenigvuldig met die effektiewe diepte (d). Hierdie vereenvoudiging lei tot oorkonserwatiewe skuifkapasiteit voorspellings en dan ook

oneffektiewe gebruik van beton. Dit is gevind dat die hele deursnit area van die web ‘n bydrae lewer tot die skuifsterkte.

Verder het die vesels ‘n aansienlike bydrae gelewer tot skuifkapasiteit, asook ‘n verhoging van 49% in genormaliseerde skuifspanning vir ‘n veselinhoud van 0.6% en ‘n verhoging van 74% vir ‘n veselinhoud van 1%, in vergelyking met balke wat geen vesels bevat nie.

Deur die voorspelde waardes te vergelyk met eksperimentele waardes wys dat die voorgestelde model die skuifkapasiteit van balke met onreëlmatige deursnitte met redelike akkuraatheid voorspel met ‘n gemiddelde skuifsterkte verhouding van 0.95 en ‘n standaardafwyking op die gemiddelde skuifsterkte verhouding van 0.10. Dit word egter aanbeveel om ‘n groter steekproef te ontwikkel om die akkuraatheid van hierdie skuifmodel te bevestig.

Acknowledgements

I would like to express my gratitude to the following people for their assistance and support throughout my studies:

- My supervisors, Prof. Billy Boshoff and Prof. Celeste Viljoen, for their guidance and supervision, while giving me discretion and space to develop my own ideas.
- The structures laboratory and workshop staff at the Department of Civil Engineering at Stellenbosch University, for their assistance during experimental work.
- My parents, for giving me the opportunity to attend university and supported me in every step of the way.
- My brother, for his advice and support throughout my studies.
- Luné Carstens, for her unconditional love and support during this research.
- Pretoria Portland Cement and Chryso South Africa, for providing material used for this research.
- My fellow MEng students, for the friendship and entertainment throughout these two years.

Table of Contents

Page

List of Figures

List of Tables

List of Symbols

α	Inclination of diagonal shear crack
α_{avg}	Average measured inclination of diagonal shear crack
α_f	Fibre aspect ratio
β_1	Stress block depth factor
γ_c	Partial safety factor for concrete without fibres
ε_x	Longitudinal strain
η_o	Fibre orientation factor
η_L	Fibre length correction factor
η_b	Fibre bond efficiency factor
θ	Assumed angle of compression strut
v_{cu}	Ultimate shear stress
ρ	Longitudinal reinforcement ratio as a percentage of the cross-sectional area
ρ_1	Longitudinal reinforcement ratio
ρ_f	Volumetric fraction of fibres
σ_{cp}	Average stress acting on the concrete cross-section due to prestressing
σ_{cu}	Normal compressive stress
σ_{fu}	Fracture strength of a fibre
$(\sigma)_{t\ avg}$	Average tension stress transferred across a crack by fibres
σ_{tu}	Residual tensile stress due to fibres
τ OR τ_b	Fibre-matrix interfacial bond stress
τ_{cr}	Average shear stress at cracking
τ_u	Ultimate shear stress
a_g	Aggregate size

a_v	Shear span
b	Width
b_{ef}	Effective width
b_f	Width of flange
b_w	Width of web
$b_{w,top}$	Width at top edge of web
$b_{w,bot}$	Width at bottom edge of web
c	Distance from top of beam to neutral axis
d	Effective depth
d_f	Fibre diameter
d_g	Maximum diameter of aggregate
f	Average pullout force per fibre
f'_c	Cylinder compressive strength of concrete
f_{ck}	Characteristic value of cylinder compressive strength of concrete
f_{cu}	Cube compressive strength of concrete
f_{ctk}	Characteristic value for tensile strength of concrete without fibres
f_f	Flexural strength of concrete
f_{Ftuk}	Characteristic value of the ultimate residual tensile strength for FRC
f_{R1}, f_{R2}, f_{R3},f_{R4}	Residual flexural tensile strength at 0.5, 1.5, 2.5, 3.5 mm CMOD
f_{spfc}	Split-cylinder strength of fibre concrete
f_t	Split tensile strength of concrete
f_y	Yield stress of reinforcement
h	Height of beam
h_{sp}	Beam height excluding notch

k	Size effect factor
k_{dg}	Factor accounting for aggregate size
k_{fd}	Fibre dispersion reduction factor (0.82)
k_v	Parameter determining aggregate interlock stresses
l_{crit}	Critical fibre length
l_f	Fibre length
p	Volume percentage of fibres
p_f	Fibre perimeter
r_f	Fibre radius
v_u	Ultimate shear stress
w_{35}	Average measured width of critical shear cracks at a service load of 35 kN
w_u	Average measured width of critical shear cracks at ultimate resistance
w_{crit}	Critical shear crack width
w_m	Crack opening at shear failure
w_{ts}	Maximum crack width for concrete
z	Internal lever-arm
A	Area
A_C	cross-sectional area of concrete
A_f	Fibre cross-sectional area
A_{fc}	Fibre contribution area
A_p	Area of prestressing
A_s	Area of longitudinal reinforcement
D_f	Fibre bond efficiency factor
E_p	Modulus of elasticity of prestressing

E_s	Modulus of elasticity of reinforcement
F	Fibre factor
F_u	External load resulting in failure
G_c	Fracture energy of concrete
G_m	Shear modulus
K_f	Global orientation factor of fibres
L	Length of span
M	Bending moment
M_{Ed}	Bending moment resulting from factored design loads
M_i	Maximum internal moment
N	Number of fibres bridging a unit area of diagonal crack
N_{Ed}	Normal stress resulting from factored design loads
S	Mean centroid spacing of fibres
T_f	Resultant tensile force due to fibres bridging crack
V	Shear force
V_c	Shear resistance of concrete
V_{cc}	Shear resistance of concrete compression zone
V_{exp}	Experimental shear capacity
V_{Ed}	Shear stress resulting from factored design loads
V_f	Volume fraction of fibres
V_{FRC}	vertical component of tension resistance provided by fibres
V_{pr}	Predicted ultimate shear capacity
$V_{Rd.c}$	Contribution of concrete towards shear capacity
$V_{Rd,f}$	Contribution of fibres towards shear capacity

$V_{Rd,s}$	Contribution of transverse reinforcement towards shear capacity
V_{sy}	Shear resistance due to web reinforcement
V_u	Ultimate shear resistance
$\mathbf{V_a}$	Shear capacity due to aggregate interlock
$\mathbf{V_c}$	Shear capacity of uncracked concrete compression zone
$\mathbf{V_d}$	Shear capacity due to doweling of longitudinal reinforcement
$\mathbf{V_f}$	Shear resistance provided by fibres

List of Abbreviations

ACI	American concrete institute
ASTM	American Society for Testing and Materials
CMOD	Crack mouth opening displacement
COV	Coefficient of variation
CPF	Controlled permeability formwork
CS	Control set
CSM	Critical sliding model
DIC	Digital Image Correlation
DT	Diagonal tension
EC2	Eurocode 2
EFNARC	European Federation of National Associations Representing for Concrete
FF	Fabric formwork
FFB	Fabric formed beams
FIB	International Federation for Structural Concrete
FRC	Fibre reinforced concrete
FR-SCC	Fibre reinforced self-compacting concrete
FS	Flexural shear
ISB	Irregular shaped beams
LVDT	Linear Variable Differential Transformer
MCFT	Modified Compression Field Theory
MSS	Mean shear strength ratio
PVA	Polyvinyl alcohol
PPC	Pretoria Portland Cement

RC	Reinforced concrete
RD	Rebar debonding
SANS	South African National Standard
SC	Shear compression
SCC	Self-compacting concrete
SD	Standard deviation on the shear strength ratios
SFRC	Steel fibre reinforced concrete
SFR-SCC	Steel fibre reinforced self-compacting concrete
SLS	Serviceability limit state
ULS	Ultimate limit state
VEM	Variable engagement model

CHAPTER 1

INTRODUCTION

1.1 Background

Engineers and researchers invest a significant amount of time in the development of concrete and alternative cement-based materials to optimise the use of cement, both economically and environmentally. More specifically, there is an endeavour to reduce the costs of construction and the amount of adverse effects on the environment. This lead to the newly developed technology known as fabric formwork (FF). Traditional, non-permeable formwork usually made from wood or steel is replaced by a permeable fabric. Using FF to cast beams has multiple advantages. Fabric formed structures can be optimised in terms of geometry, to reduce the amounts of consumed material without compromising structural strength of the element and on top of that can be aesthetically pleasing. Casting concrete in fabric formwork results in structures with variable cross-sections that are irregularly shaped. However, this can be used to an advantage. The flexible FF can be manipulated to achieve a structure with variable cross-sections in which the flexural and shear capacities at any section in the element reflects the demands of the external loading.

Cement production is one of the world's leading carbon dioxide emitter and accounts for approximately 7% of the world's anthropogenic carbon emissions (Gao *et al.*, 2015). Reducing the use of cement can contribute significantly to the reduction in CO_2 emissions, thus further inspiring the design of optimised structures. Concrete savings of up to 40% can be achieved by casting beams using FF when compared to a prismatic beam with an equivalent strength (Orr et al., 2011). It has also been suggested that labour cost associated with the assembly and stripping of fabric formwork and long term costs on maintenance and repairs can be reduced (Abdelgader *et al.*, 2008). Moreover, casting concrete in permeable formwork leads to reduced water-cement ratios towards the external face of the member, resulting in more durable concrete structures (Orr et al., 2013).

However, using fabric as formwork results in members with variable and irregular sections that are different to the regular prismatic beam or T-beam. This brings rise to various new challenges in terms of structural design and construction-related problems. In-situ application, along with the installation of reinforcement and compaction of the concrete, are challenging tasks when using a flexible formwork made from fabric. Proper compaction of the concrete in geometrically optimised, variable section members can become onerous, especially in thin members with tightly packed reinforcement. The reinforcement of variable cross-section members complicates the construction process (Orr et al., 2011). Although the fundamentals remain the same, varying shapes and sizes of reinforcement are required especially for stirrups used as shear reinforcement. All this can add time and costs to the construction.

Possible solutions to the challenges that arise from using FF are to make use of self-compacting concrete (SCC) and to add steel fibres to the concrete mix. Using SCC simplifies the compaction issue since no external vibration is required. SCC can flow under its own weight and through dense reinforcing to fill all gaps and corners in the formwork. Steel fibres can be used to enhance the shear capacity of concrete and potentially replace or reduce the varying shear reinforcement required in irregular shaped members that do not have a regular prismatic cross-section (Singh and Jain, 2014).

Shear is one of the few research areas in the construction world which has been a source of contention between scholars for many years. The shear mechanisms and the individual contributions of these mechanisms have been researched significantly, but remain an ongoing debate (Thamrin et al., 2016). Since the earliest days of construction, researchers have been

determined to find models and methods to accurately determine the behaviour and resistance of structural members in shear. Since the early 1900s, researchers started using a truss model to visualise the flow of forces in a member by assigning tensile and compressive forces to steel ties and compression struts. Ever since, this has been the basis for the development of most design models (FIBa, 2010). The last four decades, significant amounts of research has been done to investigate the potential of steel fibre reinforced concrete (SFRC) to improve the performance of reinforced concrete (RC) beams. Since steel fibres improve the post-cracking tensile strength of concrete and considering that shear capacity is highly dependent on the tensile behaviour of concrete, fibres can improve the shear capacity of concrete beams. Existing shear strength models for steel fibre reinforced concrete beams are usually based on shear models developed for conventional RC beams with slight alterations to accommodate the effect of fibres (Tung & Tue, 2016).

However, researchers have not yet investigated how beams with irregular and variable sections would influence the mechanical performance under shear. Design codes and standards developed up to now do not provide criteria and guidelines which can be used to design and accurately determine the shear capacity of such beams. It has been found that codified methods which have been applied to optimised structures have provided inaccurate results and are unable to account for beams with irregular and varying cross-sections (Orr *et al.*, 2014).

1.2 Scope and Methodology

This study forms an initial step for the research of the shear behaviour of FFB containing steel fibres. This investigation focuses specifically on the shear behaviour of beams with irregular cross-sections that are uniform along the length of the beam. The irregularity of the beam results from the web thickness that varies over the depth of the beam resulting in a V-shaped web. These beams contain longitudinal reinforcement and steel fibres, but no transverse reinforcement. Fabric was not used in this investigation since beams were tested which are uniform along the length, however, it is advised that FF is used in future studies.

The primary objectives of this investigation are as follows:

- Investigate the shear behaviour of irregular shaped beams (ISB) in the ultimate limit state compared to traditional T-beams, by considering maximum loads, ultimate shear

stresses, cracking pattern and crack widths. ISB have cross-sections that are different to the regular prismatic cross-section of conventional beams.

- Investigate the effect of fibre content on the shear behaviour of ISB and the potential of steel fibres to replace transverse reinforcement in ISB in beams where minimum shear reinforcement is required.
- Propose an analytical shear model for ISB and start a database of test results for ISB tested in shear.

The methodology followed to achieve the objectives of this study is:

1. Thoroughly understand the fundamentals of shear in simply supported beams and other variables forming part of the research such as fabric formwork and steel fibre-reinforced self-compacting concrete (SFR-SCC).
2. Investigate existing shear models for FRC beams and provide a comprehensive summary of these shear models. Propose an analytical shear model for the ISBs tested in this investigation.
3. Develop a SFR-SCC that conforms to the SCC criteria, with adequate workability and passing ability (ability of SCC to flow through gaps between reinforcement bars), and can be used for further investigations in this study.
4. Develop a test set-up which exposes a beam to high shear stresses and would potentially cause shear failure. This test set-up is used to investigate the shear behaviour of the beams.
5. Design ISB, inspired by the shape of FFB that will fail in shear when tested. Perform tests on a number of beams to investigate the shear behaviour. This includes the maximum loading, maximum shear stress, cracking pattern, crack widths and main shear crack angles.

Even though fabric formed structures can be appealing in terms of aesthetics and structural efficiency, design engineers are fairly reluctant when it comes to designing fabric formed structures. The lack of knowledge on mechanical behaviour and design guidelines of such members has caused engineers to conform to conventional prismatic sections. Concerning the research significance, this study aims to provide a fundamental understanding of the mechanisms of shear in fibrous beams and provide an understanding of the shear behaviour of ISB. This research involves tests performed on beams with irregular shapes that, to the

knowledge of the author, have not been tested up to date. The irregular section shapes of the beams tested in this investigation are inspired by geometrically optimised, simply supported FFBs. Therefore, this research will serve as the basis of the investigation of shear behaviour of FFB and brings rise to opportunities for further research to build onto this investigation.

1.3 Outline of Thesis

Chapter 2 consists of a background study covering the emerging technology of fabric formwork which inspires the shape of the beams investigated in this research. Relevant information on fibre reinforcement and SCC is given. Finally, the mechanisms of shear in beams, shear failure modes and the contribution of fibres in shear are covered.

Chapter 3 summarises nine shear strength prediction models that have been developed since the late 1980's. These shear models are considered in the development of the predicted shear model of this investigation and have been modified to accommodate the ISB tested in this investigation.

Chapter 4 explains the modifications of the investigated shear models to accommodate the shape of beams in this investigation and proposes an analytical shear model for the prediction of ISB containing fibres and no shear reinforcing.

Chapter 5 lays out the experimental framework according to which this research was conducted. This includes the development of SFR-SCC, preliminary tests performed on fresh and hardened concrete, and the results thereof. Finally, all aspects regarding the primary tests performed to investigate the shear behaviour are discussed.

Chapter 6 shows the experimental results of the primary tests performed, and the shear predictions of the various modified shear models for the various beams tested in this investigation.

Chapter 7 provides detailed discussions on the results presented in Chapter 6.

Chapter 8 provides the conclusions drawn from this investigation and gives relevant recommendations for future research in this field.

CHAPTER 2

LITERATURE REVIEW

This chapter deals with relevant literature and fundamental knowledge about all aspects of this investigation. It begins with reporting literature on fabric formwork, which is the inspiration of the primary tests performed in this investigation. Followed by fibre reinforced concrete, with the focus on steel fibres and self-compacting concrete. Finally, the phenomenon of shear in concrete beams and the various aspects of shear are discussed in detail.

2.1 Fabric Formwork

Fabric formwork was originally development in the early 1900s and was used in offshore and geotechnical engineering (Orr *et al.*, 2013). Only in the 1950s, it was further developed and used for architectural and structural purposes (Chandler and Pedreschi, 2007). The earliest use of fabric formwork was in the construction of low-cost housing in Mexico, where the fabric formwork system consisted of timber ribs and fabric spanning between the supporting timber members. During the 1960s, a famous Spanish architect started using flexible plastic sheets to cast interesting wall panels (Chandler and Pedreschi, 2007). Fabric formwork used nowadays is known as a flexible, permeable, light-weight and high-strength material, usually made of

polypropylene or polyethene. It can be used as a replacement for the conventional wooden or steel formwork or in combination with traditional formwork. The numerous advantages of using fabric formwork over traditional formwork to cast structural members is what makes this technology so appealing. Figure 2.1 shows examples of beam moulds consisting of a combination of fabric formwork and pressed wood.

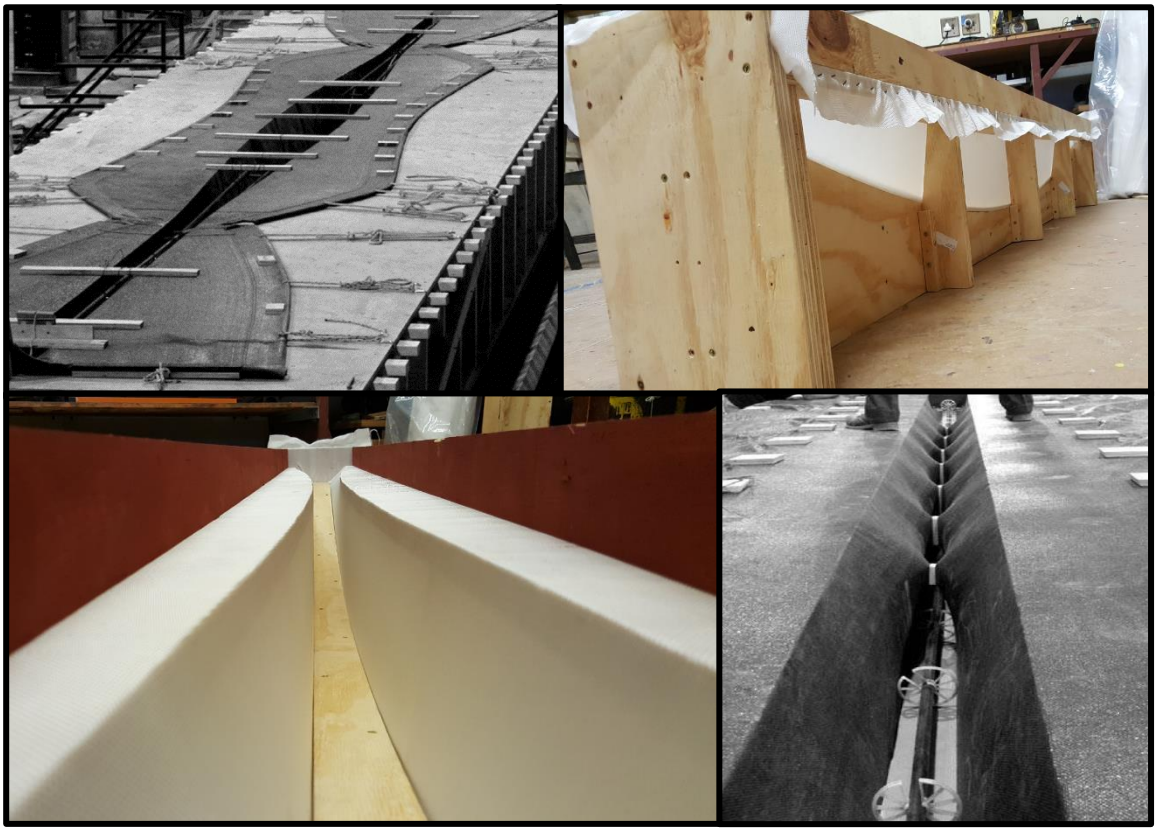

Figure 2.1: Beam moulds consisting of Fabric formwork combined with pressed wood (West, 2016).

2.1.1 Advantages and Disadvantages of Fabric Formwork

The benefits of using fabric formwork in construction are:

- Optimisation of the members, producing more economical and sustainable concrete structures.
- Durability enhancements due to the permeability of the fabric by allowing air bubbles and excess bleeding water to escape through the permeable fabric resulting in a higher concrete density close to the surface of the member.

- Structures created using fabric formwork are aesthetically pleasing. Due to the flexibility of the fabric, concrete structures with sophisticated shapes and impressive surface finishing can be cast.
- Reduced labour costs associated with assembly and stripping of fabric formwork (Abdelgader *et al.*, 2008)
- Significant savings in terms of storage and logistics due to the thin and lightweight nature of the fabric. Especially if the construction site is in a remote location or if the fabric must be manufactured abroad and transported to site.
- Due to the physical properties of the fabric, it has a wide variety of applications. It can be reused, and its geometry can be changed to suit a large variety of different shapes of structures (Chandler and Pedreschi, 2007).
- Fabric formwork is a zero-waste mould system and provides significant savings on material costs - wooden moulds become construction waste after a few uses. Polypropylene and polyethene are inexpensive materials and are available world-wide (West, 2017).
- Increased compressive strength of concrete compared to conventional formwork by filtering out the access water resulting in lower water/cement ratios towards the external surfaces. Figure 2.2 shows a comparison of compressive strengths for the same concrete mix cast in fabric and conventional formwork (Lee, 2010).

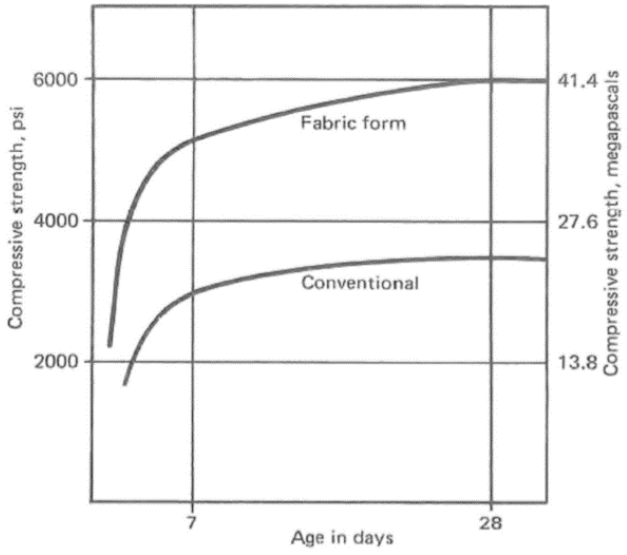

Figure 2.2: Comparison of compressive strength of concrete cast in fabric and conventional formwork (Lee, 2010).

Despite the list of advantages provided by fabric formwork, it has several disadvantages as well:

- Fabric formwork does not protect the concrete until it has cured and hardened like conventional formwork does.
- Controlling the geometries of the final structure is a difficult task, and careful analysis is required to obtain the desired geometries. This is time-consuming, but once it has been done, it can easily and effectively be repeated.
- Digital design tools, design codes and guidelines for fabric formed structures are not yet readily available.
- Flexible mould-walls can make the installation of reinforcement challenging, since it cannot rigidly support or brace rebar (West, 2017).

2.1.2 Member optimisation

Member optimisation refers to the optimisation of the final shape of the member to reduce the material used without compromising the strength and load-carrying capacity of a member. This leads to a significant amount of material savings. Up to 40% less concrete (Orr et al., 2013) and up to 50% less structural steel (West, 2016) is used in a fabric formed element compared to an equivalent strength prismatic element. The shape of an optimised beam is typically such that material is provided at the regions where it is structurally required. At sections with high bending moments, the internal lever-arm, between the longitudinal steel and compression zone is increased to enhance the moment capacity. At sections with significant shear stresses, sufficient material is provided to resist the internal shear forces. Therefore, moment and shear capacities at any section in the member satisfy the requirements of the external loading. Such optimisation of a member would be impossible to achieve without a significant effort and time if wooden or steel formwork is used.

Traditional formwork, referred to as ‘zero-deflection’ formwork systems by Orr *et al.* (2013), must resist considerable hydrostatic pressures and are therefore often large and heavy elements. These elements consume significant amounts of material and are difficult to manoeuvre. Furthermore, elements cast using traditional formwork require more concrete and steel, resulting in higher deadweight than an equivalent fabric formed member. By optimising the shape of the beam and thereby preventing the use of unrequired material, leads to lighter members. Since the self-weight of the member is considerably less, the dead weight of the

entire structure reduces, resulting in smaller members required in structures. According to Firth (2018), in exceptional cases up to 78% of the strength of a bridge is needed to carry the dead load of the bridge, and as little as 22% is used to resist the imposed loading. Similarly to bridges, in long-span beams a large portion of the strength is required to resist the dead load compared to the strength required for the imposed loads. The SANS 10100 Part 1 code for structural use and design of concrete (SANS, 2000) limits the span-to-effective depth ratio for a simply supported beam to $l/d < 16$, which means that for a beam of effective depth equal to 200 mm the span is limited to 3.2 m. These limits are based on restricting the deflection. Hence, by reducing the self-weight of beams, maximum spans can significantly be extended.

The design procedures for optimised beams are based on a sectional approach. This approach aims to satisfy the shear and bending requirements at every section along the entire length of the beam (Orr *et al.*, 2013). Considering a double-cantilevered beam with a uniform distributed load (UDL), as in Figure 2.3, the resulting moment from the UDL is parabolic (red line). Since the moment capacity of a beam, with the same amount of longitudinal reinforcing over the entire length, is solely dependent on the lever-arm between the longitudinal steel and the centroid of the compression block. Therefore, to satisfy the demands of the bending moment envelop, the required effective depth along the beam will vary parabolically. Figure 2.3 shows how the beam depth varies parabolically in proportion to the bending moments caused by the UDL. For simply supported beams, the bending moment graphs will be similar, but will have no hogging moments at supports and will have larger sagging moments at mid-span.

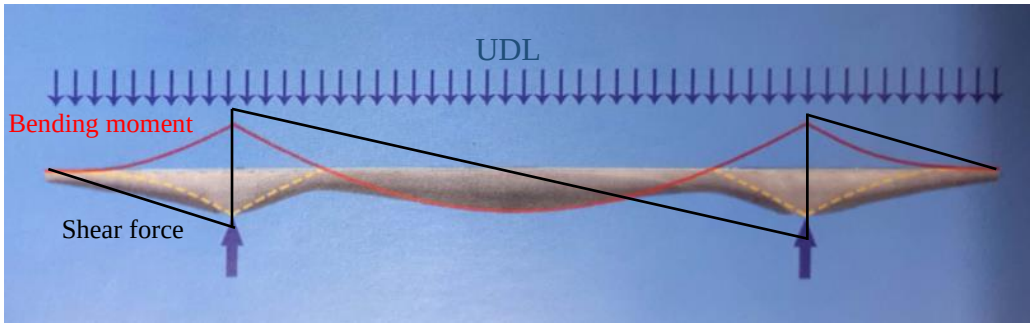

Figure 2.3: Beam subjected to UDL with resultant bending moments and shear forces (adapted from West, 2016).

The internal shear forces resulting from the applied UDL in Figure 2.3 are indicated with a black line. The shear forces do not follow the same parabolic curve as the bending moments and are rather distributed linearly with maximum shear forces over the supports. Therefore it must be ensured that the beam has sufficient shear capacity at every section along the length of the beam.

2.1.3 Durability enhancement

By replacing the standard wooden or steel formwork with a permeable fabric not only facilitates optimisation of structures but also has been proven to significantly enhance the durability of such structural members (Orr *et al.*, 2013). The key to this is the permeability of the fabric. Controlled permeability formwork (CPF) is a formwork system that removes air and water from the concrete. Fabric formwork acts similarly by allowing mixing water to bleed through the permeable fabric during the curing phase. Air can escape through the fabric, which prevents the formation of blowholes or any form of honeycombing. Other advantages of permeable formwork, which contribute to durability include:

- Reduced water absorption and permeability.
- Enhanced surface hardness and tensile strength.
- Reduced oxygen diffusion rates, chloride ingress and carbonation.
- Improved resistance in freeze-thaw climate.

Fabric formwork has one major advantage over CPF systems since the fabric acts as the formwork and the permeable liner for the concrete. The improved durability of the concrete raises the potential to reduce the cover depth required in structures, which further reduces concrete volume and embodied carbon (Orr *et al.*, 2013).

2.1.3.1 Carbonation

The high alkalinity of concrete generally protects the steel reinforcement from corrosion through the protective passivation layer. Due to the alkalinity in the pore solution, an extremely thin inert layer forms around the steel's surface (Steffens *et al.*, 2002). Carbon dioxide penetrates the concrete through air-filled pores, mainly by gaseous diffusion, and chemically reacts with the calcium hydroxide in the concrete. This reduces the alkalinity of the concrete, destroying the passivation layer. Thus, the steel becomes susceptible to corrosion.

Accelerated carbonation tests performed by Orr *et al.* (2013) showed a significant reduction in the coefficient of carbonation for specimens cast in fabric compared to specimens cast in impermeable formwork. After 180 days, the carbonation depth of samples cast in impermeable formwork was 12.7 mm and only 6.7 mm in specimens cast in fabric formwork. Similar results were shown by CPF systems, proving that the carbonation depth for both low and high strength concrete are reduced by using a permeable formwork (Suryavanshi and Swamy, 1997).

2.1.3.2 Chloride ingress

The ingress of chlorides significantly influences the corrosion rate of reinforcement in concrete by increasing internal moisture content and decreasing pore water pH (Orr *et al.*, 2013). Corrosion of reinforcement in concrete induced by chlorides has become one of the major causes of deterioration, especially in structures exposed to marine environments and de-icing salts (Martín-Pérez *et al.*, 2000). The corrosion of steel causes a significant increase in volume due to the products of the corrosion reaction. Local high pressures build up in the concrete, leading to cracking and spalling of the concrete cover. Furthermore, corrosion of the reinforcing steel leads to a reduction in reinforcement cross-sectional area, which is of significant concern since it may result in premature failure of a structure, without carrying the loads for which it was designed. Using permeable formwork results in a denser concrete layer close to the surface of the specimen, potentially reducing the rate of chloride ingress.

According to the study conducted by Orr *et al.* (2013) the non-steady state chloride coefficient reduced by 58% at 53 days and by 41.5% at 90 days for specimens cast in permeable formwork. However, it was recommended that further work is required to provide a method to predict the chloride ingress in fabric formed members. Similar results were obtained by Suryavanshi and Swamy (1997), where short term tests performed on specimens cast using a CPF made from C30 grade concrete showed a 50% reduction in chloride diffusion coefficient.

2.1.3.3 Sorptivity and surface hardness

Orr *et al.* (2013) performed sorptivity tests and compared the results of specimens cast with permeable and impermeable formwork. Results suggest that permeable formworks results in fewer large pores, reducing the short term surface absorption.

Furthermore, in the same study performed by Orr *et al.* (2013), the tests results showed an increase in surface hardness of 13% over 35 days which reduced to 7% after 95 days. This is

most probably due to the reduction in water and increase in cement particle concentration at the surface of the concrete cast against a permeable surface. However, more research is required to clarify this matter. Figure 2.4 presents the benefits of concrete cast in fabric formwork.

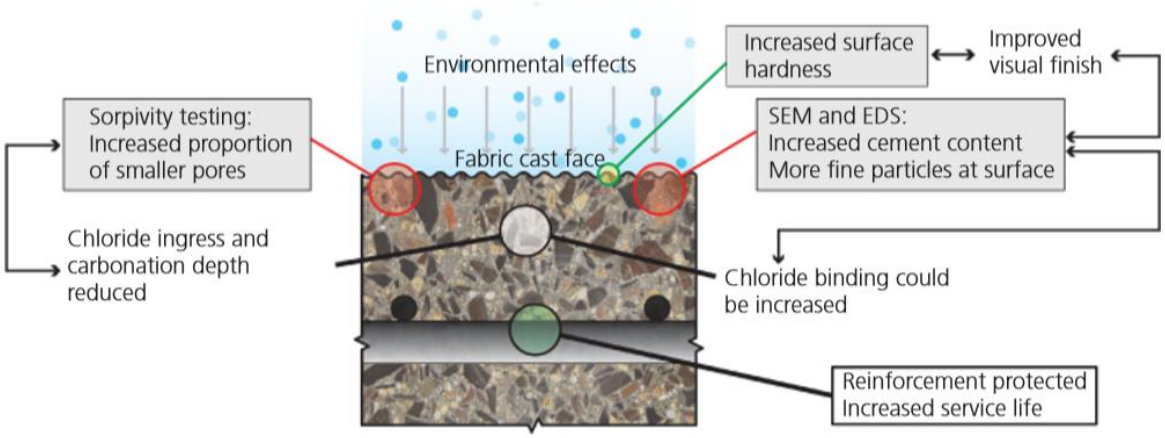

Figure 2.4: Proposed effects on the surface zone of concrete cast in fabric formwork (Orr et al., 2013).

2.2 Fibre reinforcement

The use of fibres in concrete to enhance the post cracking behaviour is becoming more popular in the construction industry. According to EN 14889-2 (2006), fibres can be categorised into two general geometric groups, namely macro-fibres (lengths of > 30 mm) and micro-fibres (lengths of < 15 mm). Various materials are used to manufacture fibres such as steel, glass, polypropylene or even natural materials. There are a large variety of fibres in the market which are used in construction. The choice of fibres generally depends on the performance outcome desired for the final structure. Advantages provided by fibres include improved post-cracking tensile strength (Mohammadi *et al.*, 2008), enhanced ductility (Minelli and Conforti, 2014), reduction of risk of plastic shrinkage cracking (Illston et al., 2001) and improved shear strength of concrete (Tung & Tue, 2016). The performance of the FRC depends significantly on the physical properties, content, orientation and distribution of the fibres, and the fibre-matrix interfacial bond.

This section covers the various aspects of using fibres to enhance the shear capacity of the concrete. The main focus will be placed on steel fibres since this is the chosen fibre type in this investigation.

2.2.1 Fibres influence on toughness, cracking and ductility

Steel fibres control and stabilize the formation and propagation of cracks in concrete. Once cracks have formed, the fibres can potentially transmit higher stresses across the cracks resulting in enhanced toughness in FRC composites (Minelli and Conforti, 2014). In FRC, the load at which cracking becomes unstable is significantly higher than conventional RC. Furthermore, at ultimate limit states (ULS) fibres cause smaller crack spacing and allow for larger crack widths before failure. This all contributes to the enhanced bearing capacity and ductility of FRC. Fibres allow for smaller crack widths which results in improved durability.

Minelli and Conforti (2014) found that RC beams fail shortly after the formation of the first diagonal cracks appears. In FRC, multiple shear cracks form and failure only occurs once the critical crack reaches a width of 1-3 mm. In RC beams, failure usually occurs at a crack width of 0.25-0.5 mm. For these circumstances, longer fibres perform better than short fibres. Furthermore, in the same investigation, it was found that the addition of fibres reduce the angle of inclination of the shear cracks.

2.2.2 Post-cracking behaviour of FRC

Post-cracking residual stresses that are transferred across cracks by the fibres are the bases of the structural design of FRC members (FIB, 2010a). Fibres only come in action once the concrete has cracked and the fibres are stressed in tension. The post-cracking residual stresses are caused by fibre bridging mechanisms across the surface of cracks (Buratti *et al.*, 2011). Lower volume of steel fibres in concrete result in strain-softening behaviour of the composite after cracking. This behaviour is usually favoured over strain-hardening since higher fibre volumes are required to achieve strain-hardening behaviour, which makes the composite uneconomical. In strain-softening behaviour, the peak stress is reached just before the first crack occurs, after which the stress reduces as deformation increases. In strain-hardening behaviour, stresses increase after the first crack occurred and multiple cracks form afterwards. The peak stress is not reached at first crack but rather at a later stage. Refer to Figure 2.5, showing softening and hardening behaviour under uniaxial tension (Mohammadi *et al.*, 2008).

Furthermore, many existing shear models for steel fibres only accommodate strain-softening composites.

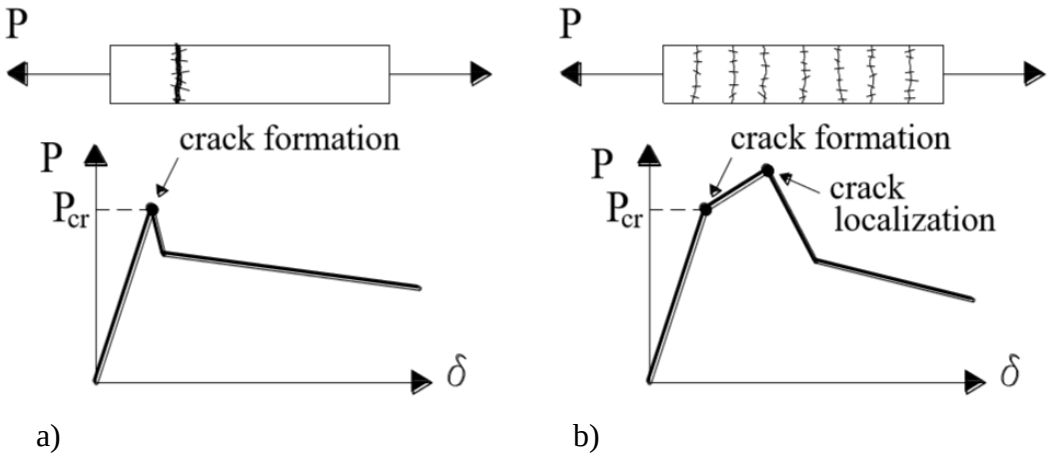

Figure 2.5: Strain softening (a) and hardening (b) behaviour under uniaxial tension (FIB, 2010a).

2.2.3 Fibres as minimum shear reinforcement

Steel fibres significantly improve the shear behaviour of concrete. Therefore, the American Concrete Institute (ACI) Building Code allows designers to use deformed steel fibres as minimum shear reinforcing in elements with low shear stresses (Singh and Jain, 2014). Research done by Greenough & Nehdi (2009) and Parra-montesinos (2006) has proven that beams containing as little as 0.75% of fibres can satisfy the minimum shear reinforcement criteria by providing sufficient shear strength. This is, however, a vague statement since the contributions of fibres are highly dependent on the physical parameters of the fibres. Test results from Singh & Jain (2014) showed that the shear strength of deep beams could be more than doubled with the addition of only 50 kg/m^3 (roughly 0.63%) steel fibres and increased by up to 85% in shallower beams.

2.2.4 Economic benefits of fibres

Fibres can potentially replace shear reinforcement in beams were minimum shear reinforcement is required and reduce conventional shear reinforcement in members carrying substantial loading. Replacing shear stirrups with fibres can significantly reduce construction time and cost (FIB, 2010c). Since the installation of stirrups involves high labour input, it is ideal to use fibres in construction projects, especially in locations where labour costs are high

or labour force is scarce. Furthermore, fibres are the quintessential solution for thin members such as architectural panels where it is impossible to insert steel reinforcement.

2.2.5 Influence of steel fibres on fresh concrete

Fibres are known to enhance the mechanical properties of concrete in its hardened state. However, it has been found that fibres could have adverse effects on concrete in its fresh state. Results from the research of Mohammadi *et al.* (2008) indicate that the workability of concrete decreases uniformly with the increase of fibre content. Furthermore, the aspect ratio of fibres has a significant influence on the workability, and higher aspect ratios tend to affect workability more. It was also found that fibres clumping together is a concern in concrete where fibres of high aspect ratios are used. This is lesser of a concern in FRC where fibres with low aspect ratios are used.

The effect of fibres is more severe in the case of SCC since the grade and performance of SCC relies heavily on its rheological properties. Mohammadi *et al.* (2008) stated that the introduction of steel fibres causes a perceptible increase in stiffness of the concrete mix. According to Yehia *et al.* (2016), the workability of concrete is reduced more by steel fibres than synthetic fibres due to the higher stiffness of steel fibres. Pajak and Ponikiewski (2017) found that for SCC containing more than 2% fibres, the passing ability does not meet the required criteria for SCC.

2.3 Fibre Reinforced Self-compacting Concrete

Self-compacting concrete (SCC) and fibre reinforcement have been introduced previously and are further discussed in more detail in this section. The important characteristics, requirements and design approach of SCC are presented, focussing mainly on fibre reinforced self-compacting concrete (FR-SCC).

2.3.1 Self-compacting Concrete

The concept of SCC was originally developed by Okamura in Japan in the year 1986. SCC was developed to adapt to the growing shortage of skilled labour, and it was only made possible due to the earlier development of superplasticisers. According to the European standards (EN

206-1:2000), SCC is defined as "concrete that can flow and consolidate under its own weight, completely fill the formwork even in the presence of dense reinforcement, whilst maintaining homogeneity and without the need for any additional compaction". Su *et al.* (2001) described it more clearly as "a type of concrete with special rheological properties allowing it to flow into all corners of the formwork and fill gaps in areas with dense reinforcement, without the need of vibration or compaction during the placing or pouring process, while at the same time having enough cohesion to resist segregation and excess bleeding". Different to conventional concrete, SCC should have the following three key properties:

- Filling ability – the ability to flow into the gaps, spaces and all corners of the formwork under its own weight.
- Passing ability – the ability to pass between highly congested reinforcing without segregation and blocking.
- Segregation resistance – the ability to remain a homogenous material through the production, transportation and the placing processes.

SCC has a significant number of advantages over conventional concrete which include the ability to flow under its own weight, the self-compacting ability and the resistance against segregation (Su *et al.*, 2001). These properties eliminate the requirement for additional vibration when placing the concrete, which results in a faster rate of construction and a reduction in labour. The functional filling capacity of fresh SCC makes it possible to apply concrete in areas of highly congested reinforcement and reducing the risk of honeycombing in the final structural product (Shi *et al.*, 2015). Further advantages of SCC include improved quality of concrete surfaces, improved durability, lower levels of noise and vibrations, and safer working environment (EFNARC, 2002).

2.3.2 Conformity criteria of SCC

The requirements for a concrete mix to be classified as a SCC are based on three properties which are passing ability, filling ability and segregation resistance. These properties can be further classified into different classes. The main determining factors for the required class of concrete mix are: application of the concrete (i.e. confinement conditions such as element geometry and reinforcement spacing), placing method and finishing method.

Table 2.1 summarises the various test methods, prescribed by EFNARC (2002) and the typical performance ranges for the various properties of SCC.

Table 2.1: Prescribed test methods and conformity criteria for SCC (EFNARC, 2002).

Property	Test method	Unit	Typical range
Filling ability	Slump-flow	mm	650 - 800
	T_{500} slump-flow	sec	2 - 5
	V-funnel	sec	6 - 12
	Orimet	sec	0 - 5
Passing ability	L-box	(h_2/h_1)	0.8 – 1.0
	J-Ring	mm	0 - 10
	U-box	$(h_2 – h_1)$ mm	0 - 30
	Fill-box	%	90 - 100
Segregation resistance	Segregation resistance (Sieve) test	%	0 - 15
	V-funnel at T_{5min}	sec	0 – (+3)

2.3.3 Design principles for SCC

Many institutions have developed their own method for SCC mix design since there is no standard method (SCCEP, 2005). Similar constituent materials are used in SCC and traditional concrete, however, the compositions are different in several respects. SCC has a higher paste content with less coarse aggregates, a lower water to powder ratio, higher quantities of superplasticiser and often contains viscosity modifying agents (VMA).

The design sequence for SCC provided by EFNARC (2002) is as follows:

1. Selection of desired air content (usually 2%)
2. Designation of coarse aggregate volume percentage (50-60% of total volume)
3. Designation of fine aggregate volume percentage (40-50% of total volume)
4. Design composition of paste:
5. By performing flow tests with various water contents determine the water demand of the powder composition.
6. Determine the desired water/powder ratio and optimum superplasticiser quantity for the mortar:
    - Analyse the effect of superplasticiser in combination of the selected powder contents.

- Adjust the water/powder ratios and superplasticiser dosages to achieve desired characteristics
- If desired characteristics are not obtained, commence by first changing the type of superplasticiser, alternatively change the powder composition and as a last resort, change the type of cement.

7. Selecting the coarse aggregate size and grading with the application in mind.
8. Assessing the properties of the concrete by performing standardised tests.

The previously described design sequence can be adapted to design FR-SCC, by simply incorporating the volume of fibres that must be added to the mix. Fibre volumes are chosen based on the desired mechanical properties of the mix. Fibres volumes usually range between 0.5% and 2.0% of the total concrete volume.

2.3.4 Steel Fibre Reinforced Self-compacting Concrete (SFR-SCC)

The combination of SCC and steel fibres provide the combined benefits of the SCC in its fresh state and the enhanced mechanical properties due to the fibres in the hardened state. The combined benefits result in several new fields of application (SCCEP, 2005). The ideal application for this composite would be for elements with complex and irregular shapes where the application of traditional shear reinforcement is inconvenient and compaction with external vibration is difficult. As mentioned previously, the addition of fibres (metallic or polymer) tend to reduce the workability and flowability of the SCC in its fresh state. The magnitude of these adverse effects tend to be higher for steel fibres due to their high stiffness (Yehia *et al.*, 2016).

Characteristics that influence the workability are (1) fibre aspect ratio and the shape of the fibres. (2) The stiffness and density differences between the fibres and the matrix. This difference is usually higher for steel fibres resulting in the larger influence on workability and flowability. (3) The geometry of the fibre not only influences the fibre anchorage and strength of the composite but also influences the friction between fibres and matrix in the fresh state, therefore affecting the workability as well. However, with the addition of superplasticisers, the desired workability and flowability for SCC can be obtained.

2.3.5 Fibre alignment and distribution in SCC

The potential of fibres to enhance post-cracking resistance of concrete, and the magnitude thereof, is dependent on the fibre alignment in the cracked section. An investigation performed by Vandewalle *et al.* (2008) to study the effect of fibre orientation in self-compacting concrete found that fibres align along the flow direction during the placement of SCC leading to higher post-cracking strength. In another study by Ponikiewski & Golaszewski (2013), similar results were observed and this phenomenon intensifies for longer fibres and larger volume percentages of fibres. Therefore, the application of FR-SCC can lead to significant beneficial effects in narrow structural members such as T-beams or beams formed with fabric formwork, due to the alignment of fibres.

2.4 Shear behaviour of Beams

The phenomenon of shear is highly complex as it consists of multiple interdependent mechanisms. Significant research is done in the pursuit to clarify and understand this complex phenomenon. This section covers the various shear failure modes and shear mechanisms. Furthermore, the influences of fibres on shear behaviour and size effect are discussed.

2.4.1 Shear failure modes

Shear failures, which in reality are a result of a combination of shear forces as well as bending moments, are generally failures that occur suddenly and with no prior warning signs. Designers typically try to design a beam in which failure is governed by flexural strength, reducing the possibility of shear failure (Kong & Evans, 1987). Shear failures are mostly brittle failures and can result in severe consequences such as loss of people's lives as a result of structural failure.

Studies have shown that failure modes of rectangular beams are strongly dependent on the shear span-to-effective depth ratio (a_v/d). This is the ratio of the distance between an applied point load and the nearest support (shear-span), and the effective depth of the beam. It has been found that the failure mode can be transformed from a brittle shear failure to ductile flexural failure by incorporating steel fibres in the concrete (Zhang et al., 2016). A general rule of thumb is that beams with $a_v/d > 6$ usually fail in bending.

If a_v/d falls between 2.5 and 6, a crack forms somewhere in the shear-span, often referred to as a flexure-shear crack. The flexure-shear crack initiates as a vertical crack, but as the shear force increases, the crack starts forming diagonally towards the point where the load is applied (blue line in Figure 2.6). Furthermore, in some cases numerous smaller cracks form where longitudinal reinforcement is located, which may lead to splitting the beam horizontally as the shear force increases. This failure mode is often referred to as shear-tension failure.

For beams where the a_v/d is between 1 and 2.5, the shear crack forms independently and does not develop from an initial flexure crack. The diagonal crack penetrates into the compression zone of the concrete towards the point of load application where the concrete eventually undergoes crushing (red line in Figure 2.6). This is known as shear-compression failure.

Beams with a_v/d less than 1 approaches the behaviour of deep beams and undergoes deep beam failure. The diagonal shear crack approximately forms on a straight line linking the beam support and the point of load application. The crack usually starts forming at about a third of the depth of the beam and then simultaneously propagates towards the support and point of load application (green line in Figure 2.6).

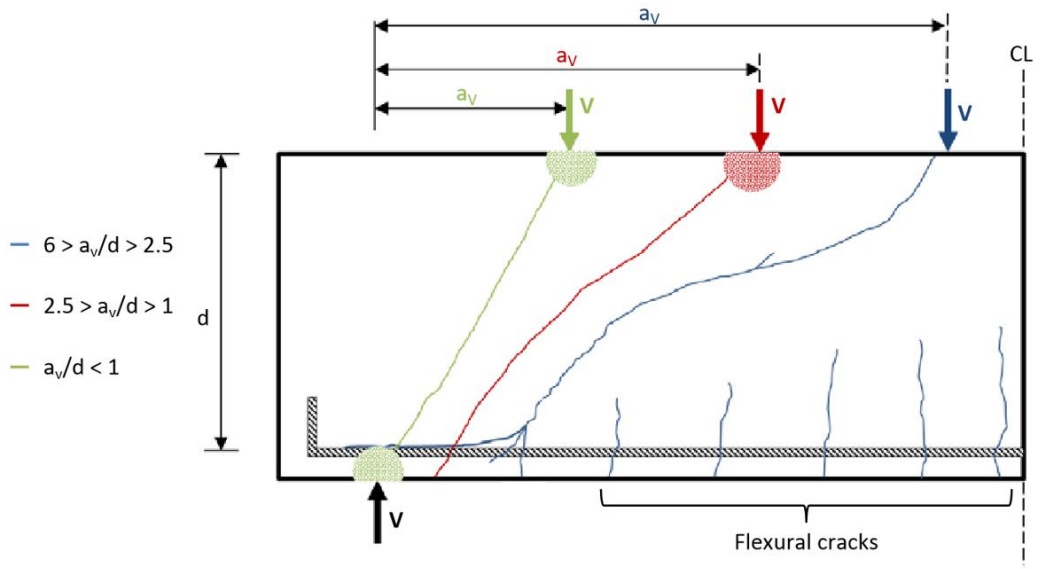

Figure 2.6: Influence of shear span-to-effective depth ratio of failure modes (reworked from Kong and Evans (1987)).

2.4.2 Mechanisms of shear transfer

Shear forces in beams are resisted by a combination of doweling of the longitudinal reinforcement, aggregate interlock and the shear in the concrete under compression (Kong & Evans, 1987). As the shear force increases the various shear mechanisms reach their full capacity and can resist no more load. When the final mechanism reaches its full capacity a sudden and brittle failure of the beam occurs.

The above mechanisms suggests that the shear capacity of a beam depends not only on the shear span-to-effective depth ratio but is affected by several alternative shear parameters. The various parameters and their effects can be summarised as follows:

a) Concrete strength – Increased concrete strength generally enhances the capacity of the doweling action, the aggregate interlock as well as the concrete compression zone to resist shear.

b) Longitudinal steel ratio – Large longitudinal steel ratios mainly increase the shear capacity by increased doweling action and by restricting the formation of wide cracks, which in turn increases the aggregate interlock capacity. Thamrin et al. (2016) also showed that shear capacity increases as the reinforcement ratio increases.

c) Aggregate type – The strength of aggregates used in concrete affects the shear capacity through aggregate interlock. More angular and stronger aggregates generally enhance the shear capacity.

d) Beam size – Ultimate shear stress reduces as beam size increases. This means that larger beams are proportionally weaker in shear than smaller beams. This concept is often referred to as size-effect.

Shear reinforcement is mainly used to enhance the shear capacity of beams and to provide confinement to longitudinal steel to prevent it from "popping out" under high loads. Stirrups are vertical or sometimes diagonally positioned reinforcement bars in the beams. As shear cracks form, a portion of the shear force is carried over to the shear reinforcement. Fibres can be used to enhance the shear capacity of concrete and potentially replace or reduce shear reinforcement in structural members (FIB, 2010c).

2.4.3 Contribution of fibres to shear resistance

Fibres contribute to shear resistance in two ways; (1) by the shear resistance, i.e. doweling action and stress transfer across cracks, of the fibres themselves and (2) by enhancing the contribution of the shear transfer mechanisms (Tung and Tue, 2016). The effects of fibres on the shear transfer mechanisms include:

a) Enhance doweling action – Fibres increase the tensile strength of the concrete along the dowel zone of longitudinal reinforcement and in turn, enhance the effectiveness of the doweling action by restraining the propagation and widening of dowel cracks (Li *et al.*, 1992).

b) Aggregate interlock – Aggregate interlock contributions to shear resistance diminishes as the cracks widen. It is believed that fibres enhance the aggregate interlock by limiting the crack widths, therefore promoting aggregate interlock. However, according to Zeranka (2017), further investigation is required.

c) Fibres under size-effect – It has been shown that as the size of the beam increases, the effectiveness of fibres becomes less (Dinh *et al.*, 2010). However, fibres reduce the crack spacing and therefore may lead to potential reduction, or with a rather tough FRC, elimination of the size effect in beams (FIB, 2010c).

Furthermore, fibres enhance the loading capacity of structures and provide significant ductility. Shear failure in RC members is associated with a brittle-like behaviour and mostly causes a sudden collapse of a structure. The enhanced ductility provided by fibres determines visible deflections and warnings prior to forthcoming failure or collapse (FIB, 2010c). Figure 2.7 shows the various components contributing to the shear strength of fibrous beams with no transverse reinforcement.

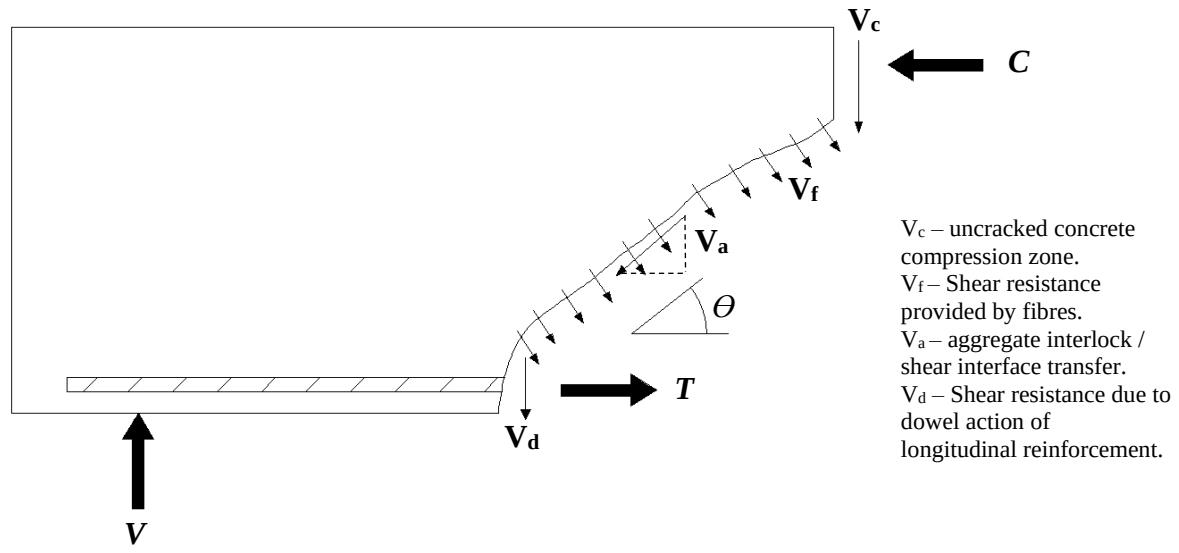

Figure 2.7: Internal forces in cracked FRC beam (reworked from Kong & Evans, 1987 and Tung & Tue, 2018).

2.4.4 Size effect in shear and the influence of fibres on size effect

The concept of size effect significantly influences the shear capacity of deep beams. The term size effect generally refers to the decay in the ultimate shear capacity of a beam, as the effective depth increases (Minelli and Conforti, 2014). The main reason for the occurrence of size effect is the larger shear crack widths in beams with larger effective depths. However, the best way to model this phenomenon is still an ongoing debate in the research community.

The major consequence of wider cracks, according to Bazant & Kim (1984), is the diminishing of the tensile residual stresses across a crack and the reduced contribution of aggregate interlock to shear resistance. According to Bentz (2005), wider cracks reduce the crack interface shear stresses, which result in lower shear capacity. However, Frosch (2001), found that influence of size effect on shear capacity is insignificant in beams with minimum or no transverse reinforcement and suggested that further research is done regarding this. Researchers have a general agreement that FRC imitates similar behaviour to well-distributed reinforcement and can, therefore, substantially influence size effect in beams loaded in shear (Minelli and Conforti, 2014).

Minelli and Conforti (2014), investigated the effect of steel fibres on size effect by testing beams with various depths (500, 1000 and 1500 mm) containing various fibre volumes of 0%, 0.63% and 1.0%, and no transverse reinforcement. The research concluded that size effect is substantially mitigated by fibres. The results show that as the effective depth increases, the influence of size effect reaches a horizontal asymptote indicating no further change in shear capacity. This horizontal asymptote is reached significantly sooner in FRC beams than in classical RC beams.

2.4.5 Shear behaviour of non-prismatic beams

Structural members that have been optimised tend to be non-prismatic, leading to the top or bottom flange being inclined. Theoretically, the shear force may partially be resisted by inclined flanges. However, according to Orr et al. (2014), premature failure often occurs in such optimised members. Compression and tension forces in the inclined flanges can effectively change the shear force in the section. Assuming the vertical components of the inclined compression and tension chords could be made equal to the shear force acting on the cross-section, the requirement for transverse reinforcement could be negated. This can be achieved by placing the longitudinal reinforcement bar at a specific depth in the beam to create an internal lever arm at every section along the beam that is sufficient to resist the bending moment at that section, provided that the tensile steel has yielded and has a constant cross-sectional area (Orr *et al.*, 2014). However, this approach faces two major challenges. Using longitudinal steel to provide vertical force resistance in beams requires the steel to be yielded along its entire length and completely anchored at its ends. Furthermore, beams are subjected to multiple load cases throughout their lifespan, and it is impossible to configure reinforcement to satisfy this for all load cases. Longitudinal reinforcement is determined by the load case inducing the maximum bending moment in the beam. However, this is not necessarily the load case that induces maximum shear stresses. Therefore, reinforcement placed for maximum moment resistance will be incorrectly placed for maximum shear resistance.

2.4.6 Shear behaviour of webbed beams

Design codes such as the Eurocode (EN 1992-1-1, 2004) and the ACI Building Code (ACI Committee 318, 2008) make use of the assumption that the shear forces in a T-beam are entirely resisted by only the web. This assumption is widely used in the structural design practice but has been proven to be incorrect according to Zararis (2006). Tests have shown that T-beams,

consisting of a web and flange, have considerably higher shear strengths than beams consisting only of a rectangular web. This indicates that the flange has a significant influence on the shear resistance of a T-beam. Thamrin et al. (2016) investigated the effect of the width of the flange and web on the shear capacity of T-beams and found that the shear capacity of beams consisting of a flange and web is between 5 and 25% higher compared to rectangular beams. In the same study, the correlation between the flange width *(b_f)* and the shear strength was found to be significantly higher than the correlation between the web width *(b_w)* and the shear strength. This indicates that flange has a significant influence on the shear strength of a beam, however, more research is required to investigate this matter.

Zararis (2006) proposed that the effective cross-sectional area of a T-beam considered when predicting shear capacity is approximately defined by the shaded region in Figure 2.8. Therefore, an effective width *(b_{ef})* for the beam can be defined as the shaded area *A* in Figure 2.8 divided by the depth of the neutral axis *c*.

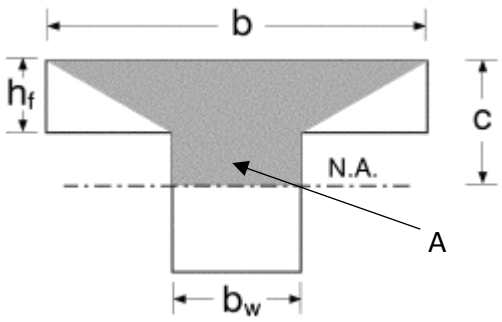

Figure 2.8: Cross-section of T-beam with shaded effective shear area (Zararis, 2006).

2.4.7 Shear resistance comparison of FR-SCC to conventional FRC beams

Significant amount of research is done to investigate the effect of fibres on the performance of FRC beams under shear, however few researchers consider fibres in combination with SCC. An investigation done by Greenough and Nehdi (2009), showed that FR-SCC performs better under shear loading than conventional FRC, mainly due to an improved interfacial bond between the fibres and concrete matrix

To compare the performance in shear of FR-SCC to FRC, Greenough and Nehdi (2009) investigated the increase in shear strength of the relevant beams consisting of FR-SCC

compared to their reference beam consisting of FRC. The approach that was used, accommodated the variety of beams sizes, longitudinal reinforcement ratios, concrete compressive strengths, fibre volumes and fibre types. Furthermore, all beams considered contained the reinforcement with a yield stress of 400 MPa and no transverse reinforcement.

The research found that ultimate shear capacity was higher in FR-SCC beams compared to conventional FRC. More significant improvements in shear capacity were observed for higher fibre volumes. This was most likely attributed to self-compacting ability and denser microstructure of SCC. The higher percentage of fines in SCC also plays a significant role in this by improving the interfacial bond between fibres and cement matrix. However, this feature merits additional research (Greenough & Nehdi, 2009).

2.5 Concluding summary

In this chapter, the numerous benefits of using permeable fabric formwork and steel fibres in construction were discussed. Furthermore, various challenges that arise from the use of fabric formwork were highlighted and focus was placed on the shear behaviour of beams. A gap in literature on the shear behaviour of ISB, such as beams formed with fabric formwork, was identified which lead to potential of further research and the main focus of this investigation.

The description of various shear prediction models for FRC beams found in literature follow in Chapter 3.

CHAPTER 3

SHEAR PREDICTION MODELS FOR CONCRETE BEAMS

Various shear models have been developed in the past to predict the shear capacity of rectangular RC beams, most of which rely on empirical and semi-empirical formulas. These models have shown good agreement with the test results from which they have been developed but poor agreement with test results obtained in other investigations. Recently, several analytical approaches have been proposed in which the physical mechanisms of shear are considered in the development of the shear models. Most of the models are adapted from conventional RC shear models to accommodate the effect of the fibres. In this section, nine alternative shear prediction models that have been developed in the last three decades and reported in literature, are explained.

3.1 Shear Strength prediction method proposed by Mansur *et al.* (1987)

According to Mansur *et al.* (1987), the external shear is resisted by aggregate interlock, the concrete compression zone, doweling action of longitudinal reinforcement and the web reinforcement. However, the individual contribution of the first three mentioned shear components is difficult to predict and is often considered as a combined contribution. Therefore, the total shear resistance of a section is:

$$V_u = V_c + V_{sy} \qquad \textit{Eq 3.1}$$

where: V_c is the combined resistance due to aggregate interlock, doweling action and compression zone, and V_{sy} is the vertical component of the resistance due to web reinforcement.

Mansur *et al*. (1987) adopted the approach proposed by the ACI-ASCE Committee 426 to calculate the shear strength of beams without transverse reinforcement. This approach takes into account aggregate interlock, doweling action and shear resistance in the compression zone, which is component V_c in Eq 3.1. The concrete contribution V_c depends on the concrete compressive strength f'_c, longitudinal reinforcement ratio ρ and the moment-to-shear ratio. The concrete contribution can be determined by:

$$V_c = (0.16\sqrt{f'_c} + 17.2\frac{\rho V d}{M})bd \leq (0.29\sqrt{f'_c})\ bd \qquad \textit{Eq 3.2}$$

where: *V/M* is the shear-to-moment ratio at the critical section, and *b* and *d* are the width and effective depth of the section, respectively.

The critical section depends on the shear span-to-effective depth ratio a_v/d. For beams with $a_v/d \leq 2$, the critical section is at midsection of the shear span. For beams with $a_v/d > 2$, the section is a distance equal to the effective depth *d* away from the point of maximum moment. Hence, the following expressions are derived for the moment-to-shear ratio at the critical section for simply supported beams with two symmetrical point loads:

$$\frac{M}{V} = \left(\frac{M_{max}}{V} - \frac{a}{2}\right) when \frac{a_v}{d} \leq 2 \qquad Eq\ 3.3$$

$$\frac{M}{V} = \left(\frac{M_{max}}{V} - d\right) when \frac{a_v}{d} > 2 \qquad Eq\ 3.4$$

Mansur *et al.* (1987) tested the effect that fibres have on V_c by comparing the calculated result to the tested result of V_c, and it was concluded that the impact is negligible. Furthermore, Mansure *et al.* (1987) found that SFRC beams possess a substantial amount of strength after diagonal cracking has occurred. This was investigated by studying the stress-strain characteristics in direct tension which is graphically represented in Figure 3.1. The dashed line represents the experimental curve and the solid line the idealised curve. The residual stress σ_{tu} is the reserved strength after diagonal cracking, which depends on multiple factors such as length, shape, fibre volume and surface characteristics of fibres as well as concrete properties.

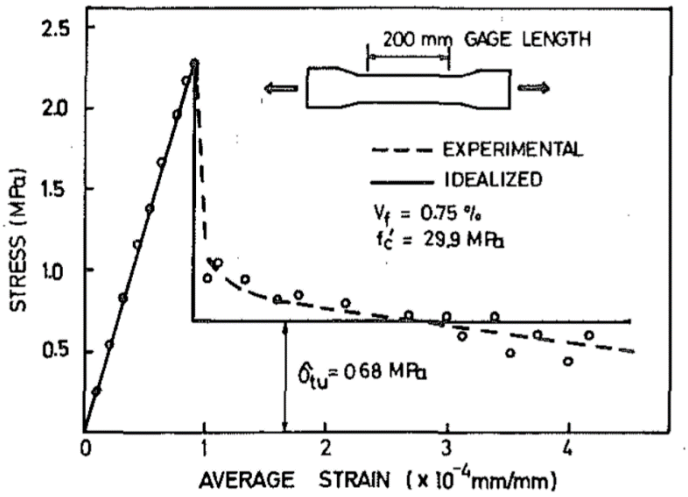

Figure 3.1: Stress-strain relationship of fibre reinforced concrete in direct tension (Mansur et al., 1987).

Considering the forces acting at a diagonal crack in a beam consisting of SFRC without transverse reinforcement, the residual stress σ_{tu} contributes to the shear resistance. With the diagonal crack assumed to form at 45˚, the horizontal projection of the crack is equal to the effective depth *d*. The ultimate shear strength of a beam can be determined with:

$$V_u = V_c + \sigma_{tu}\, bd \qquad Eq\ 3.5$$

To determine σ_{tu}, Mansure *et al.* (1987) suggests using the method proposed by Swamy & Mangat (1976). According to Swamy & Mangat (1976), once concrete reinforced with fibres cracks, the entire stress is transferred to the fibres. Therefore the composite strength can be taken as the fracture strength of the fibres. The ultimate tensile strength of the composite, by considering the length, bond characteristics and random orientation of the fibres, is determined with:

$$\sigma_{tu} = \eta_o\, \eta_L\, \eta_b\, 2\, \tau \frac{l_f}{d_f} V_f \qquad Eq\ 3.6$$

The value for the fibre-matrix interfacial bond stress τ can be determined from the modulus of rupture. A relationship between the interfacial bond stress and the compressive strength of the concrete was found by Swamy and Mangat (1976), but no emphasis was put on the fibre geometry (Figure 3.2). Therefore, in this investigation, a more recent method was used to determine the interfacial bond stress which was proposed by *fib* Model Code 2010 (FIB, 2010b), since it applies to hooked end fibres. The interfacial bond stress was taken as $0.8 * \sqrt{f_c'}$.

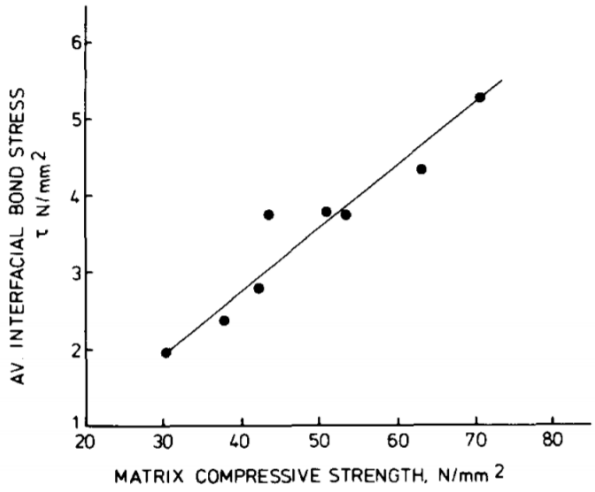

Figure 3.2: Fibre-matrix Interfacial bond stress – matrix compressive strength relationship (Swamy & Mangat, 1976).

The orientation factor η_o for three-dimensional random orientation of fibres can be taken as 0.41 as suggested by Swamy & Mangat (1976). The length correction factor η_L is calculated using a formula that takes into account the stress distribution along the fibres length l_f therefore, is a function of the length of the fibres as well as the material properties of the fibres and the matrix. The length correction factor can be calculated with:

$$\eta_L = 1 - \frac{\tanh(\beta\, l_f/2)}{(\beta\, l_f/2)} \qquad \textit{Eq 3.7}$$

where β is given by:

$$\beta = \sqrt{\frac{2\pi\, G_m}{E_f A_f \ln(S/r_f)}} \qquad \textit{Eq 3.8}$$

where G_m is the shear modulus of the matrix, A_f is the fibre cross-sectional area, r_f the radius of an individual fibre, and S is the mean centroid spacing and is given by:

$$S = 25\left(\frac{d_f}{p\, l_f}\right)^{0.5} \qquad \textit{Eq 3.9}$$

where p is the volume percentage of fibres in the matrix.

The bond efficiency factor η_b is considered to be not critical by Swamy & Mangat (1976) and can be taken as 1.

The following steps are followed to determine the shear strength using the model proposed by Mansur *et al.* (1987):

1. Determine the position of the critical section and calculate the moment-to-shear ratio. For beams with two symmetrical point loads Eq 3.3 or Eq 3.4 can be used.
2. Calculate V_c using Eq 3.2;
3. Calculate S using Eq 3.9;
4. Calculate β using Eq 3.8;
5. Calculate η_L using Eq 3.7;

6. Calculate σ_{tu} using Eq 3.6;
7. Determine the shear strength of the critical section V_u using Eq 3.5.

3.2 Shear strength prediction method of Li *et al.* (1992)

Li *et al.* (1992) investigated the effect of fibre type, fibre volume fractions, spear span-to-effective depth ratio, reinforcement ratio and beam depth on the shear capacity of beams. It was suggested that fibres do not significantly increase the compressive strength of concrete and should, therefore, not be considered as a parameter when determining the shear strength of FRC. However, Li *et al.* (1992) stated that better indicators of improved performance are the split tensile and flexural strength.

From the test results obtained, Li *et al.* (1992) proposed an empirical model to determine shear capacity of FRC beams which is a function of the product of the flexural strength f_f and the split tensile strength f_t. Furthermore, to take into account arch effect, Li *et al.* (1992) proposed two different formulae for beams with $a_v/d \leq 2.5$ and $a_v/d > 2.5$. In this investigation, f_f was calculated from CMOD tests according to EN 14651 (2007) and f_t was calculated using Eq 3.21 from Kwak *et al.* (2002).

The following formulae are proposed by Li *et al.* (1992) to calculate the ultimate shear stress and showed a good straight-line correlation with the results obtained in the investigation by Li *et al.* (1992). To obtain the shear strength, multiply the shear stress by the cross-sectional area:

a/d ≥ 2.5

$$f_v = 1.3 + 4.68\,[\,(f_f f_t)^{3/4}\left(\rho\,\frac{d}{a_v}\right)^{1/3} d^{-1/3}\,] \qquad \textit{Eq 3.10}$$

a/d < 2.5

$$f_v = 9.16\,[\,(f_f)^{2/3}\,(\rho)^{1/3}\left(\frac{d}{a_v}\right)] \qquad \textit{Eq 3.11}$$

where ρ is the longitudinal reinforcement ratio as a percentage of the cross-sectional area.

3.3 Shear Strength prediction method proposed by Swamy *et al.* (1993)

Swamy *et al.* (1993) performed symmetrical four-point bending tests on SFRC beams to assess the shear behaviour of beams with steel fibres as shear reinforcement. Concrete T-beams with a thin web were used in this investigation, because better alignment of the fibres in the principle tensile stress direction can be achieved in members with thin webs (Swamy *et al.*, 1993). In this investigation, three major parameters that affect shear strength were considered; shear span-to-effective depth ratio, longitudinal steel ratio and amount of steel fibres. Furthermore, Swamy *et al.* (1993) proposed a simple model to determine the ultimate shear strength of fibrous reinforced concrete beams, based on a truss model where strut inclination of 45˚ is assumed. The shear resistance consists of the shear resistance of the compression chord V_c and the shear resistance of the web reinforcement V_w, which are steel fibres in this case. In the proposed model, the effect of fibres on concrete compression strength is neglected. Swamy et al. (1993) proposed the following equations for V_w and V_c:

$$V_w = 0.9\,\sigma_{tu}\,b_w\,d \qquad \textit{Eq 3.12}$$

$$V_c = 3.75\,\tau_R\,b_w\,d \qquad \textit{Eq 3.13}$$

where b_w is the width of the web. σ_{tu} is the ultimate tensile strength of fibre reinforced concrete. τ_R is defined as the concrete shear strength, which depends on the compressive strength. However, Swamy et al. (1993) did not specify how to determine τ_R. Therefore, the method proposed by the *fib* Model Code 2010 (FIB, 2010b) for Level I approximation was used:

$$\tau_R = k_v\sqrt{f'_c} \qquad \textit{Eq 3.14}$$

where: $k_v = \frac{180}{1000+1.25z}$;

z is the internal lever-arm between the longitudinal steel and the centroid of the compression block.

f'_c is the cylinder compressive strength of the concrete.

Short beams have a higher shear resistance, therefore V_c is increased by a factor equal to $2d/a_v$. No further definition for a short beam is provided by Swamy *et al.* (1993). With a limit of compression force equal to $0.3\,f'_c b_w\,d$ in the inclined struts, the shear strength can be calculated with:

$$V_u = 0.9\,\sigma_{tu}\,b_w\,d + 3.75\,\tau_R\,b_w\,d \qquad \textit{Eq 3.15}$$

Based on work done by Swamy *et al.* (1993), the post-cracking tensile strength of the composite σ_{tu} can be calculated with:

$$\sigma_{tu} = \eta_o\,\eta_L\,\sigma_{fu}\,V_f \qquad \textit{Eq 3.16}$$

where σ_{fu} is the fracture stress of a fibre and V_f is the volume percentage of fibres. The orientation factor η_o and length efficiency factor η_L take into consideration the random orientation of fibres in a three-dimensional space and stress distributions along the length of an individual fibre, respectively. An orientation factor η_o of 0.41 is considered to be exact (Swamy & Mangat, 1976). The post-cracking tensile strength depends on the length of the fibres and is determined using two various equations distinguishing between failure caused by fibre slippage (Eq 3.17) and fibre rupture (Eq 3.18). The post-cracking tensile strength for beams with fibres either smaller or equal to critical length l_c or with fibres larger than l_c can be calculated with:

$l_f \le l_c$

$$\sigma_{tu} = 0.41\,\tau\,\frac{l_f}{d_f}\,V_f \qquad \textit{Eq 3.17}$$

$l_f > l_c$

$$\sigma_{tu} = 0.41\left(1 - \frac{\sigma_{fu}\,d_f}{4\,\tau\,l_f}\right)\sigma_{fu}V_f \qquad \textit{Eq 3.18}$$

where τ is the fibre-matrix interfacial bond stress and d_f is the fibre diameter. Swamy *et al.* (1993) determined the interfacial bond strength from flexural strength tests, for the fibres used in the investigation to be approximately 4 MPa. Alternatively τ be calculated as $0.8\sqrt{f'_c}$ for hooked-end fibres according to the *fib* Model Code 2010 (FIB, 2010b). The critical length is defined as double the length required to allow the fibre to reach its breaking stress without slippage occurring. The critical length can be determined by:

$$l_{crit} = 2\frac{\sigma_{fu}\, A_f}{p_f\, \tau} \qquad \textit{Eq 3.19}$$

where A_f is the fibre cross-sectional area, p_f is the fibre perimeter and τ is the interfacial bond strength.

3.4 Shear strength prediction method of Kwak *et al.* (2002)

The proposed shear strength prediction model of Kwak *et al.* (2002) is derived empirically. It consists of a combination of shear strength equation developed by Zsutty (1971), to take into account the influence of concrete tensile strength and arch action that might develop in short beams. An additional term takes into account the direct shear contribution of the fibres.

Originally, Zsutty (1971) stated that a positive rate of shear strength increase occurs when the a_v/d ratio is decreased below a certain value described by Kwak *et al.* (2002) as $a_v/d_{transition}$. The $a_v/d_{transition}$ ratio indicates whether a beam is considered as a short beam or a slender beam. The term in the shear strength formula accounting for arch action and tensile strength is multiplied by a factor $e = a_v/d_{transition} * d/a_v$ for short beams and $e = 1$ for slender beams. The $a_v/d_{transition}$ ratio suggested by Kwak *et al.* (2002) is equal to 3.5. The proposed equation for ultimate shear stress is:

$$v_u = 2.1\, e\, f_{spfc}^{0.7}\, (\rho \frac{d}{a_v})^{0.22} + 0.8\, v_b^{0.97} \qquad \textit{Eq 3.20}$$

where f_{spfc} is the split-cylinder tensile strength of fibre concrete [MPa] and is equal to:

$$f_{spfc} = \frac{f_{cu}}{(20 - \sqrt{F})} + 0.7 + 1.0\sqrt{F} \qquad \textit{Eq 3.21}$$

where: ρ is the flexural reinforcement ratio;

$v_b = 0.41\, \tau\, F$;

F is a fibre factor = $(l_f / d_f)\, V_f\, D_f$;

l_f is the fibre length;

d_f is the fibre diameter;

V_f is the volume fraction of steel fibres;

D_f is the bond factor: 0.5 for round fibres, 0.75 for crimped fibres and 1.0 for indented fibres;

τ is the average fibre-matrix interfacial.

To obtain the shear strength, the ultimate shear stress is multiplied with the cross-sectional area.

3.5 Shear strength prediction model in *fib* Model Code 2010 (FIB, 2010c)

The shear strength prediction model suggested in the *fib* Model Code 2010 (FIB, 2010b) is a model that was adapted from the shear formula in the Eurocode 2 (EC2) for beams without shear reinforcement (EN 1992-1-1, 2004). The equation to calculate shear capacity of beam provided by EC2 has been adapted for SFRC by adding a term that takes into account the shear component of fibres. This model has only been verified strictly for steel fibres in conventional concrete, therefore this model does not accommodate special types of concrete such as reactive powder concrete or alternative fibre reinforcement (FIB, 2010b). The following represents the shear formulae proposed in EC2 for RC beams with no shear reinforcement (Eq 3.22) and the model proposed in the *fib* Model Code 2010 (FIB, 2010b) which is the EC2 equation that has been adapted to incorporate steel fibres (Eq 3.23):

$$V_{Rd,c} = \left(\frac{0.18}{\gamma_c}\, k\, (100\, \rho_1\, f_{ck})^{1/3} + k_1\, \sigma_{cp}\right) b_w\, d \qquad \textit{Eq 3.22}$$

$$V_{Rd,c} = \left(\frac{0.18}{\gamma_c}\, k \left[100\, \rho_1 \left(1 + 7.5\, \frac{f_{Ftuk}}{f_{ctk}}\right) f_{ck}\right]^{1/3} + 0.15\, \sigma_{cp}\right) b_w\, d \qquad \textit{Eq 3.23}$$

where: γ_c is a partial safety factor for concrete without fibres;

k is a factor taking the size effect into account and is equal to:

$$k = 1 + \sqrt{200/d} \leq 2.0$$

ρ_1 is the ratio of longitudinal reinforcement and is equal to: $\rho_1 = A_s/b_w d$

A_s is the cross-sectional area of longitudinal reinforcement;

f_{ck} characteristic value of concrete cylinder strength [MPa];

f_{Ftuk} is the characteristic value of the ultimate residual tensile strength for FRC;

f_{ctk} is the characteristic value for tensile strength of concrete without fibres;

σ_{cp} is the average stress acting on the concrete cross-section due to prestressing action [MPa];

b_w is the smallest width of the concrete in the tension area [mm];

d is the effective depth of the beam;

The factor f_{Ftuk} can be determined by performing the bending test on notched beams according to EN 14651 (2007). From this test, nominal values of the residual flexure strengths $f_{R,1}$, $f_{R,2}$, $f_{R,3}$ and $f_{R,4}$ corresponding to different crack mouth opening displacement values (CMOD) of 0.5, 1.5, 2.5 and 3 are obtained. The nominal values are used to calculate f_{Ftuk} for the relevant FRC with:

$$f_{Fts} = 0.45\, f_{R1} \qquad \textit{Eq 3.24}$$

$$f_{Ftu} = f_{Fts} - \frac{w_u}{CMOD_3}(f_{Fts} - 0.5\, f_{R3} + 0.2\, f_{R1}) \geq 0 \qquad \textit{Eq 3.25}$$

where w_u is the maximum crack width acceptable in structural design.

3.6 Plastic Model for SFRC Beams by Spinella *et al.* (2010)

The shear model proposed by Spinella *et al.* (2010) is based on the Critical Sliding Model (CSM), which was initially developed for RC beams without shear reinforcement. The CSM is based on the assumption that yield lines are formed as shear cracks form in the beam. The

model proposed by Spinella *et al.* (2010) is a simplified version of the CSM and adapting it for the shear capacity increase due to arch effect, specifically in short beams. The CSM was also modified to account for the ability of fibres to restrain the widening of cracks and prevent slippage at the shear crack by implementing effectiveness factors.

In the theory of plasticity, it is accepted that cracked concrete subjected to compressive stresses is exposed to compression strains and orthogonal tensile strains, simultaneously. Therefore, it has a reduced strength compared to uncracked concrete. The effective compressive strength in is computed as:

$$f_{c,ef} = v_c f_c = v_s v_0 f_c$$

$$= v_s \left\{ \left(\frac{5.6}{\sqrt{f_c}} \right) \left[0.27 \left(1 + \frac{1}{\sqrt{h}} \right) \right] (0.15\rho + 0.58) \right\} f_c \qquad \textit{Eq 3.26}$$

where: v_s is the sliding reduction factor = 0.5

ρ is the longitudinal reinforcement percentage = $100A_s/bh$

h and b are the height and width of the beam, respectively

f'_c is the compressive cylinder strength

CSM for SFRC beams

It is more suitable to apply the plastic theory to SFRC than to RC due to the flattening of the stress-strain relationship. The residual tensile stress resulting from the fibres influence the mechanical behaviour of members, especially in slender beams (Spinella *et al.*, 2010). The Variable Engagement Model (VEM) proposed by Foster *et al.* (2006) has been adopted in this model and is used to estimate the effective tensile strength of SFRC (Eq 3.27).

$$f_{ctf,ef} = v_{tf} f_{ctf} \qquad \textit{Eq 3.27}$$

The VEM assumes that fibres fracture rather than pull out of the concrete and that slippage between the fibres and concrete matrix occurs prior to the full development of bond stress. The relationship of tensile stress and crack opening displacement is determined from the matrix and fibre stress contributions. With an allowable crack opening at shear failure (w_m) equal to *0.01h,* the effectiveness tensile factor can be computed as:

$$v_{tf} = \left(1 - \frac{w_m}{w_{ts}}\right) + \left[\frac{tan^{-1}(w_m/\alpha)}{\pi}\left(1 - \frac{2w_m}{l_f}\right)^2 F_\tau\right] \quad \textit{Eq 3.28}$$

where: α is a material parameter = $d_f/3.5$

$F_\tau = \beta_\tau V_f(l_f/d_f)$;

l_f is the fibre length;

d_f is the fibre diameter;

V_f is the volume fraction of steel fibres;

β_τ is the ratio of fibre-matrix shear stress and the direct tensile strength of the material = τ_b/f_{ct} with $d_f = c\sqrt{f'_c}$ (c ranges between *0.5* and *1* for straight, crimped or hooked-end fibres)

w_{ts} is the maximum crack width for the matrix = $2G_c/f_{ct}$;

G_c is the fracture energy of concrete depending on the maximum aggregate size (a_g) and is = $0.00375 f_c^{2/3} a_g^{1/4}$ [MPa];

The critical section of the beam is located at the start of the shear crack, which propagates and becomes the critical yield line. To determine the location of the critical section, the average cracking stress τ_{cr} (Eq 3.29) and the average ultimate shear stress τ_u (Eq 3.30) must be solved.

$$\tau_{cr} = \frac{P_{cr}}{bh} = 0.5\, f_{ct,ef}\, \frac{1 + [(a-x)/h]^2}{a/h} \quad \textit{Eq 3.29}$$

$$\tau_u = 2\frac{\tau_{cr}}{(a-x)/h} \quad \textit{Eq 3.30}$$

Finally, the location where the critical shear crack starts to develop can be calculated as follows:

$$\frac{(a-x_o)}{h} = \frac{\sqrt[3]{2}\left(\sqrt{12+81q^2} - 9q\right)^{2/3} - 2\sqrt[3]{3}}{\sqrt[3]{6^2}\left(\sqrt{12+81q^2} - 9q\right)^{1/3}} \leq \frac{a}{h} \quad \textit{Eq 3.31}$$

$$q = -4\left(\frac{\tau_{cf}}{f_{ct,ef}}\right)\left(a/h\right) \qquad \textit{Eq 3.32}$$

$$\tau_{cf} = 0.11\, v_{0f} f_{cf} \qquad \textit{Eq 3.33}$$

By applying the simplifications developed by Spinella *et al.* (2010), the average ultimate shear stress of fibrous concrete can be calculated as follows:

$$\tau_u = 0.220\, v_{0f}\, f_{cf}\; h/(a - x_o) \qquad \textit{Eq 3.34}$$

$$v_{0f} = \left\{\left(\frac{5.6}{\sqrt{f'_c}}\right)\left[0.27\left(1 + \frac{1}{\sqrt{h}}\right)\right](0.15\rho + 0.58)\right\} \qquad \textit{Eq 3.35}$$

The following steps are followed to determine the shear strength using the model proposed by Spinella *et al.* (2010):

1. Determine the effectiveness factor in compression using Eq 3.26.
2. Estimate the shear crack width w_m. For this model, it is proposed to use $w_m = 0.01h$.
3. Using Eq 3.28 determine the effectiveness factor in tension and then the effective tensile strength using Eq 3.27.
4. Determine the starting position of the critical shear crack by computing Eq 3.31.
5. Use Eq 3.34 to calculate the average shear stress at failure.

3.7 MCFT-VEM Shear prediction model

The following model is proposed in the *fib* Model Code - Bulletin 57 (FIB, 2010c). The basis of this model is the Modified Compression Field Theory (MCFT) combined with the VEM for the fibre contribution towards shear resistance of SFRC beams. In this model, the shear capacity is a combination of the shear contributions of the concrete $V_{Rd,c}$, the transverse reinforcing steel $V_{Rd,s}$ and the steel fibres $V_{Rd,f}$. The VEM, however, shows that the contribution of the concrete and the fibres are interlinked and are functions of the critical shear

crack width w_{crit} and should therefore be solved simultaneously. Figure 3.3 represents the coupling of the concrete matrix and fibres' contributions to shear capacity.

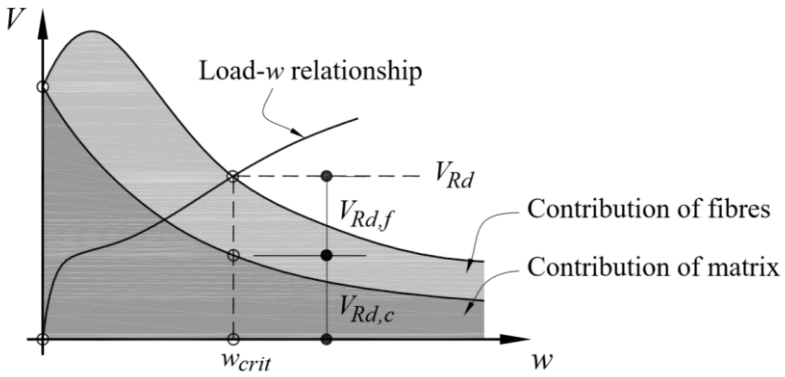

Figure 3.3 Combination of concrete matrix and fibres' shear contributions (FIB, 2010c).

From the work of Bentz *et al.* (2006), the concrete shear component is given as follows, provided that web crushing does not control the design:

$$V_{Rd,c} = k_v \frac{\sqrt{f_{ck}}}{\gamma_c} b_w z \qquad \textit{Eq 3.36}$$

where: z is the internal moment lever arm and is taken as *0.9d;*

γ_c is a partial safety factor for concrete.

k_v is a parameter that determines the aggregate interlock stresses resisted by the concrete (Eq 3.37).

$$k_v = \frac{0.4}{1 + 1500\varepsilon_x} \cdot \frac{1300}{1000 + 0.7\, k_{dg}\, z} \qquad \textit{Eq 3.37}$$

The factor k_{dg} takes into account the maximum aggregate size d_g *(mm)* and is determined as:

$f'_c \leq 70$ MPa	$k_{dg} = \frac{48}{16 + d_g} \geq 1.15$	*Eq 3.38*
$f'_c > 70$ MPa and light-weight concrete	$k_{dg} = 3.0$	

Shear crack width at mid-height on the section *w* is calculated with:

$$w = 0.2 + 1000\varepsilon_x \geq 0.125\ mm \qquad \textit{Eq 3.39}$$

where ε_x is the longitudinal strain at mid-height of the section and is given as:

$$\varepsilon_x = \frac{M_{Ed}/z + 0.5V_{Ed}\ cot\theta + 0.5N_{Ed} - A_p f_{po}}{2\left(E_s A_s + E_p A_p\right)} \qquad \textit{Eq 3.40}$$

In Eq 3.40, M_{Ed} , V_{Ed} and N_{Ed} are the internal forces resulting from the factored design loads. A_s and E_s , and A_p and E_p are the cross-sectional area and elastic modulus of reinforcing steel and prestressing steel, respectively. The angle of the compressive strut can be calculated as:

$$\theta = 29^o + 7000\varepsilon_x \qquad \textit{Eq 3.41}$$

The fibre contribution to shear capacity $V_{Rd,f}$ is determined through the VEM (Eq 3.42) and is illustrated in Figure 3.4.

$$V_{Rd,f} = k_{fd}\ f_{tf}(w)\ b_w\ z\ cot\theta \qquad \textit{Eq 3.42}$$

where k_{fd} is a fibre dispersion reduction factor and was determined through x-ray image analysis and should be taken as 0.82.

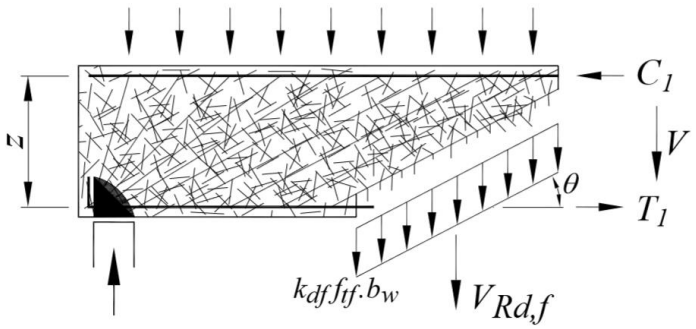

Figure 3.4: Fibre reinforcement contribution to shear capacity (FIB, 2010c).

Variable engagement model

The VEM was developed by Voo and Foster (2003). In brief, the tensile strength f_{tf} provided over a unit area by fibres is given as:

$$f_{tf} = K_f\ \alpha_f\ \rho_f\ \tau_b \qquad \textit{Eq 3.43}$$

where: α_f is the fibre aspect ratio (l_f/d_f);

ρ_f is the volumetric fraction of fibres;

τ_b is the bond stress between fibres and concrete matrix and = $k_b\sqrt{f_{ck}}$. (k_b = 0.8 for hooked end fibres, = 0.6 for crimped fibres and = 0.4 for straight fibres) and f_{ck} is the compressive cylinder strength;

K_f is a global orientation factor and is given as:

$$K_f = \frac{1}{\pi}\ tan^{-1}\left[w/\left(\alpha_l l_f\right)\right]\left(1 - \frac{2w}{l_f}\right)^2 \qquad \textit{Eq 3.44}$$

where α_l is a fibre engagement coefficient = $1/(3.5\alpha_f)$. Furthermore, it is assumed that no fibre fracture occurs and the fibres rather pull out of the concrete matrix. Thus, Eq 3.44 only applies provided:

$$l_f < l_{crit} = \frac{d_f}{2} \cdot \frac{\sigma_{fu}}{\tau_b} \qquad \textit{Eq 3.45}$$

where σ_{fu} tensile strength of an individual fibre [MPa].

3.8 Shear Strength Model proposed by Dinh *et al.* (2011)

A simple shear strength prediction model was proposed by Dinh *et al*. (2011) for slender SFRC beams without shear reinforcement. In this model, it is assumed that shear stresses are resisted by the concrete compression block and by the fibres that transfer tension across shear cracks. The failure criterion of Bresler & Pister (1958) is used to determine the shear contribution of the compression block, which considers concrete subjected to both compressive and shear

stresses, simultaneously. The contribution of fibres to shear resistance is calculated using material properties obtained from the standard bending test prescribed by the ASTM 1609 (2019). For conservatisms, in this proposed model aggregate interlock and doweling action is ignored. It is argued that as the critical crack widens the contribution of shear resistance by aggregate interlock significantly diminishes prior to failure.

In this model, a SFRC beam is assumed to fail along the idealized inclined crack represented by line MNPQ on Figure 3.5 a) which consists of the assumed shear crack MNP and the compression zone PQ. The dashed line MNN'P represents an idealised critical flexure-shear crack in SFRC beams failing in shear. Figure 3.5 b) represents the assumed linear strain distribution just prior to failure with *P* representing the position of the neutral axis and *w* crack width.

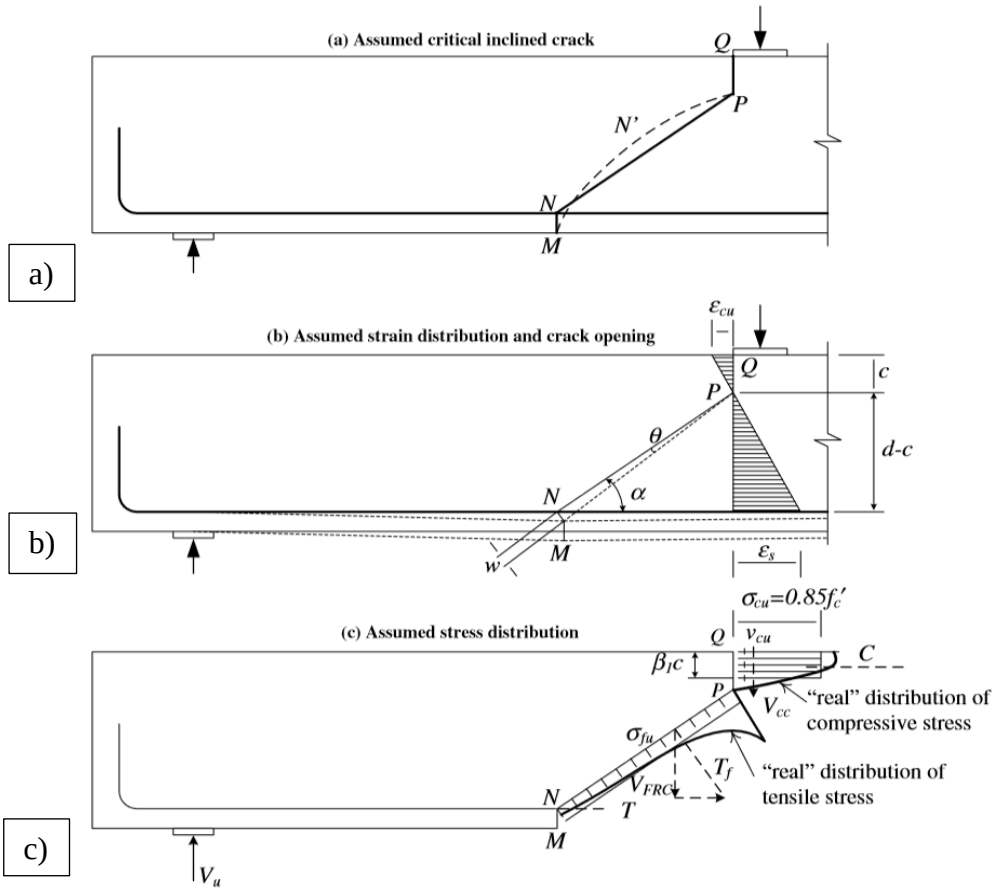

Figure 3.5: Idealised failure crack and internal stresses of SFRC beams (Dinh et al., 2011).

According to this model, the shear strength for a SFRC beam can be calculated as follows:

$$V_u = V_{cc} + V_{FRC} \qquad \textit{Eq 3.46}$$

where V_{cc} is the shear force contribution of the compression block, and V_{FRC} is the shear contribution provided by fibres through tension resistance.

Shear contribution of the compression block

In this model, concrete crushing in the compression zone is assumed to trigger shear failure. The stress state above the neutral axis is assumed to be a combination of normal compressive stress σ_{cu} and shear stress v_{cu}. Since significant experimental evidence has shown that low volume of fibres have negligible effects on the compressive stress of concrete the failure criterion of by Bresler & Pister (1958) for normal concrete (Figure 3.6) is considered adequate and can be calculated as follows:

$$\frac{v_{cu}}{f'_c} = 0.1\left[0.62 + 7.86\left(\frac{\sigma_{cu}}{f'_c}\right) - 8.46\left(\frac{\sigma_{cu}}{f'_c}\right)^2\right]^{1/2} \qquad \textit{Eq 3.47}$$

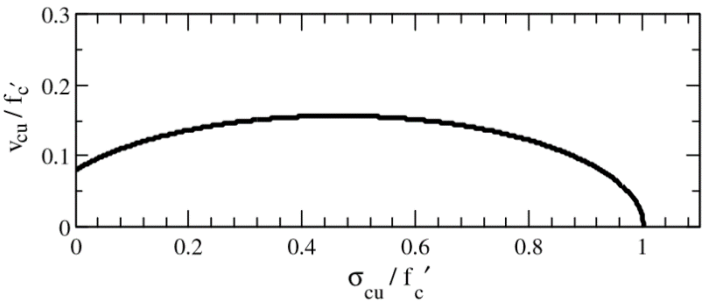

Figure 3.6: Failure criterion of concrete in compression and shear by Bresler & Pister (1958) (Dinh et al., 2011).

Assuming force equilibrium at any given section, the depth of the compression block can be calculated with Eq 3.48, assuming that the longitudinal reinforcement has yielded.

$$c = \frac{T_s}{k_1 k_3 f'_c b} = \frac{A_s f_y}{k_1 k_3 f'_c b} \qquad \textit{Eq 3.48}$$

A_s and f_y are the cross-sectional area and yield stress of longitudinal steel, respectively. f'_c and b are the compressive cylinder strength of concrete (MPa) and width of the section, respectively. The factor $k_1 k_3$ can be calculated by the simplified equation from the ACI Building Code (ACI Committee 318, 2008) as:

$$k_1 k_3 = 0.85\beta_1 \qquad \textit{Eq 3.49}$$

For $f'_c \leq 27.6$ MPa, $\beta_1 = 0.85$ and for $f'_c \geq 55.1$ MPa, $\beta_1 = 0.65$. For f'_c between 27.6 and 55.1 MPa, linear interpolation is used.

Based on the work done by Dinh *et al.* (2011), the shear carried in the compressive zone is determined as:

$$V_{cc} = 0.11 f'_c \beta_1 c b = 0.11 \frac{T_s}{0.85} = 0.13 A_s f_y \qquad \textit{Eq 3.50}$$

Fibre contribution to shear resistance

The transfer of tension force across a shear crack is dependent on the crack width. The proposed approach is illustrated in Figure 3.5 c). For simplicity, a uniform tensile stress is considered (thin line in Figure 3.5 c), which equals the resultant force of the actual stress distribution (bold line in Figure 3.5 c). The stress below the tensile reinforcement is neglected. V_{FRC} is expressed as:

$$\begin{aligned} V_{\text{FRC}} &= T_f \cos(\alpha) = \left[(\sigma_t)_{\text{avg}} b \left(\frac{d-c}{\sin(\alpha)} \right) \right] \cos(\alpha) \\ &= (\sigma_t)_{\text{avg}} b (d-c) \text{cotan}(\alpha) \end{aligned} \qquad \textit{Eq 3.51}$$

Test beams failing in shear-compression showed that the angle α lies in the range of 33˚ and 45˚, for conservatism and simplicity it is recommended to use α = 45˚. The average tension stress transferred across a crack $(\sigma_t)_{avg}$ is determined from the ASTM 1609 four-point bending

tests. Similar results can be obtained from the CMOD test prescribed in EN 14651 (2007) and was used for this investigation.

The derivation of the uniform tensile stress from the ASTM 1609 four-point bending test can be seen in Figure 3.7. Shown by test results, the depth of the neutral axis can be taken as $0.1h$ from the top of the beam. The average tensile stress at a deflection of δ can be calculated as:

$$(\sigma_t)_{\text{avg}} = \frac{2M}{0.9bh^2} \qquad \textit{Eq 3.52}$$

where M is the moment at the cracked section once a deflection of δ has been reached. The deflection δ is calculated at a crack width equal to 0.05 l_f. The deflection δ is calculated as:

$$\delta = \frac{l_f\, L}{80(h-c)} \qquad \textit{Eq 3.53}$$

where L is the span of the beam and c can be taken as $0.9h$.

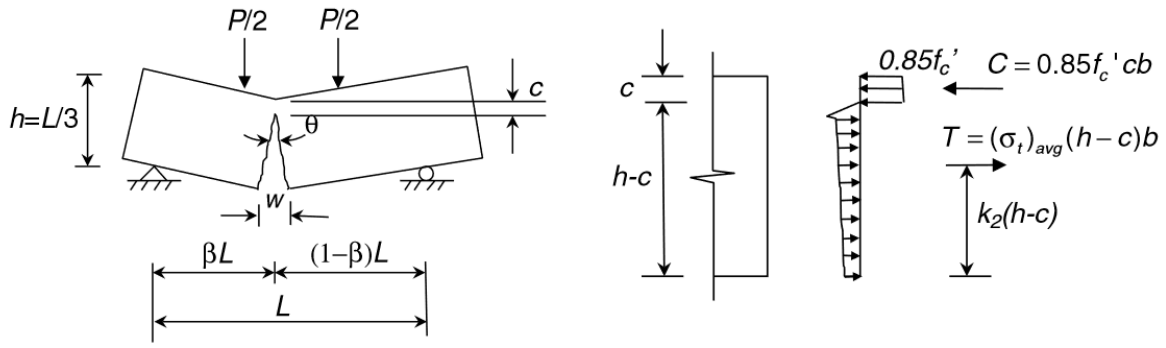

Figure 3.7: Derivation of the uniform tensile stress from the ASTM C1609 four-point bending test (Dinh et al., 2011).

3.9 Shear strength prediction method of Singh & Jain (2014).

The mechanics based shear prediction model proposed by Singh & Jain (2014) is based on the model proposed by Dinh *et al.* (2011). The contributors to shear resistance considered in this

model are that of the compressed concrete V_{CC} and the shear component of the fibres bridging the diagonal crack V_{FRC} (refer to Figure 3.8). The shear contribution of aggregate interlock is considered to be negligible since aggregate interlock diminishes as the critical shear crack widens and due to the slight possibility of the crack faces sliding over each other. The ultimate shear strength of the beam is then simply taken as the summation of these two components.

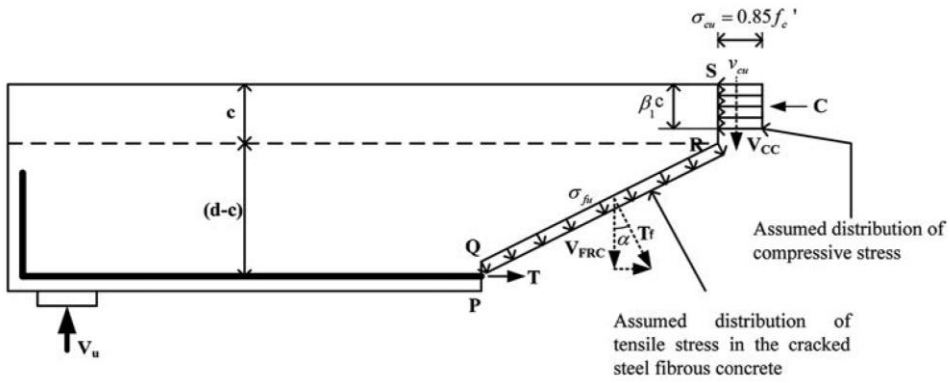

Figure 3.8: Assumed stresses of SFRC beam failing in diagonal tension (Singh and Jain, 2014).

In this model, the shear contribution of the compressed concrete is estimated by using the following formula which was derived by Dinh *et al.* (2011) from the failure criterion of Bresler & Pister (1958):

$$V_{CC} = 0.11 f_c' \beta_1 c b \qquad \text{Eq 3.54}$$

where: f'_c is the cylinder compressive strength of the concrete;

c is the depth of the neutral axis;

β_1 is the stress block depth factor and is 0.85 for $f'_c \leq 27.6$ [MPa] and 0.65 for $f'_c \geq 55.1$ [MPa]. For f'_c between 27.6 and 55.1 MPa, linear interpolation is used.

In cases were the yield stress f_y and cross-sectional area A_s of the longitudinal reinforcement is known Eq 3.54 can be replaced with, provided the beam has a rectangular cross-section:

$$V_{CC} = 0.13 A_s f_y \qquad \textit{Eq 3.55}$$

With reference to Figure 3.8, the vertical component of the uniform tensile force T_f transferred across the assumed critical shear crack, at an angle of α, through fibre tension is given as:

$$V_{FRC} = T_f \cos\alpha = [\sigma_{fu} b(d - c)\cot(\alpha)] \qquad \textit{Eq 3.56}$$

The uniform tensile stress σ_{tu} resulting from fibres bridging a unit area of the diagonal shear crack is calculated as:

$$\sigma_{tu} = N \cdot f \qquad \textit{Eq 3.57}$$

where N is the number of fibres bridging a unit area of diagonal crack and f is the average pull-out force per fibre which are is calculated as:

$$N = 0.5 \frac{V_f}{\pi r_f^2} \qquad \textit{Eq 3.58}$$

$$f = \tau \pi D_f d_f \frac{l_f}{4} \qquad \textit{Eq 3.59}$$

where V_f is the fibre content in the concrete mix, r_f is the radius of a fibre, D_f is a bond efficiency factor depending on the kind of fibres used (for hooked-end fibres $D_f = 1$ and for crimped fibres $D_f = 0.75$), d_f is the fibre diameter and l_f is the fibre length. The fibre-matrix interfacial bond strength can be estimated as:

hooked-end fibres: $$\tau = 0.85\sqrt{f_c'} \qquad \textit{Eq 3.60}$$

crimped fibres: $$\tau = 0.75\sqrt{f_c'} \qquad \textit{Eq 3.61}$$

From this, Eq 3.56 can be rewritten as:

$$V_{FRC} = \left[0.5\tau D_f V_f \frac{l_f}{d_f} b(d-c)\cot(\alpha) \right] \qquad \textit{Eq 3.62}$$

Combining Eq 3.54 and 3.62, the shear strength of a SFRC beam V_u can be calculated with:

$$V_u = 0.11 f_c' \beta_1 cb + \left[0.5\tau D_f V_f \frac{l_f}{d_f} b(d-c)\cot(\alpha) \right] \qquad \textit{Eq 3.63}$$

The diagonal shear crack inclination α was found to be in the range of 25˚ to 36˚. It was recommended that an average value of 30˚ is used.

3.10 Concluding summary

This chapter covers a detailed description of nine shear prediction models that can be applied to fibre reinforced concrete beams. These models have been applied to existing databases containing beams that failed in shear and have all shown good shear prediction quality. This collection of shear models include various analytical, empirical, semi-empirical and more complex models. It has been realised that models reported in literature are generally only developed for beams with prismatic sections and must be modified somehow to predict the shear capacity of ISB.

Table 3.1 is a summary of the input requirements or preliminary testing that must be performed prior to the application of the relevant shear models. Preliminary tests will provide certain material properties required as input parameter in the shear model.

Table 3.1: Summary of the input requirements for the application of the various shear models

Model	**Type**	**Input requirements**				
		Concrete compressive strength	User shear crack inclination angle	EN 14651 test	ASTM C1609 test	Split-cylinder tensile strength
Mansur et al.	Analytical	Yes	No	No	No	No
Li et al.	Empirical	Yes	No	No	No	Yes
Swamy et al.	Analytical	Yes	45° assumed in model	No	No	No
Kwak et al.	Empirical	Yes	No	No	No	Yes**
fib MC 2010	Empirical	Yes	No	Yes	No	No
Spinella et al.	Complex	Yes	No	No	No	No
MCFT-VEM	Complex	Yes	No	No	No	No
Dinh et al.	Analytical	Yes	Yes	Yes*	Yes	No
Singh & Jain	Analytical	Yes	Yes	No	No	No

*** Either of the EN 14651 or ASTM C1609 tests are required and not both.**
**** Tests can be performed or relevant formula presented in the model description.**

CHAPTER 4

SHEAR PREDICTION MODELS FOR IRREGULAR SHAPED BEAMS

This section explains how the shear prediction models presented in Chapter 3 have been modified to accommodate the irregular cross-sections of the beams tested in this investigation. Furthermore, an analytical shear prediction model is proposed for ISB with steel fibres.

4.1 Modification of shear models for irregular shaped beams

Most existing shear models and design codes use an effective cross-sectional area that contributes to shear resistance as equal to the narrowest part of the beam or web (b_w) multiplied by the effective depth (d) of the beam. The majority of the shear models used in this investigation specify the effective area as being equal to ($b_w \cdot d$). This means that theoretically, the four beam-types tested in this investigation should have the same shear capacity (refer to Figure 4.1). However, this is considered to be incorrect and will lead to over-conservative shear predictions.

Alternatively, EN 8110-1 (1997) specifies the shear resistance of a beam as being equal to the ultimate shear stresses multiplied by an effective cross-sectional area that is calculated as the average width of the web located below the flange multiplied by the effective depth of the beam. Furthermore, Thamrin *et al.* (2016) found that the flange of a T-beam has a significant influence on the shear capacity of a beam

The shear models used in this investigation were modified by replacing the effective area term $(b_w \cdot d)$ with an alternative effective area. Considering the guidelines of the EN 8110-1 (1997) and the findings of Thamrin *et al.* (2016) the new effective area used in the shear models incorporates the whole cross-sectional area of the web and the portion of the flange above the web.

The effective area that was used to adapt the shear models is graphically presented in Figure 4.1, with the exception of the models proposed by Dinh *et al*. (2011) and Singh & Jain (2014). For the case where the neutral axis lies in the flange, the effective cross-sectional area is taken as the gross cross-sectional area of the web, plus the part of the flange which lies directly above the web, i.e. the part of the flange that has the same width as the top of the web. If the neutral axis lies within the web, the effective area is calculated as the gross cross-sectional area of the web under the neutral axis, plus the part of the web and flange above the neutral axis with the same width as the width at the neutral axis (refer to Figure 4.1).

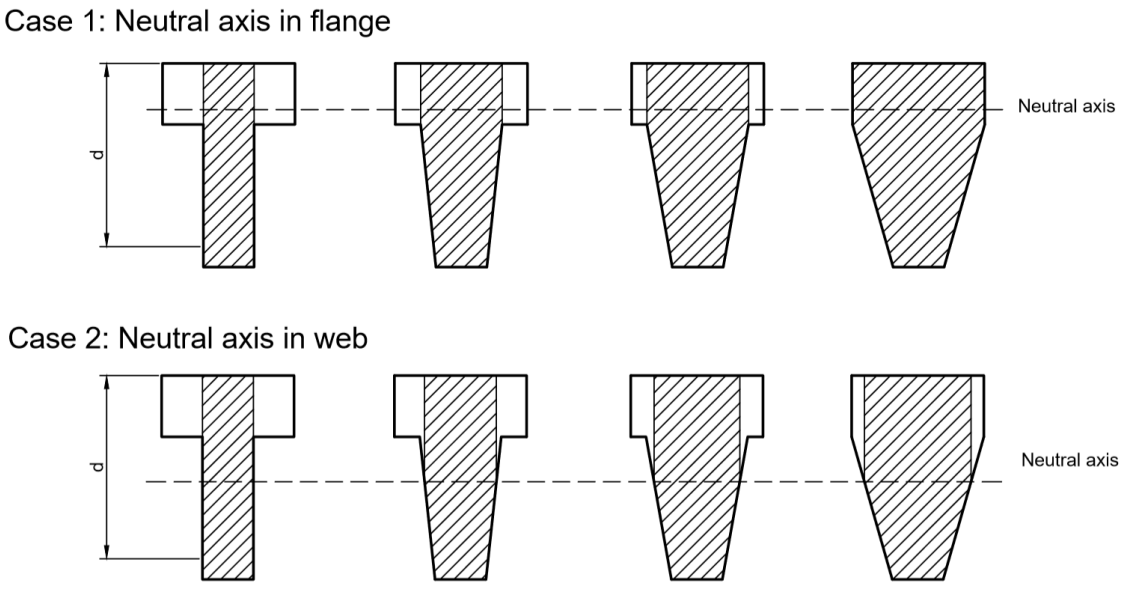

Figure 4.1: Alternative effective areas used to adapt shear models.

The cross-sectional area used to predict the shear capacity with the models of Dinh *et al.* (2011) and Singh & Jain (2014) were modified differently to other shear models used in this investigation since these models require the inclination of the diagonal shear crack as input parameter. For the shear contribution of the concrete compression block, the whole area of concrete above the neutral axis is used. For the contribution of fibres towards shear resistance, the cross-sectional area of the beam in the plane of the main shear crack is used. Therefore, the cross-sectional area of the beam on a plane angled at α (the angle between the main shear crack and the horizontal) between the centroid of the reinforcement and the neutral axis is used. This is similar to the proposed model and is explained in the following section.

The final equations of all modified shear models used in this investigation were modified with an alternative effective area and are summarised in Table 4.1 with further important notes.

Table 4.1: Summary of adapted shear model formulae.

Model	Year	Formula	Note
Mansur et al.	1987	$V_u = \left[\left(0.16\sqrt{f'_c} + 17.2\frac{\rho V d}{M}\right) + \left(\eta_o\,\eta_L\,\eta_b\,2\,\tau\frac{l_f}{d_f}V_f\right)\right]\cdot A_{eff}$	
Li et al.	1992	$V_u = \left(1.3 + 4.68\,[\,(f_f f_t)^{3/4}\left(\rho\frac{d}{a}\right)^{1/3} d^{-1/3}\right)\cdot A_{eff}$	
Swamy et al.	1993	$V_u = (0.9\,\sigma_{tu} + 3.75\,\tau_R)\cdot A_{eff}$	$\sigma_{cu} = \eta_o\,\eta_L\,\sigma_{fu}\,V_f$
Kwak et al.	2002	$V_u = \left(2.1\,e\,f_{spfc}^{0.7}\,(\rho\frac{d}{a})^{0.22} + 0.8\,v_b^{0.97}\right)\cdot A_{eff}$	$f_{spfc} = \frac{f_{cu}}{(20-\sqrt{F})} + 0.7 + 1.0\sqrt{F}$ $F = (l_f / d_f)\,V_f\,D_f$
fib Model Code 2010	2010	$V_{Rd} = \left(\frac{0.18}{\gamma_c}\,k\left(100\,\rho_1\,(1 + 7.5\cdot\frac{f_{Ftuk}}{f_{ctk}}\cdot f_{ck}\right)^{1/3} + 0.15\cdot\sigma_{cp}\right)\cdot A_{eff}$	
Spinella et al.	2010	$V_u = \left(0.22\left[\left(\frac{5.6}{\sqrt{f_c}}\right)\left[0.27\left(1+\frac{1}{\sqrt{h}}\right)\right](0.15r + 0.58)\right]f_{cf}\,\frac{h}{(a-x_0)}\right)\cdot A_{eff}$	
MCFT-VEM	2010	$V_{Rd} = \left(k_v\frac{\sqrt{f_{ck}}}{\gamma_c} + k_{fd}\cdot f_{tf}\cot\theta\right)\cdot A_{eff}$	
Dinh et al.	2011	$V_u = 0.11\,f'_c\,\beta_1 c\,b_f + (\sigma_t)_{avg}\cdot(d-c)\left(\frac{b_c + b_d}{2}\right)\cot\alpha$	The term $b(d-c)$ was replaced with $(d-c)\left(\frac{b_c+b_d}{2}\right)$
Singh and Jain	2014	$V_u = 0.11\,f'_c\,\beta_1 c\,b_f + 0.5\,\tau\cdot D_f\cdot V_f\frac{l_f}{d_f}\cdot(d-c)\left(\frac{b_{NA}+b_d}{2}\right)\cot\alpha$	Where: b_c is the width of the beam at the neutral axis and b_d is the width of the beam at effective depth
A_{eff} is calculated as the full area of the web plus the portion of the flange equal to the width of the top of the web. Refer to Chapter 3 for detailed descriptions of the shear models and equations in this Table.			

4.2 Proposal of Shear Model

A simple model is proposed, based on shear mechanics, to predict the shear strength of irregular shaped SFRC beams with no stirrup reinforcement. ISB in this case refers to beams consisting of a flange and an unconventionally shaped web. These ISB can also be described as V-beams, referring to the shape of the web. The development of a shear model for V-beams is inspired by the relatively new technology known as Fabric Formwork which generally produces beams of irregular shapes with similar sections as a V-beam.

The proposed model is adapted from the model proposed by Singh & Jain (2014) and was modified slightly to accommodate the irregular cross-section of a V-beam. This analytical model was chosen based on the principles used to developed the model, and this model has proven to be significantly accurate in predicting the shear capacities of numerous regular prismatic and T-beams (Singh & Jain, 2014). Furthermore, it is a simple model that can easily be applied by designers in practice to predict the shear capacity of irregular shaped V-beams in order to produce safe designs.

4.2.1 Limitations of Model

The proposed model is limited to the shear prediction of beams containing steel fibres and no transverse reinforcement undergoing diagonal tension failure, which generally occurs in beams with a shear span-to-effective depth ratio (a_v/d) in the vicinity of 2.5 to 6. The model has been developed for conventional SFRC but can also be applied to beams consisting of SFR-SCC, even though it has been proven that FR-SCC has higher interfacial bond strengths between fibres and concrete matrix (Greenough & Nehdi, 2008) compared to FRC. Due to the limited knowledge on the improved interfacial bond strength in SCC, the model has not been adjusted for this feature, which will only lead to slightly more conservative predictions in cases where SFR-SCC is used. Furthermore, the model is only applicable for hooked-end and crimped steel fibres and will not lead to accurate predictions for beams containing straight steel fibres or fibres consisting of alternative materials such as polypropylene or glass fibres.

Shear resistance of slender FRC beams without vertical reinforcement is attributed to a complex interaction of various mechanisms that contribute to shear resistance such as the compression block, aggregate interlock, dowel action and the residual stresses from fibres bridging diagonal cracks. For simplicity and conservatism, the shear mechanisms considered

in this model are the contribution of the concrete in compression and the vertical component of residual stresses produced by the steel fibres bridging the critical diagonal shear crack. According to Dinh *et al.*, (2011), the contribution of aggregate interlock is considered to be insignificant because as diagonal crack widens, the steel fibres are mobilised and the shear contribution of aggregate interlock would start to decay. Similarly, in beams that are under-reinforced in flexure, doweling action would have a minor contribution and is ignored in this model, for the sake of conservatism. The ultimate shear resistance of the beam can therefore be calculated as the superimposed shear resistance of the two mentioned components, and is expressed as:

$$V_u = V_{cc} + V_{FRC} \qquad Eq\ 4.1$$

where: V_{cc} is the shear component of the concrete in compression and V_{FRC} is the shear resistance contributed by the steel fibres.

4.2.2 Description of Model

For the development of this model, the assumption is made that a SFRC beam fails along an idealised line (1-2-3) representing the main flexural-shear crack and the compression block (3-4), as shown in Figure 4.2.

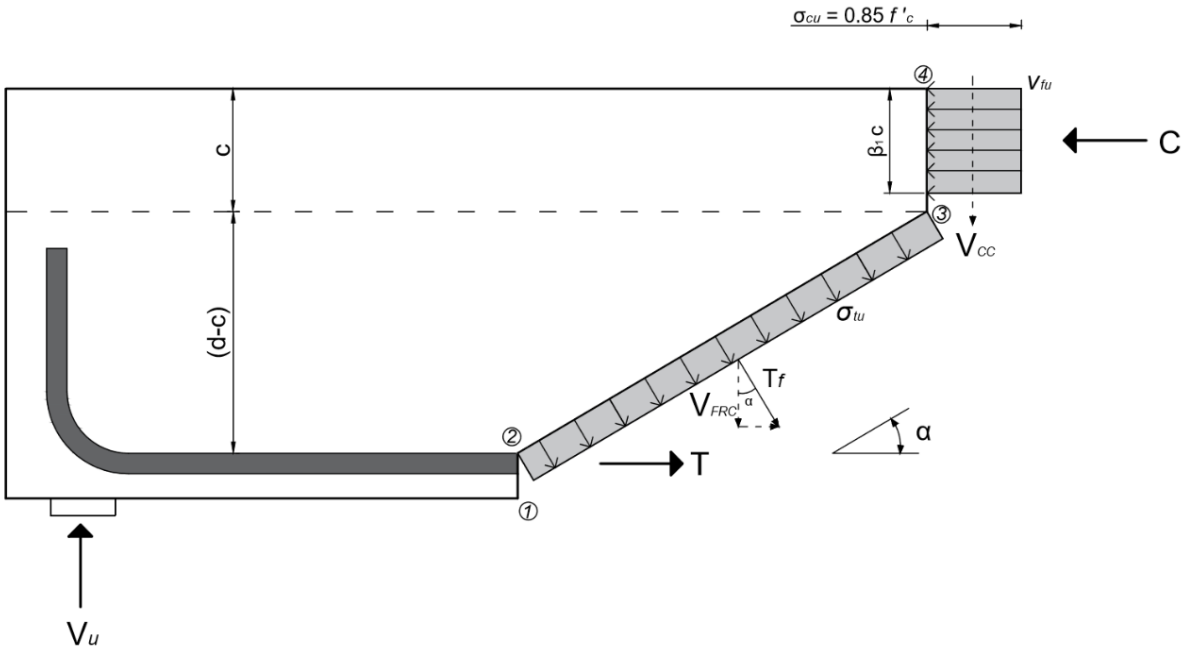

Figure 4.2: Assumed failure mode and simplified internal stresses of FRC beam (reworked from Dinh et al. 2011).

4.5.2.1 Prediction of Shear Resistance of Compression Block

In the proposed model, it is assumed that the crushing of concrete above the neutral axis triggers shear failure. Since significant experimental evidence shows that low volumes of fibres in concrete have a negligible effect on the compressive strength of FRC, it is reasonable to use the stress-based failure criterion of normal concrete to determine the failure envelope of concrete subjected to a combination of compressive and shear stresses. The failure criterion of Bresler & Pister (1958) was used and is presented by Eq 4.2 and Figure 4.3.

$$\frac{v_{cu}}{f'_c} = 0.1\left[0.62 + 7.86\left(\frac{\sigma_{cu}}{f'_c}\right) - 8.46\left(\frac{\sigma_{cu}}{f'_c}\right)^2\right]^{1/2} \qquad \textit{Eq 4.2}$$

where: v_{cu} and σ_{cu} are the shear and normal stresses at failure, respectively.

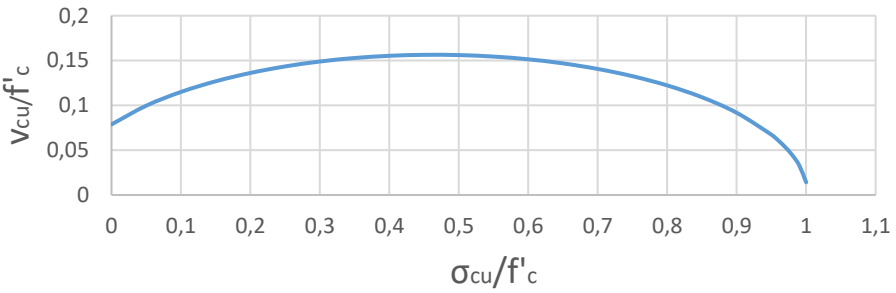

Figure 4.3: Bresler & Pister (1958) failure criterion for normal concrete exposed to compressive and shear stresses, simultaneously.

In the model of Bresler & Pister (1958), a uniform stress distribution over a certain depth of the compression zone is assumed as $k_1 k_3 f'_c$, shown in Figure 4.4 . Therefore, the depth of the compression zone c can be calculated by considering force equilibrium at a given section and assuming the reinforcement has yielded:

$$c = \frac{A_s f_y}{k_1 k_3 f'_c b_f} = \frac{A_s f_y}{0.85\beta_1 f'_c b_f} \qquad \textit{Eq 4.3}$$

where: $k_1 k_3$ can be obtained from:

$$k_1 k_3 = 0.85\beta_1 \quad \begin{cases} \beta_1 = 0.85 \; for \; f'_c \leq 27.6 \; MPa \\ \beta_1 = 0.65 \; for \; f'_c \geq 55.1 \; MPa \end{cases} \qquad Eq\ 4.4$$

Liner interpolation for $27.6 < f'_c < 55.1$ MPa

When $\beta_1 c$ is computed and falls within the web, Eq 4.3 must be rightly adjusted to incorporate the part of the web in compression.

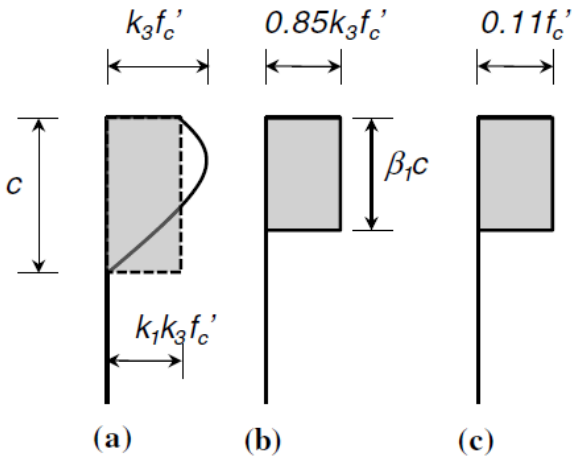

Figure 4.4: Stress distributions of beams compression block: a) Average (dashed line) and actual (curve) normal stress distribution, b) Assumed stress block; c) shear stress distribution (Dinh et al. 2011).

A conservative assumption is made by calculating the resultant shear force from a uniform shear stress distribution acting over the depth of $\beta_1 c$, corresponding to $\sigma_{cu} = 0.85k_1 f'_c$ (with $k_3 = 1$ for horizontally cast beams). This leads to a uniform shear stress of $v_{cu} = 0.11 f'_c$ (refer to Figure 4.4). This assumption is made since the resultant shear force from the uniform normal stress distribution of $k_1 k_3 f'_c$ is higher than the shear force induced by the non-linear stress distribution. The equation used to calculate the shear contribution of the compression block has been adjusted slightly to incorporate the case where the neutral axis falls within the web. Therefore, the shear contribution of the beam compression block is defined as:

$$V_{cc} = 0.11 f'_c A_{cc} \qquad Eq\ 4.5$$

where: A_{cc} is the area of concrete over which the uniform compressive stress acts (cross-sectional area above $\beta_1 c$.). In cases were the neutral axis falls within the web, A_{cc} must include the area of the flange and the area of the web above $\beta_1 c$.

4.5.2.2 Prediction of Shear Resistance contributed by Fibres

The major adjustment made to the model proposed by Singh & Jain (2014) is in calculating the contribution of fibres towards shear resistance, which depends on the tensile force in the fibres bridging the diagonal shear crack. The fibre contribution depends on the cross-sectional area of the beam in the plane of the diagonal shear crack. The actual stress distribution at the critical crack is shown in Figure 4.5 a), by the thick curve in the figure. For simplicity, an idealised equivalent uniform tensile stress (σ_{tu}) distribution acting over an effective area (A_{fc}) referred to as the Fibre contribution area, is assumed, which has a similar resultant force (T_f) as the actual stress distribution (refer to Figure 4.5 b). The term A_{fc} has been incorporated into the model to account for the irregular cross-sections of V-beams. Furthermore, only forces above centroid of longitudinal reinforcement are considered and the shear strength contribution of the fibres V_{FRC} is expressed as:

$$\begin{aligned} V_{FRC} &= T_f \cos(\alpha) \\ &= \sigma_{tu} A_{fc} \\ &= \sigma_{tu}(d - c)\left(\frac{b_c + b_d}{2}\right) cot\ \alpha \end{aligned} \qquad Eq\ 4.6$$

where: α is the inclination of the main diagonal shear crack. b_c and b_d represent the top and bottom width of the fibre contribution area, respectively (Figure 4.5 b).

If the neutral axis lies within the web b_c is the width of the web at the neutral axis. If the neutral axis lies in the flange, the width b_c is taken as the width of the web assuming the web continues into the flange up to the neutral axis. Refer to Figure 4.5 b) for clarity.

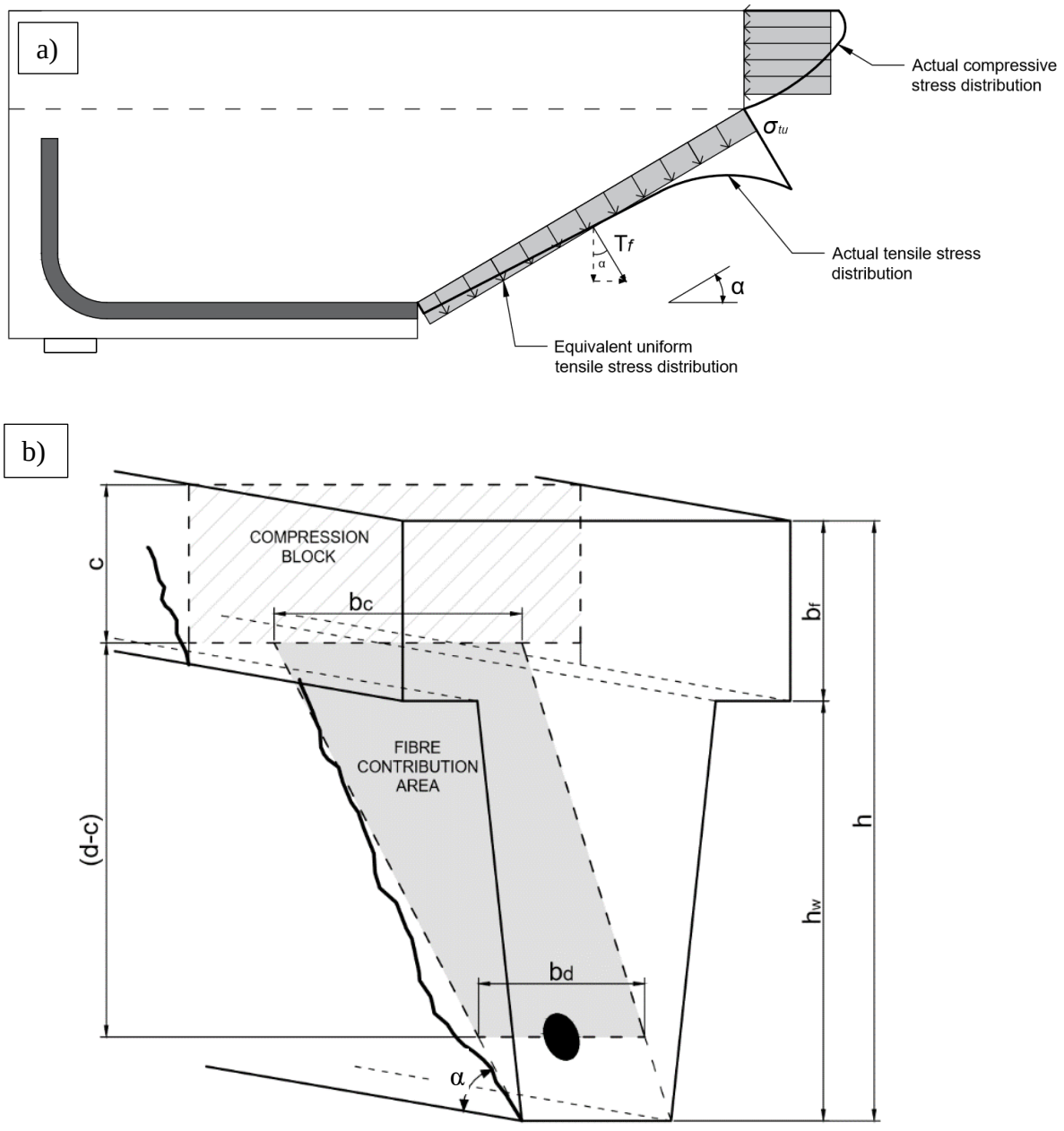

Figure 4.5: a) Actual and assumed stress distributions (rework from Dinh et al., 2011); b) Image of the 3-D view of an irregular shaped beam indicating the Compression block and Fibre contribution area

The equivalent uniform tensile stress σ_{tu} in fibres that are bridging a unit area on the surface of the critical shear crack is calculated as:

$$\sigma_{tu} = N \cdot f \qquad \textit{Eq 4.7}$$

where: N is the amount of fibres crossing a unit area on the surface of the critical crack and f is the average pull-out force per fibre. The amount of fibres crossing a unit area is estimated as:

$$N = 0.5\frac{V_f}{\pi\, r_f^2} \qquad \textit{Eq 4.8}$$

where: V_f represents fibre volume in the SFRC and r_f is the fibre radius. f represents the average pull-out force per fibre and is estimated by:

$$f = \tau\, \pi\, D_f d_f \frac{l_f}{4} \qquad \textit{Eq 4.9}$$

where: l_f and d_f are the length and diameter of a fibre, respectively. D_f is the fibre efficiency factor ($D_f = 1$ for hooked-end fibres and $D_f = 0.75$ for crimped fibres). The average fibre-matrix interfacial bond strength τ is calculated as follows and can be applied to normal and high strength concrete (Singh and Jain, 2014):

$$\tau = C\sqrt{f'_c} \quad \begin{cases} C = 0.85\ for\ hooked\ end\ fibres \\ C = 0.75\ for\ crimped\ fibres \end{cases} \qquad \textit{Eq 4.10}$$

Using Eq 4.6 through 4.10, the fibre contribution to shear resistance can be rewritten as:

$$V_{FRC} = 0.5\,\tau\, D_f V_f \frac{l_f}{d_f}\,(d-c)\left(\frac{b_c + b_d}{2}\right)\cot(\alpha) \qquad \textit{Eq 4.11}$$

Combining Eq 4.1, Eq 4.5 and Eq 4.11, the shear strength for an irregular shaped SFRC beam is calculated as:

$$V_u = 0.11 f'_c A_{cc} + 0.5\,\tau\, D_f V_f \frac{l_f}{d_f}\,(d-c)\left(\frac{b_c + b_d}{2}\right)\cot(\alpha) \qquad \textit{Eq 4.12}$$

4.3 Concluding summary

This chapter covered the modification of existing shear models for the application of ISB by incorporating a larger effective area that contributes to the shear resistance of the beam. Furthermore, the analytical shear prediction model was proposed which is based on the model of Singh & Jain (2014) which has been slightly adjusted to accommodate ISB reinforced with steel fibres. The major adjustment was made to the equation used to calculate the cross-sectional area over which fibres act and contribute to the shear resistance of the beam. Eq 3.56 was modified to accommodate the V-shaped webs of the ISB tested in this investigation, which lead to Eq 4.6. Due to the irregular V-shaped webs, fibres act over a larger cross-sectional area which results in larger shear contribution by the fibres leading to higher shear capacity.

The experimental framework follows in Chapter 5, giving detailed explanations of all the tests performed in this investigation.

CHAPTER 5

EXPERIMENTAL FRAMEWORK

This chapter covers the development procedure of SFR-SCC with properties in the fresh and hardened state that are considered to be adequate for the experimental work in this investigation. Preliminary tests performed on the developed concrete mix are discussed and the results are presented. Furthermore, the primary tests of this investigation are discussed. This includes the inspiration of the shape and design of beams tested, naming convention of the beams, pre-experimental procedures and test details.

5.1 Development of SFR-SCC

Complex moulds are used to cast the ISB tested in this investigation. Since normal concrete requires external vibration during the casting stage, which will be a major challenge due to the complexity of the shape of the moulds, a SCC is developed. SCC is used to simplify the production of beams by eliminating the need of external vibration for proper compaction and by reducing the risk of honeycombing. However, the SCC must have adequate workability and passing ability to flow under its own weight and pass through narrow gaps between reinforcing steel in thin webs.

This section presents the method followed to obtain a SFR-SCC mix that is adequate for experiments in this investigation. Furthermore, the final mix design and more details on the constituent materials are given.

5.1.1 Design Method and Mix design

The design method of Zeranka (2017) was used in this investigation to obtain SFR-SCC suitable for the experiments conducted in this investigation. This method was adapted from a method developed by Okamura and Ouchi (1999) and is similar to the design sequence prescribed by EFNARC (2002). The approach consists of developing and optimising the mix in various stages before proceeding to the next. The stages are paste, mortar, SCC and then SFR-SCC. A new mix has to be made when proceeding to the next stage.

The paste is developed by adding all the powders and mixing it with water and superplasticizer. Powders include cement and cement extenders such as fly ash, slag or condensed silica fumes. Mortar is obtained by adding fine aggregate or sand to the constituents of the paste stage. Thereafter, large aggregates are added to the constituents to obtain the SCC stage. Finally, fibres are added to obtain the SFR-SCC. The various components of FR-SCC are shown in Figure 5.1.

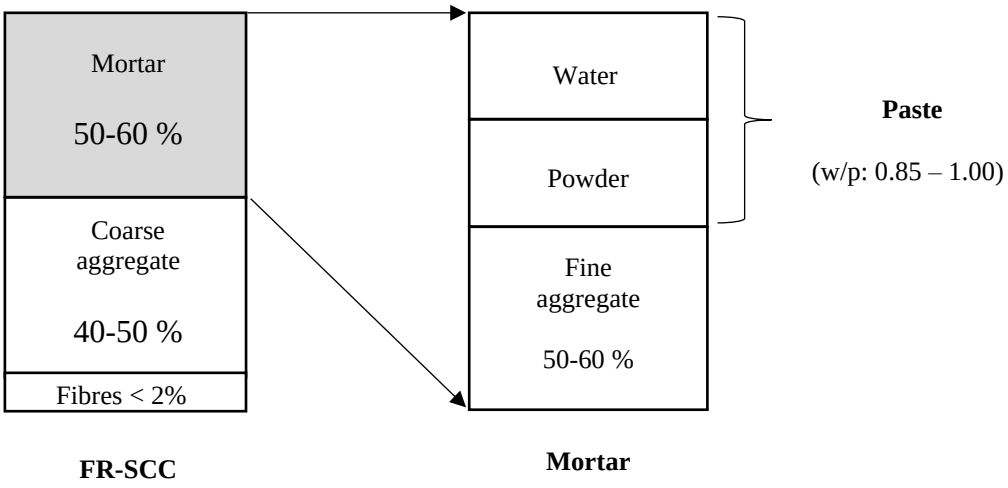

Figure 5.1: Components of FR-SCC (adapted from Okamura & Ouchi, 1999).

For the development of the SFR-SCC mix used in this investigation, the paste stage was skipped. Instead of starting from scratch, guidelines from Zeranka (2017) were used to get an indication of the quantities required of various constituent materials to develop a mortar. To determine the required amount of superplasticizer, small amounts were added at a time until the desired slump flow was obtained. This procedure involves trial and error mixes until a desired mix design is obtained.

Concrete mixes with various amounts of fibres were used in this investigation. The mixes were slightly altered to accommodate the various fibre contents and to produce favourable fresh concrete properties. Higher fibre contents demanded larger amounts of superplasticizer to retain sufficient slump flow. Fibre contents investigated in this study are 0.6% and 1% by volume.

The powder composition (percentage by weight of binder) consisted of 60% cement and 40% fly ash. The volume percentage of sand and coarse aggregates was 55% and 26%, respectively. The final SFR-SCC mix designs for the various beam sets tested in this investigation are shown in Table 5.1.

Table 5.1: SFR-SCC mix designs.

Constituent Material	**Type**	**Control mix**	**Mix 1**	**Mix 2**
		no fibres	**0.6 % fibres**	**1 % fibres**
			Content (kg)	
Cement	*Surebuild CEM II 42.5 (N)*	238.1	236.7	235.8
Fly Ash	*DuraPozz*	158.8	157.8	157.2
Water		185	183.9	183.2
Sand	*Coarse Malmesbury*	1074.5	1068	1063.7
Aggregate	*Greywacke 9mm*	709.9	705.5	702.7
Superplasticizer	*Chryso Optima 310*	3.143	3.171	3.395
Fibres	*Bekeart Dramix RL 45/50*	0	47.1	78.5

5.1.2 Constituent materials

The following constituent materials were used in the SFR-SCC mixes:

5.1.2.1 Cement

SUREBUILD CEM II/A-L 42.5 (N) with a relative density of 3.08 as supplied by PPC (Pretoria Portland Cement Co. Ltd).

5.1.2.2 Fly Ash

DuraPozz fly ash as supplied by Ash Resources (Pty) Ltd with a relative density of 2.2. Fly ash is used as a cement extender to improve the properties of concrete and comply with the specifications of SANS 50450-1:2014.

5.1.2.3 Aggregate

The sand used is locally known as Coarse Malmesbury sand which is formed by the natural degradation of rock.

The coarse aggregate used had a nominal diameter of 9 mm and is locally known as Greywacke stone, which is produced by the crushing of Malmesbury shale. Relative densities of 2.64 and 2.73 were used for the sand and stone, respectively.

5.1.2.4 Superplasticizer

MAPEI Dynamon SP1 was used, it consists of a water-based solution containing acrylic polymers which sufficiently disperse the cement grains, therefore increasing the workability of the concrete, making it easy to apply when fresh. The relative density of superplasticizer was taken as 1.08.

5.1.2.5 Fibres

DRAMIX 3D 45/50BL fibres, supplied by Bekaert, were used. These fibres are hooked end fibres with a single hook (refer to Figure 5.2). These fibres are described in the general catalogue as cost-effective fibres, sound to be used in structural concrete submitted to regular load-bearing and dynamic loading. The physical properties of these fibres can be seen in Table 5.2.

Table 5.2: Physical properties of Bekaert DRAMIX 3D 45/50BL fibres.

Name	Length (mm)	Diameter (mm)	Aspect ratio	Tensile strength (MPa)	Modulus of elasticity (GPa)
Dramix 3D 45/50BL	50	1.05	48	1115	200

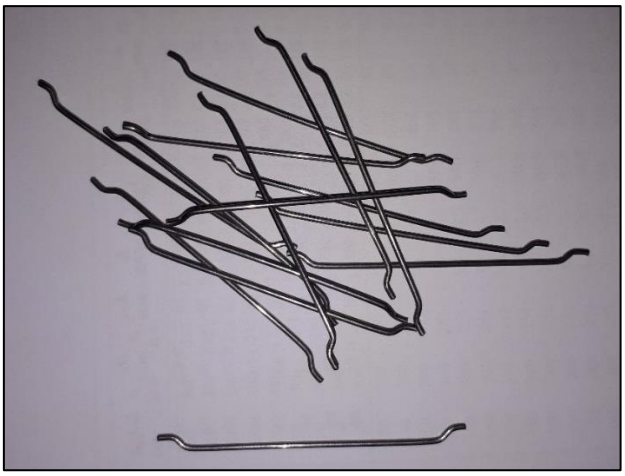

Figure 5.2: Bekaert DRAMIX 3D 45/50BL fibres.

5.2 Preliminary tests

To ensure that the concrete used has adequate properties for the experiments in this study, preliminary tests were performed on the SFR-SCC mix to determine the concrete properties, in its fresh and hardened state. Preliminary tests performed in this investigation are described in this section, which include slump flow, J-ring, compressive strength and crack mouth opening displacement (CMOD) tests.

5.2.1 Preliminary tests on fresh concrete

Tests were performed on the fresh concrete to obtain certain rheological properties of the SFR-SCC in order to determine whether the mix is suitable to be used in the ISB moulds. Furthermore, steel fibres were added to the SCC to replace the shear reinforcement in the beams, since the bending and placing of stirrups would be a cumbersome process due to the complex shape of the moulds. The following tests were performed on fresh concrete, to get an indication of the workability and passing ability of the SFR-SCC:

- Slump-flow and T_{500} slump-flow test.
- J-Ring test.

5.2.1.1 Slump flow test and T_{500} slump-flow test

These two tests can be performed simultaneously, and the same apparatus is required. These tests give an indication of the workability of the concrete mix and can also be used to inspect the concrete for signs of segregation. These tests were performed in accordance with SANS 5862-1 (SANS, 2006b), with apparatus adhering to the standards. The required apparatus includes a slump cone, a smooth steel plate with the centre and a circle of 500 mm over the centre marked on the plate, a measuring tape and a stopwatch. Figure 5.3 represents a slump flow test, and the apparatus is labelled.

The test is performed on a level surface. The cone is placed in the centre of the steel plate with the small opening facing to the top. The cone is then filled with one continuous layer to the top rim and the top surface of the concrete is levelled. The cone should be firmly pressed against the plate to prevent concrete leaking out at the bottom. From the start to the end of filling the cone should be within 2 minutes. The cone is immediately raised by a steady vertical motion without any interruption.

To obtain the T_{500} result, a stopwatch is used to measure the time from the beginning of the uplift of the cone until the apparently maximum diameter of the concrete flow reaches 500 mm. To obtain the slump flow, the apparently maximum diameter and the diameter perpendicular to it is measured once it has stopped flowing and the average flow diameter is used as the slump flow result. The slump flow is measured to the nearest 5 mm and T_{500} to the nearest 0.1 seconds.

Figure 5.3: Slump flow test.

5.2.1.2 J-ring test

This test is performed according to ASTM C1621 (2017) to determine the passing ability of SCC. The apparatus used for this test adheres to the standards and includes a slump cone, smooth steel plate and a J-Ring. The J-Ring consists of a steel ring 300 mm in diameter at the centre of the ring with 16 evenly spaced, smooth rods with diameter of 16 mm. The J-Ring can be seen in Figure 5.5.

The J-Ring is placed on the smooth steel plate, and the slump cone is placed concentric with the J-Ring with the larger opening facing to the top. The inverted slump cone is filled with freshly mixed concrete without any tamping or vibration. The top of the concrete in the cone is scraped off using a tamping rod with a sawing motion and spilt concrete is wiped off the steel plate. To start the test, the slump cone is lifted with a steady vertical movement without any lateral or torsional motion.

Once the concrete has stopped flowing, measure the apparently maximum diameter and the perpendicular diameter of the circular flow and calculate the average to obtain the J-Ring Spread. The distance from the top of the J-Ring to the concrete at four points located on the outside rim of the J-Ring and at the centre of the J-Ring is measured. The centre reading is subtracted from the average of the four outside readings to obtain the J-Ring Blocking reading in millimetres. Table 5.3 summarises all the results obtained from the preliminary tests performed on the fresh SFR-SCC.

Table 5.3: Results of tests performed on SFR-SCC in its fresh state.

Test		**Result**			**Unit**
		Mix 1	**Mix 2**	**Control mix**	
		0.6% fibres	**1% fibres**	**no fibres**	
Slump-flow		620	655	625	mm
T_{500} slump-flow		4.1	4.3	4.4	sec
J-Ring	***Spread***	570	530	590	mm
	Blocking	24	29	18	mm

Figures 5.4 and 5.5 represents the slump flow tests and the J-ring tests performed on the three different SCC mixes, respectively. After the slump flow test was performed, the mix was visually inspected for segregation and fibre clumping. No signs of segregation or fibre clumping were visible in either of the three concrete mixes.

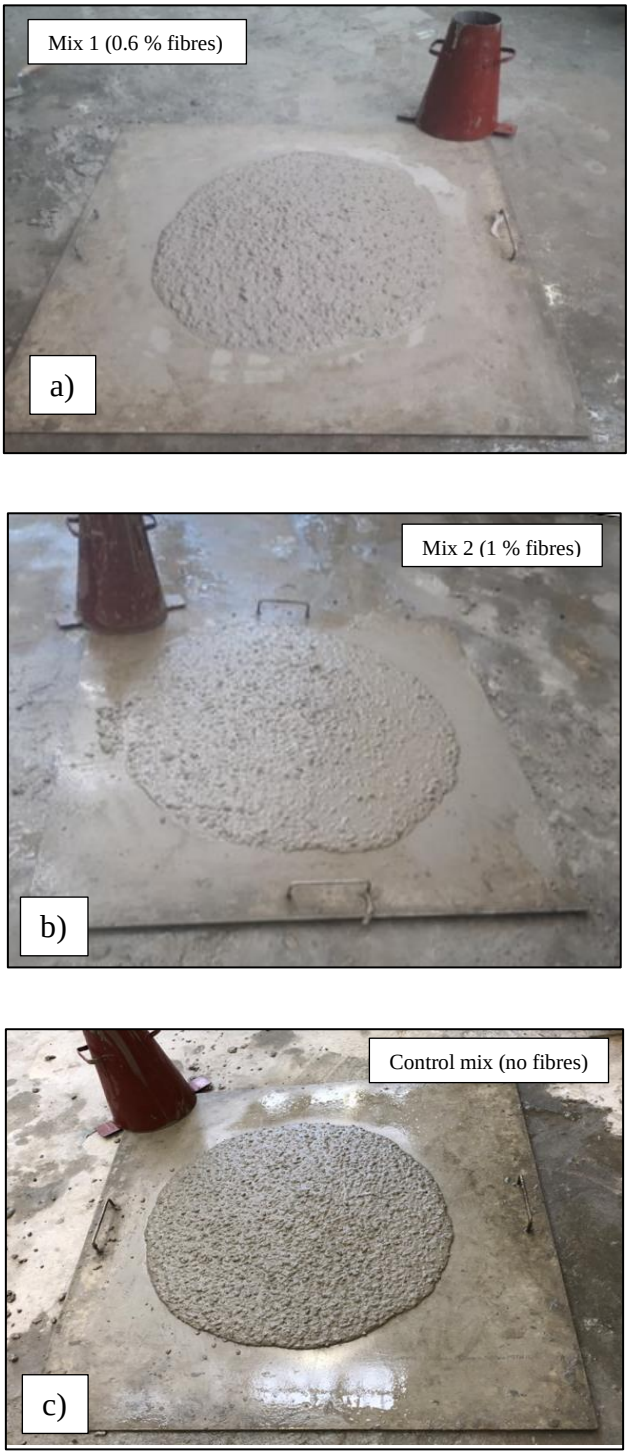

Figure 5.4: Slump flow test results of a) Mix 1, b) Mix 2 and c) Control mix.

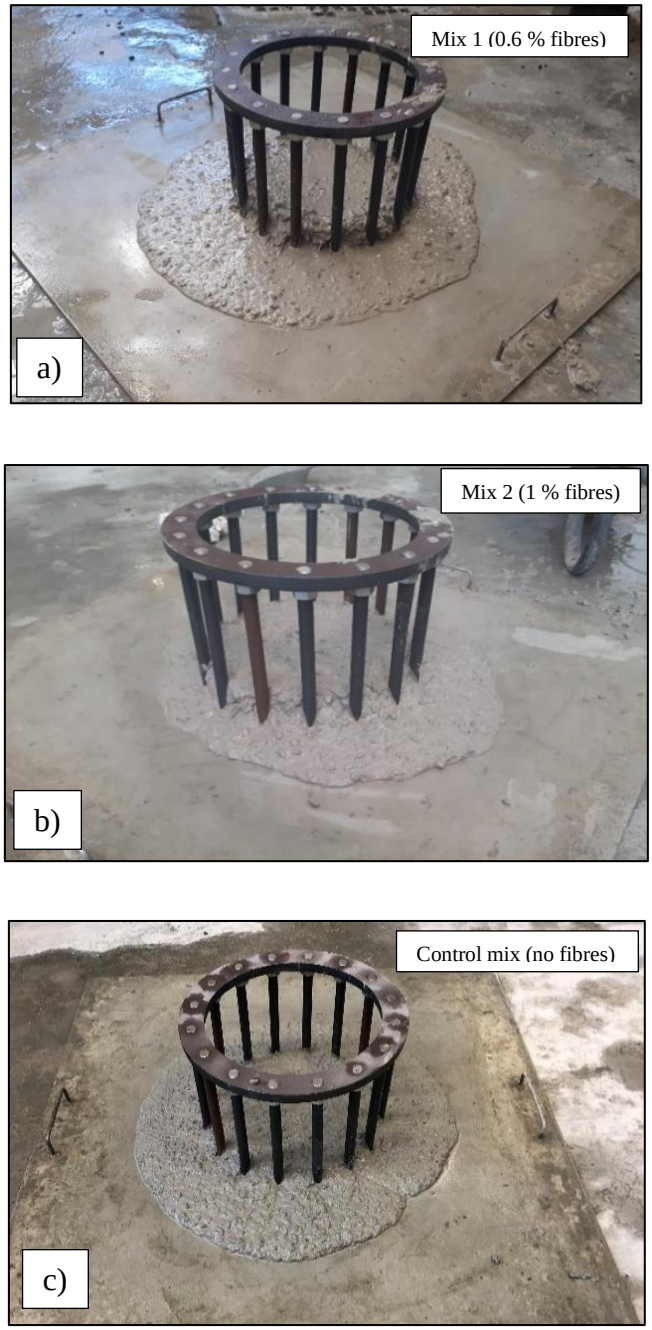

Figure 5.5: J-ring test results of a) Mix 1, b) Mix 2 and c) Control mix.

The slump flow of the control mix, Mix 1 and Mix 2 are 625 mm, 620 mm and 655 mm, respectively, indicating that all the mixes conform to the slump flow criteria of SCC according to EFNARC (2005). From the comparison of the slump flow to the J-Ring spread, and from the J-Ring blocking results it can be seen that the blocking in Mix 1 (0.6% fibres) is slightly more than in the control mix. Conversely, the blocking in Mix 2 is significantly more than

blocking in the control mix. The difference between the slump flow and J-Ring Spread for the control mix, Mix 1 and Mix 2 of is 35 mm, 50 mm and 125 mm, respectively. J-Ring blocking for the control mix, Mix 1 and Mix 2 is 18 mm, 24 mm and 29 mm, respectively. The blocking in Mix 2, containing 1% fibres, is significant compared to the control mix containing no fibres. This indicates that in cases where reinforcing is tightly packed, Mix 2 with 1% fibre content, could result in problems during the pouring stage of the concrete. The higher fibre content could result in unwanted blockages as the concrete flows through reinforcement, which may lead to adverse effects such as fibre clumping or honeycombing.

5.2.2 Preliminary tests on hardened concrete

Tests were performed on hardened concrete at various ages. These tests were performed according to the relevant standards. The two tests performed on the hardened SFR-SCC are described and results are presented in the following section.

5.2.2.1 Compressive strength tests

Compressive strength tests on the various concrete mixes were performed according to SANS 5863 (SANS, 2006a) using a Contest Hydraulic Actuator machine. Cubes were cured in water baths at 23 $\pm$ 2° c. Concrete cubes were cast with dimensions of 100 x 100 x 100 mm and were tested at ages of 14 and 28 days. For each beam that was cast for the primary tests, cubes were cast from the same mix so that the exact concrete compressive strength is obtained and could be used for the application of the shear models. The test itself involved taking the cubes from the water bath, drying off the surfaces of the cubes using paper towels and measuring the exact dimensions of each cube. Subsequently, the cubes were placed into the Contest Hydraulic Actuator machine such that the load is applied perpendicular to the casting direction. A steel plate with a perfectly square face was used to transfer the load from the machine to the concrete cube. Figure 5.6 represents a concrete compression test in the Contest Hydraulic Actuator machine.

Figure 5.6: Compressive strength test of concrete cube.

The loading is applied at a rate of 180 kN/min. At failure, the machine records the load. The compressive strength of the cube is then calculated by:

$$\sigma = \frac{P}{A} \qquad \textit{Eq 5.1}$$

where: σ represents the compressive strength of the concrete cube (MPa), P is the failure load recorded by the Contest Hydraulic Actuator machine (N) and A is the area of the face of the cube onto which the load was applied (mm^2).

The compressive strength test results are summarised in Table 5.4. In cases where a shear model required the cylinder compressive strength as input parameter, 80% of the cube strength was used. The coefficient of variation in compressive strength is shown in brackets to give an indication of variability.

Table 5.4: Compressive strengths of various concrete mixes.

Age (days)	Mix 1	Mix 2	Control mix
	Cube compressive strength [MPa]		
14	34.9 *(5.6%)*	36.4 *(2.2%)*	34.0 *(4.9%)*
28	44.7 *(6.8%)*	46.8 *(4.3%)*	41.3 *(5.2%)*
	Cylinder compressive strength [MPa]		
14	27.9 *(5.6%)*	29.1 *(2.2%)*	27.2 *(4.9%)*
28	35.8 *(6.8%)*	37.4 *(4.3%)*	33.0 *(5.2%)*

5.2.2.2 Crack Mouth Opening Displacement (CMOD) tests

Tests were performed according to EN 14651-A1 (2007) using an Instron 2000KPX testing machine. CMOD tests are a method of measuring the flexural tensile strength of SFRC specimens. A set of residual flexural tensile strength values is determined from the flexural stress-CMOD curve that is obtained from the tests. Figure 5.7 represents the tests set-up of a typical CMOD test that was used in this investigation.

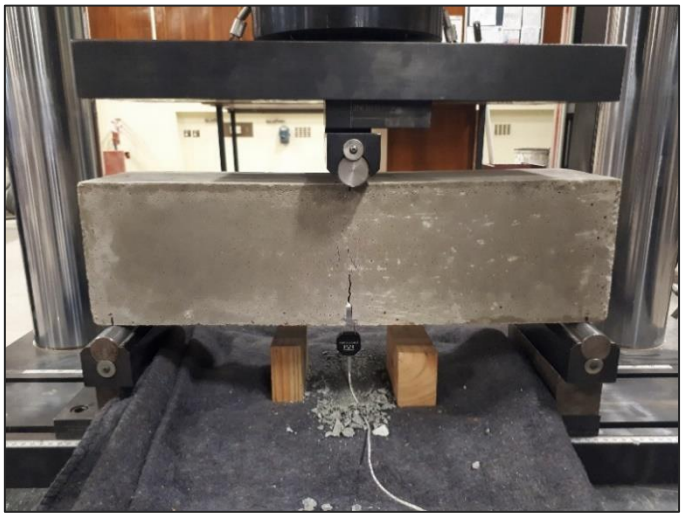

Figure 5.7: CMOD test set-up.

Specimens with dimensions of 150 x 150 x 600 mm were cast. The procedure of filling the mould is important due to the fibres in the concrete mix. The mould is filled in three increments (refer to Figure 5.8), increment 1 in the centre of the mould, and increments 2 and 3 at the ends

of the moulds. The increments should be sized such that increment 1 contains twice as much concrete as increment 2 and 3.

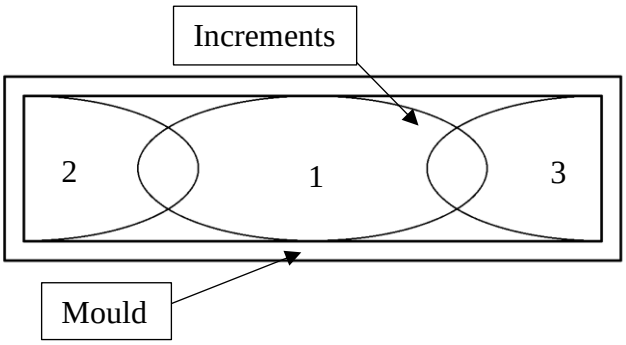

Figure 5.8: CMOD mould filled in increments (reworked from BS EN 14651-A1 (2007)).

Specimens were cured in water baths at 23 ± 2° c up to an age of 14 days when they were tested. Tests are normally performed at the age of 28 days, but since primary tests were performed on beams aged 14 days, flexural tensile strength values were required for the concrete at the age of 14 days. Prior to testing, the specimens are notched using wet sawing at mid-span of the specimen. Specimens are rotated 90° around its longitudinal axis so that the notch is situated on the face adjacent to the casting surface. The notch had a width of 5 mm and was approximately 25 mm deep such that the distance from the tip of the notch to the top surface of the specimen (h_{sp}) is 125 ± 1 mm (refer to Figure 5.9).

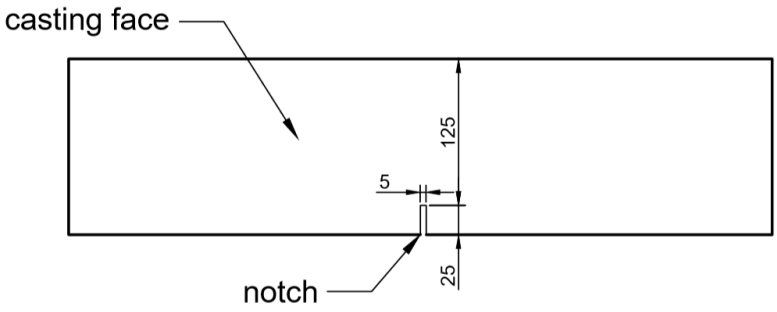

Figure 5.9: Notching details of CMOD specimen.

After a notch is cut into the specimen, small sharp metal pieces known as knife-edges are fixed to the specimen on either side of the notch. The knife-edge pieces were used to mount the clip gauge transducer to the specimen. The clip gauge is used to measure the crack mouth opening

displacement throughout the test. The knife-edge pieces were mounted onto the test specimen, using Pratley Steel Quikset adhesive, such that the distance between the knife-edges are 8 mm apart, in order for the clip gauge transducer to fit in-between the knife-edges. Figure 5.10 shows the typical arrangement for CMOD measurements. The knife-edge pieces must have a thickness of less than 5 mm (refer to Figure 5.10).

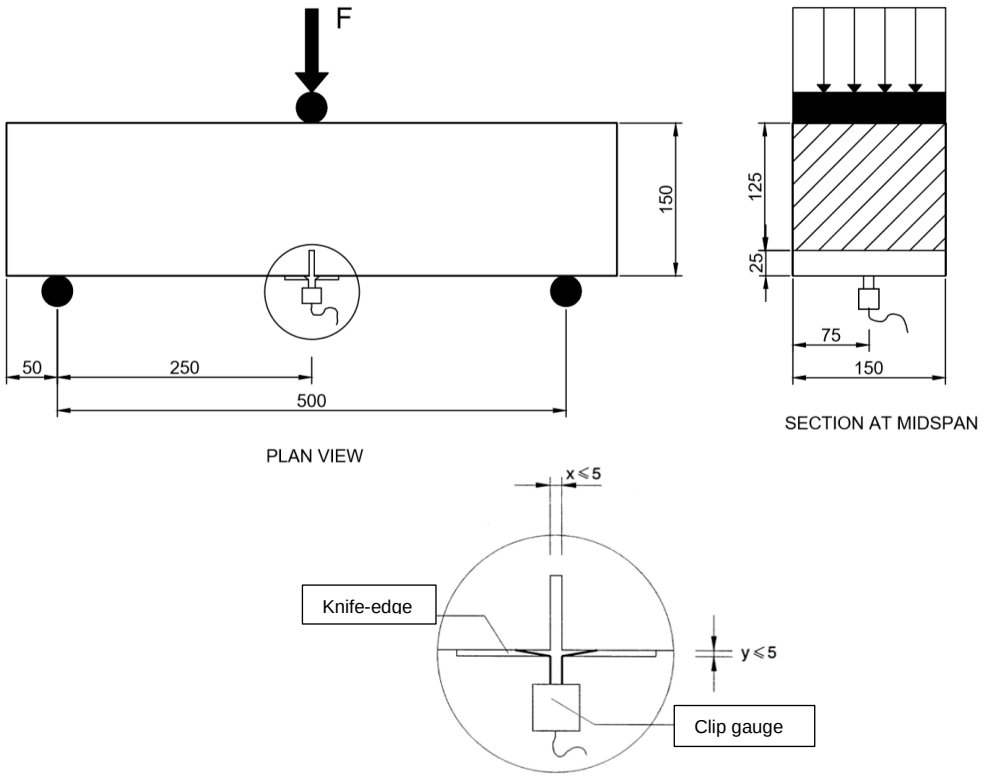

Figure 5.10: Arrangements for the CMOD test measurements (reworked from BS EN 14651-A1 (2007)).

The test itself involved placing the test specimen onto two roller supports, 500 mm apart (refer to Figure 5.10). The force gets transferred to the specimen through a roller at mid-span (vertically above the notch). The machine inducing the force onto the specimen is operated such that the CMOD is controlled at a constant rate of 0.05 mm/min. When the CMOD reaches 0.1 mm, the rate at which CMOD increases is changed to 0.2 mm/min.

From the tests results, the residual flexural tensile strength $f_{R,j}$ values are calculated as:

$$f_{R,j} = \frac{3\,F_j\,l}{2\,b\,h_{sp}^2} \qquad Eq\ 5.2$$

where: $f_{R,j}$ is the residual flexural tensile strength in MPa calculated at $CMOD_j$ ($j = 1, 2, 3, 4$) equal to 0.5, 1.5, 2.5 and 3.5 mm. F_j is the load at to $CMOD_j$ *and* l represents the span length [mm]. b and h_{sp} are the width of the specimen and the distance from the tip of the notch to the top of the specimen, respectively. The residual flexural tensile strength values of the various SFR-SCC mixes are shown in Table 5.5, and the load-CMOD results obtained from the tests are presented in Figure 5.11 and 5.12 for Mix 1 and Mix 2, respectively. The coefficients of variation are shown in brackets to give an indication of variability in the residual flexural tensile strength values.

Table 5.5: Residual flexural tensile strength values.

Residual flexural tensile strength (MPa)					**MC 2010 Classification**
	fR_1	**fR_2**	**fR_3**	**fR_4**	
Mix 1	4.30 *(17.6%)*	4.54 *(17.3%)*	4.45 *(16.8%)*	4.20 *(16.9%)*	4 c
Mix 2	6.10 *(26.7%)*	5.81 *(18.5%)*	5.26 *(15.6%)*	4.73 *(16.9%)*	6 b

The two SFR-SCC mixes were classified according to the classification method in *fib* Model Code 2010 (FIB, 2010a). In particular, two parameters are specified, the number representing the strength interval (f_{R1k}) and the letter representing the f_{R3k}/f_{R1k} ratio. Mix 1 and Mix 2 are classified as 4 c and 6 b mixes, respectively.

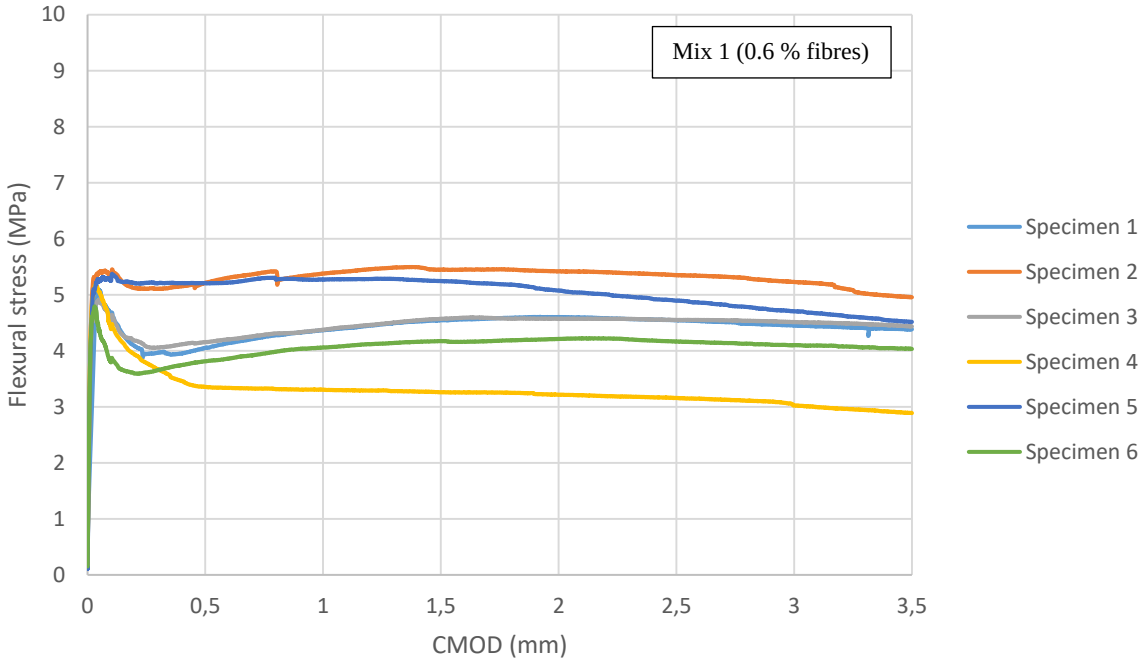

Figure 5.11: CMOD test results of SFR-SCC Mix 1.

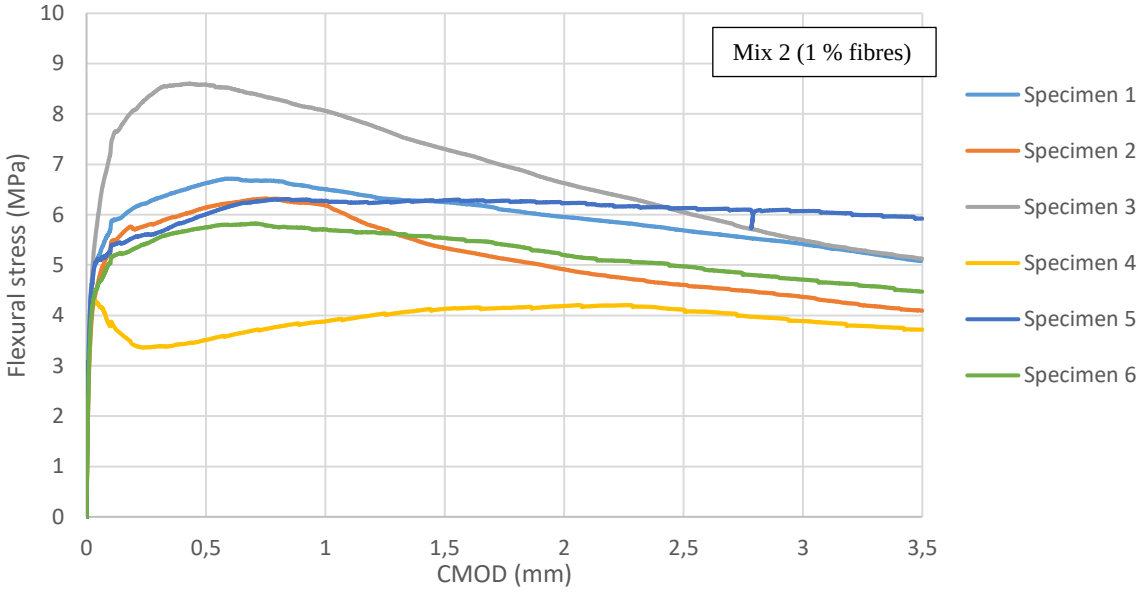

Figure 5.12: CMOD tests results of SFR-SCC Mix 2.

5.2.3 Yield strength of reinforcement steel

In order to obtain the actual yield stress of the reinforcement for the application of the shear models, tensile tests were performed on reinforcement sample pieces. A Zwick Universal Testing Machine was used to perform the tests which complied with the specifications of SANS 6892-1 (2010). Since only the yield stress was desired in this investigation, tests were manually stopped after the yield stress was reached for every individual steel sample. Table 5.6 presents the average yield stress of the reinforcement steel batches used for the control set, Set 1 and Set 2. The coefficients of variation are shown in brackets to give an indication of variability.

Table 5.6: Yield stresses of reinforcement steel used for the various beam sets.

Set	Yield stress [MPa]
Control set	500.0 *(0.7%)*
Set 1	516.2 *(6.7%)*
Set 2	501.2 *(1.5%)*

The results of the individual tensile tests are given in Appendix D.

5.3 Primary tests

The primary tests of this investigation consisted of asymmetrical three-point bending tests that were performed to investigate the shear behaviour of ISB reinforced only with longitudinal reinforcement and steel fibres. In this section, the inspiration of the beam designs, beam nomenclature, pre-experimental procedures and test details are described.

5.3.1 Inspiration of irregular shaped beams

The geometric design of the beams tested in this investigation was inspired by the shape obtained from geometrically optimised, simply supported fabric-formed beams. The geometry of such a beam would typically be designed to resist a uniform distributed loading such that the beam contains minimal amounts of material but has sufficient strength to resist imposed loads. By ensuring that the moment and shear capacity, at every section along the length of the beam, is only slightly higher than the internal moments and shear forces at the specific section,

a beam can be optimised. This is achieved by ensuring an internal lever-arm between the centroid of the compression block and the longitudinal reinforcement that is large enough to resist the induced moment at any given section. Since the internal moments vary along the length of the beams, the internal lever-arm varies proportionally. At the same time, it must be ensured that the beam has enough shear capacity at every section to resist the induced shear stresses along the length of the beam, which increases towards the ends of the beam in cases of a simply supported beam. The geometric possibilities using FF are endless, but typically such an optimised beam has two varying parameters along its length. These varying parameters are the height of the beams to ensure sufficient moment capacity and the width of the web to ensure sufficient shear capacity towards the ends of the beam.

Figure 5.13 represents the side view and various sections of a typical simply supported FFB that has been geometrically optimised to resist a UDL. This beam was used as the basis of the design of the beams tested in this investigation.

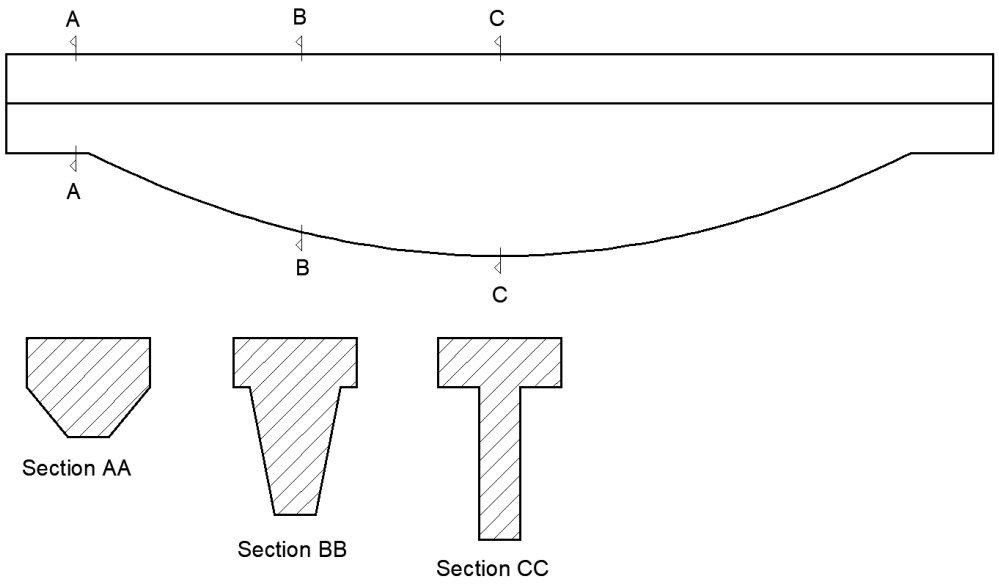

Figure 5.13: Typical sections of an optimised FFB.

5.3.2 Beam details

The beams tested in this investigation were uniform beams with varying web thickness over the depth of the beam. Beams with four various web shapes were tested to investigate what effect the shape of the web has on the shear capacity of a beam. Figure 5.14 represents the sections of the four various beams, labelled Beam A to D, tested in this investigation. The

flange dimensions, reinforcement area and bottom width of the web were kept constant with the only varying dimension being the top web width. Three sets of the same type of beams were tested with various fibre contents of 0% in the control set, 0.6% in Set 1 and 1% in Set 2. Every beam set contained 4 beams, each beam was tested twice provided it failed in the preferred shear failure mode. This provided 24 test results.

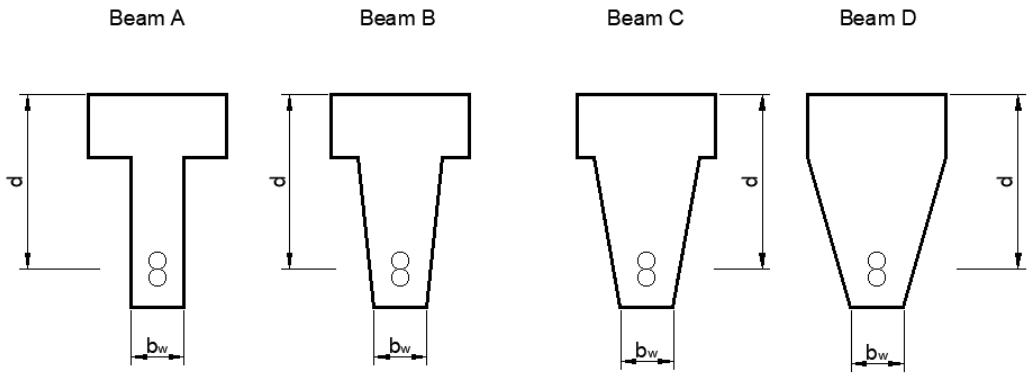

Figure 5.14: Cross-sections of beams tested in this investigation.

4.3.2.1 Beam design procedure

In order to investigate the shear behaviour of beams tested with the asymmetrical three-point bending tests, the beams had to be carefully designed to ensure that the beam fails in shear and not in bending. The following procedure was used to design a beam with cross-section type D to obtain the required longitudinal reinforcement to ensure shear failure and not bending failure. The same area of steel was provided to all other beams.

1. The shear models, described in Chapter 3, were modified and used to obtain a prediction of the shear capacity V_u of Beam D.
2. Using the test set-up, an expression was determined to calculate the load that would theoretically cause the beam to fail in shear. The expression is as follows:

$$F_u = \frac{V_u\, L}{L - a_v} \qquad Eq\ 5.3$$

where: F is the load that will theoretically result in shear failure. V_u is the ultimate shear capacity of Beam D. L and a_v are the span length and shear span length, respectively.

3. F was used to calculate the induced bending moments in the beam using:

$$M_i = \frac{F_u\, a_v (L - a_v)}{L} \qquad Eq\ 5.4$$

where: M_i is the maximum internal bending moment induced by force F_u.

4. The area of longitudinal reinforcement was determined by calculating the area of steel A_S required to resist 1.5 times the induced bending moment to ensure shear failure. The required steel was determined by:

$$A_s = \frac{1.5\, M_i}{f_y\, z} \qquad Eq\ 5.5$$

where: f_y is the yield stress of longitudinal steel and z is the internal lever arm taken as 0.9c and c is the distance from the top of the beam to the neutral axis.

5.3.2.2 Beam dimensions

Dimensions of the flange and the effective depth of the beams were determined such that the neutral axis lies approximately at the bottom of the flange. In this way the whole flange is in compression. This involved an iterative process until the desired flange dimensions were obtained. Table 5.7 gives the material properties used for the beam design and final beam dimensions.

Table 5.7: Summary of material properties and beam dimensions.

f_y (MPa)	f_{cu} (MPa)	A_s (mm^2)	h (mm)	b_f (mm)	h_f (mm)	d (mm)	$b_{w,bot}$ (mm)	$b_{w,top}$ (mm)			
								A	B	C	D
500	35	402	200	130	60	164	50	50	80	100	130

Reinforcing bars were placed on top of each other to provide sufficient cover for the reinforcement in the web. Minimum required anchorage was calculated according to SANS 10100-1 as 274 mm and sufficient anchorage of 327 mm was provided through a 90° hook in the reinforcement bars. A graphical representation of the beam dimensions is shown in Figure 5.15.

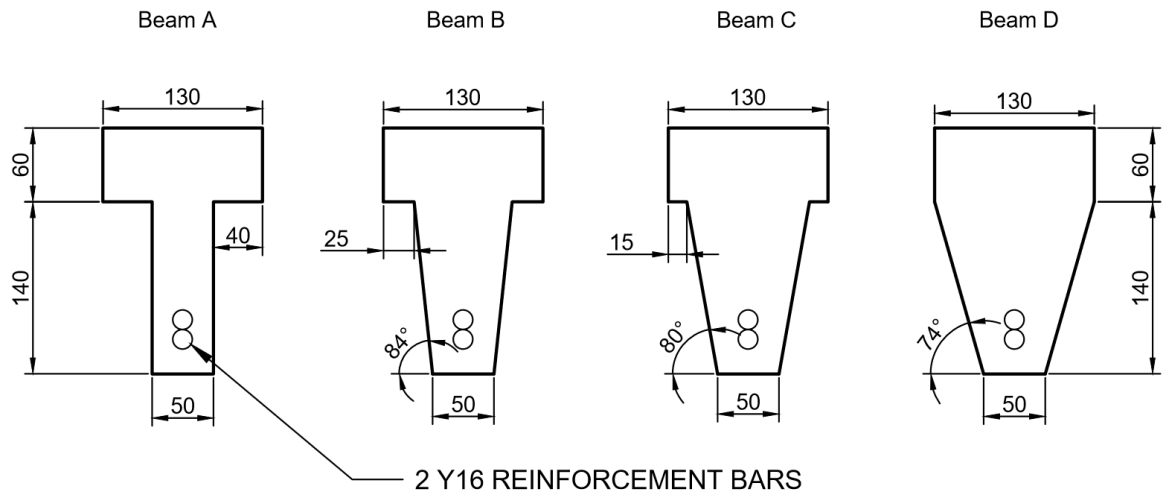

Figure 5.15: Dimensions of beams tested in this investigation.

5.3.3 Naming convention of beams

In order to easily identify a beam, nomenclature was developed which makes it possible to deduce the set number in which the beam was tested, type of the beam, the number of that specific type of beam that was tested and the percentage of fibres the specific beam contained.

Figure 5.16 clarifies the terminology that was developed and used throughout this investigation to identify the beams by giving an example of an applicable beam:

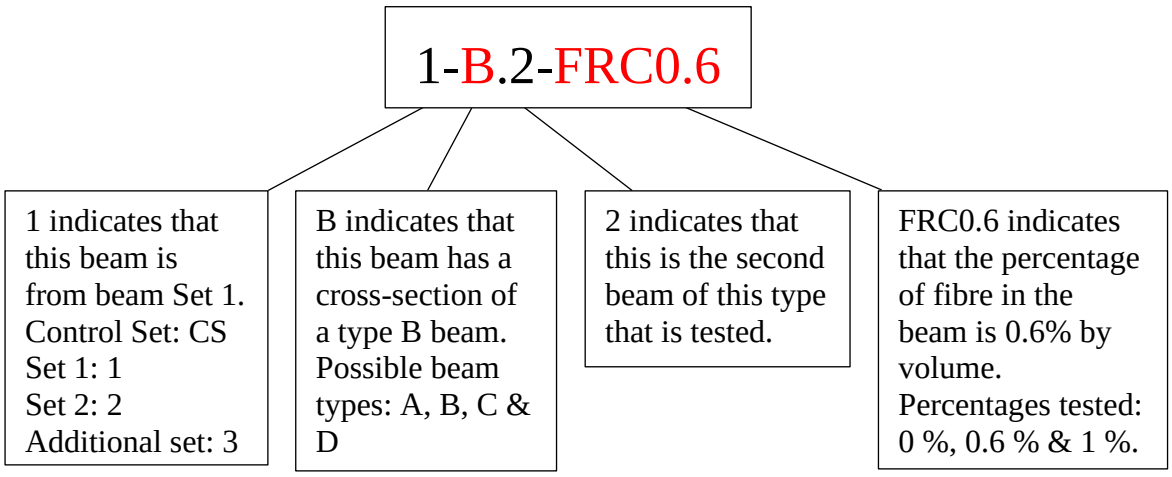

Figure 5.16: Nomenclature of beams.

5.3.4 Pre-experimental procedures

5.3.4.1 Construction of beam moulds

The moulds used for the beams were constructed from pressed wood. Pieces of wood were cut to the required shapes and fixed to one another using steel screws. The moulds were constructed in a manner that they could be disassembled during the demoulding process and reassembled for the next beam set. The moulds were painted with a layer of waterproof paint to prevent the moulds from rotting while concrete is cured and the moulds can be reused.

5.3.4.2 Mixing procedure

The mixing was done in a concrete mixer with a capacity of 0.12 m^3. This mixer was used because it is sufficient capacity to mix the enough concrete to cast a single beam, concrete cubes required for compressive strength tests and concrete to perform slump flow tests. For every beam that was cast, another concrete batch was made.

All constituent materials required for the concrete mix were weighed off to the nearest gram, prior to mixing. The mixing bowl and blades were damped to ensure these were saturated to the same extent for every mix. Aggregates, sand, cement and fly ash were added to the mixing bowl, in this specific order, for dry mixing. The dry constituent materials were mixed and then water was added to the mix at a steady rate. The concrete was allowed to mix for a while to ensure the water is thoroughly dispersed throughout the constituent materials. Then superplasticizer was added at a steady rate and the concrete was mixed for a while to allow the superplasticizer to activate. Finally, the fibres were added to the mix at small quantities, ensuring no fibre balls form within the concrete mix. After all the constituent materials have been added and mixed thoroughly, the mixer was stopped and physically mixed using a shovel. This prevented the steel fibres from settling to the bottom to the mixer. The mixing procedure took approximately between 10 and 15 minutes. The procedure and mixing durations of the mixing process can be seen in Table 5.8.

Table 5.8: Mixing procedure of SFR-SCC.

Step	Duration (s)
Dry mixing of materials	30-45
Adding water	30-45
Mixing with water	120-150
Adding superplasticizer	30-45
Mixing with superplasticizer	180-240
Adding of fibres	90-120
Physical mixing with shovel	60-120
Mixing	60-75

5.3.4.3 Casting procedure

After the mixing process, the concrete was poured from the concrete mixer into a damp wheelbarrow which was used to transport the concrete to the beam moulds. The moulds were painted with a thin layer of oil to simplify the demoulding process once the concrete has set. The reinforcement bars were bent to the required shape by the supplier and only had to be fixed to one another using thin wire. The reinforcement bars were fixed in position in the mould using three plastic spacers positioned under the bars, at the ends and mid-span to allow for 20 mm cover. Wooden clamps were constructed which were fastened to the mould from the outside, to hold the bent portions of the reinforcement bars upright.

The concrete was poured from the wheelbarrow into the mould in a similar fashion as for the specimens used for CMOD tests were the concrete was added in three different increments. The mould was filled to the top and ensured that concrete had filled all gaps and corners of the mould. Two rectangular steel pieces were inserted close to the beams ends, which served as hooks onto which the crane can be attached when the beam is transported to the testing machine. Finally, the surface of the beam was levelled using a trowel and the beams were ready for curing.

5.3.4.4 Curing procedure

After the casting process, the concrete was left to set in the mould for 24 hours. Then, wet blankets were thrown over the beams and moulds. The blankets were kept damp by spraying them with water once a day, to keep a humid environment around the beam. A large plastic sheet was used to cover the beams to reduce the amount of evaporation from the blankets.

Beams were cured inside the moulds up to an age of 7 days and were then removed from the moulds. After that, the beams were cured in the same manner up to an age of 13 days when they were removed from under the blankets, left to dry and prepared for testing

5.3.5 Test details

5.3.5.1 Test set-up

The test set-up was developed in such a way that every beam can be tested twice, provided it fails in the preferred shear failure mode. Figure 5.17 represents a) a schematic drawing and b) an image of the actual test set-up of the asymmetrical three-point bending tests. The blue markers represent the supports and point load of Test 1 and the red markers represent Test 2. Presuming that Test 1 resulted in shear failure in the short shear span, the beam can be swung around and Test 2 can be performed on the other end of the beam, without the results of Test 1 affecting the results of Test 2. Figure 5.17 b) is an image of a beam where the second test is being performed on a beam. It can be seen that the cracks from Test 1 formed outside the span of Test 2 therefore, the results have no effect on the subsequent test.

The test was performed using a Hydraulic Instron actuator. Two steady rollers, spaced 1500 mm apart, were used as beam supports, representing a roller and a pin connection. The force was applied to the beam through a smaller roller spanning the entire width of the beam, representing a point load.

Figure 5.18 is a close-up image of the beam at the point of load application on which the various components are labelled. A three-dimensional bearing is placed between the load cell of the Instron and the roller to allow for free rotational movement around any axis at the point of load application. This ensures that no unwanted lateral forces are being induced as the beam displaces. A protection plate is placed between the bearing and roller to prevent the round edge of the roller from damaging the aluminium bearing casing. The mass of these additional components were measured and added to the loading for the analyses of the results.

Furthermore, it can be seen in Figure 5.18 that the crack passed through the Linear Variable Differential Transformer (LVDT) fixing block. In the few cases where this happened, the LVDT measurements were only affected once the cracks had reached substantial widths and long after ultimate resistance was reached. However, such results were not used in the investigation and rather the measurements of adjacent LVDTs were used.

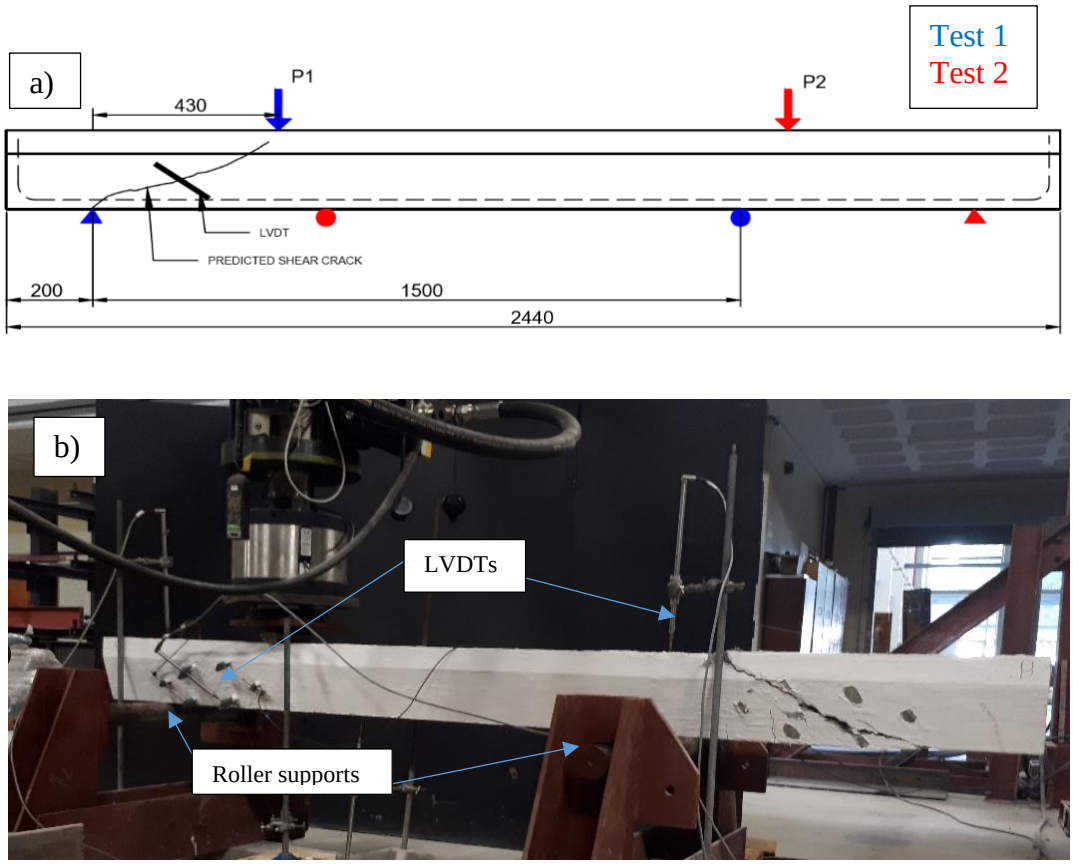

Figure 5.17: Primary test set-up

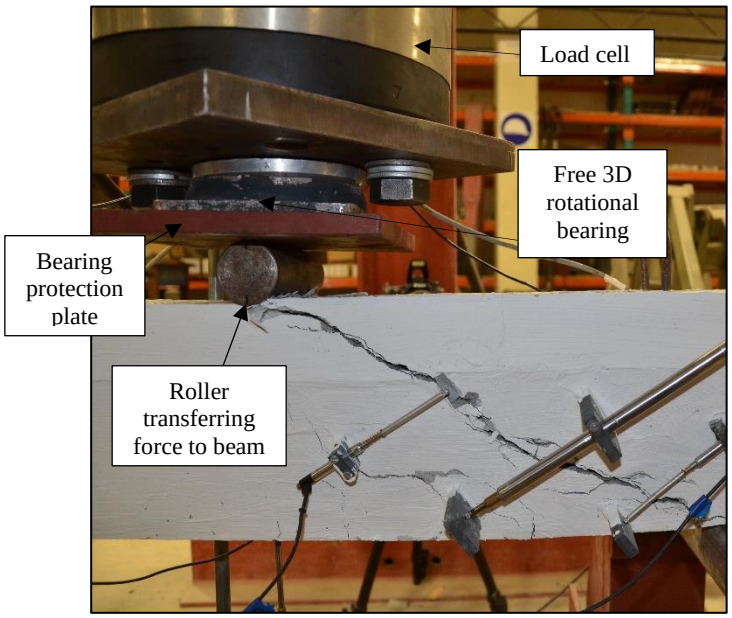

Figure 5.18: Test setup details of application of the load.

5.3.5.2 Test procedure

Beams were prepared for testing the day before the test was performed. This involved painting the beam with a thin layer of limestone ($CaCO_3$) and water mixture, giving the beams a clean, white finish so that small cracks can be identified easier during testing. The particles in the limestone layer are not adhesive and would, therefore, not affect the test results. Furthermore, the PVC clamps used to connect the LVDTs to the beam were fixed at the appropriate positions to the beam using Pratley Steel Quikset.

Before the test was started, all LVDTs were installed in their brackets, and a quick manual test was run to ensure that all LVDTs work correctly. During the test, the load was applied at 5 kN intervals, with the first interval starting at 10 kN, 15 kN and 20 kN, for the control set, Set 1 and Set 2, respectively. A loading rate of 5mm/min was used. Between loading intervals, the position of the actuator was automatically stopped and kept in position for 3 min, in which the beam was inspected. During inspection, cracks were marked off using a permanent marker and crack widths were measured by hand using a crack width measuring card. After every interval, photos of the beams were taken so that the cracking pattern could be inspected afterwards.

5.3.5.3 Test measurements

A total of ten LVDTs were used to measure deflections at various positions on the beam; however, eventually, only the data recorded by five LVDTs was used for various reasons. LVDTs were connected to the side of the beam at an angle of 35° to the horizontal, to measure diagonal shear crack widths. LVDTs were used to measure the vertical deflection of the beam under the point load and of the supports. The net deflection of the beam was calculated by subtracting the average displacement of the supports from the vertical deflection under the point load. The displacements measured by the LVDTs was captured using a HBM Spider8 data capturing device and was synced with the data recorded by the Instron. The load-cell of the Instron was used for logging the load as the test was performed.

During testing, photographs were captured of the beams at 5 kN loading intervals. The crack angles were measured by uploading these photographs onto a software called AutoCAD. The software was then used to measure the angles of the main diagonal cracks to the horizontal, as shown in Figure 5.19.

Figure 5.19: Diagonal crack angle measurement procedure.

5.4 Concluding summary

This chapter covered the development of SFR-SCC that was used for the primary investigation of this study. The tests performed on the fresh and hardened concrete, and results thereof, are discussed. The primary tests performed on ISB in this investigation are covered in detail, explaining the inspiration of the beam shapes and details, pre-experimental procedures and testing details. The results obtained from the primary tests to investigate the shear behaviour of ISB are presented in the following chapter.

CHAPTER 6

EXPERIMENTAL RESULTS AND SHEAR PREDICTIONS

The results presented in this section include the load-deflection curves for the tested beams, the crack widths of the main diagonal shear cracks, cracking angles and the final cracking pattern that formed in the beams during testing. Furthermore, the shear strength predictions by the various shear models that are investigated are presented for the various fibre percentages and beam types. The results shown hereafter are thoroughly discussed in Chapter 7.

6.1 Primary Tests

All test results obtained from the asymmetrical three-point bending tests are presented in this section.

6.1.1 Load – vertical deflection

Figures 6.1 to 6.3 show the results from the asymmetrical three-point bending test and are presented on load-deflection curves for beams in the control set, Set 1 and Set 2, respectively. The deflection was measured vertically under the point of load application and the displacements of the supports were measured vertically above the supports. The average support deflection was subtracted from the vertical deflection under the point load to obtain the

net deflection. The two curves on each graph represent the two beams that were tested of the same beam type. The Figures labelled a) through d) represent the various beam cross-sections where beam-types A, B, C and D are shown in Figures labelled a), b), c) and d), respectively. Beams in Set 1 contained 0.6% fibres, Set 2 contained 1% fibres and in the control set contained no fibres.

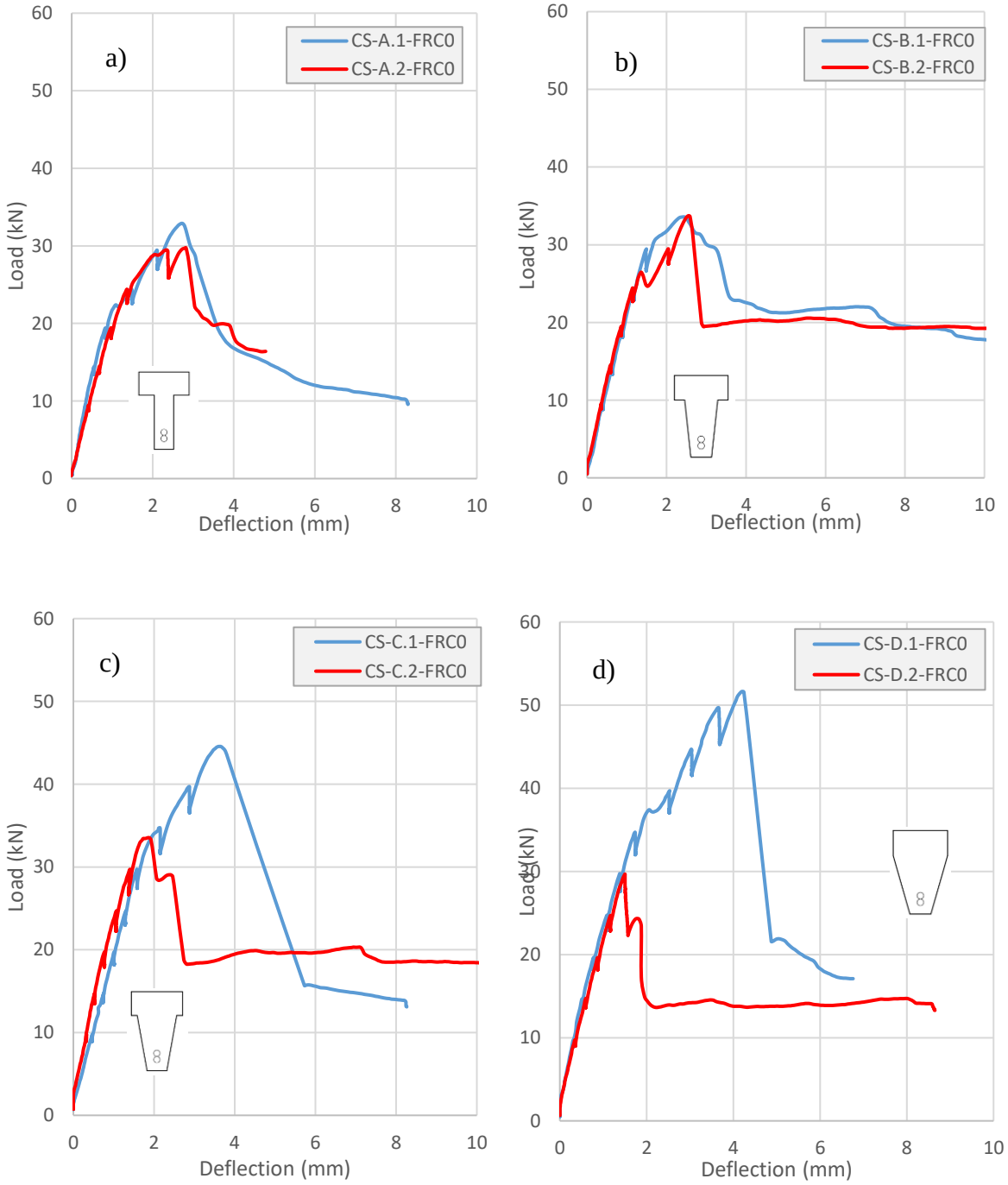

Figure 6.1: Load-deflection under point load for the control set containing no fibres: a) Beams A; b) Beams B; c) Beams C and d) Beams D.

Figure 6.2 represents the test results of Set 1 containing 0.6% fibres.

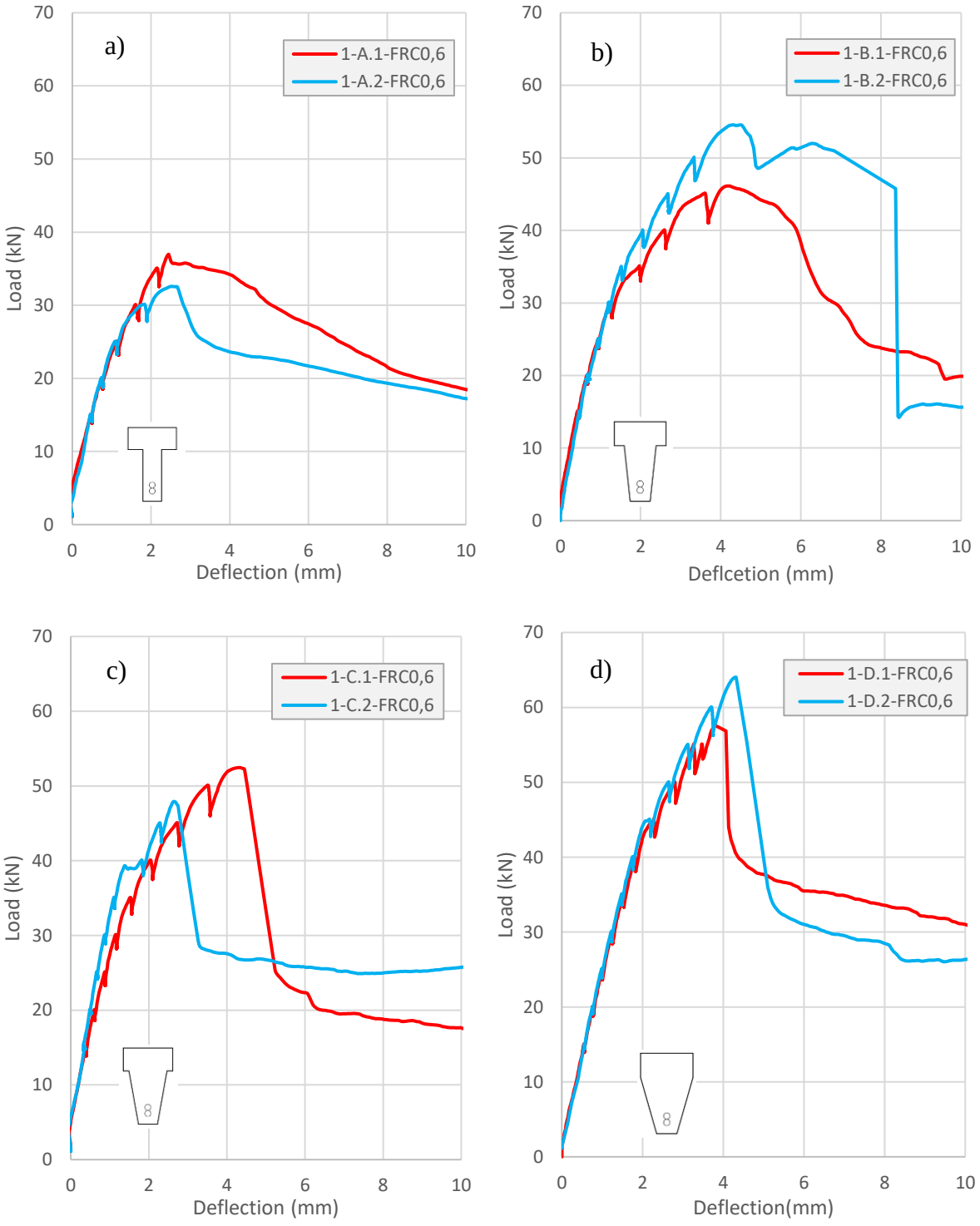

Figure 6.2: Load-deflection under point load for Set 1 containing 0.6% fibres: a) Beams A; b) Beams B; c) Beams C and d) Beams D.

Figure 6.3 represents the test results for Set 2 containing 1% fibres.

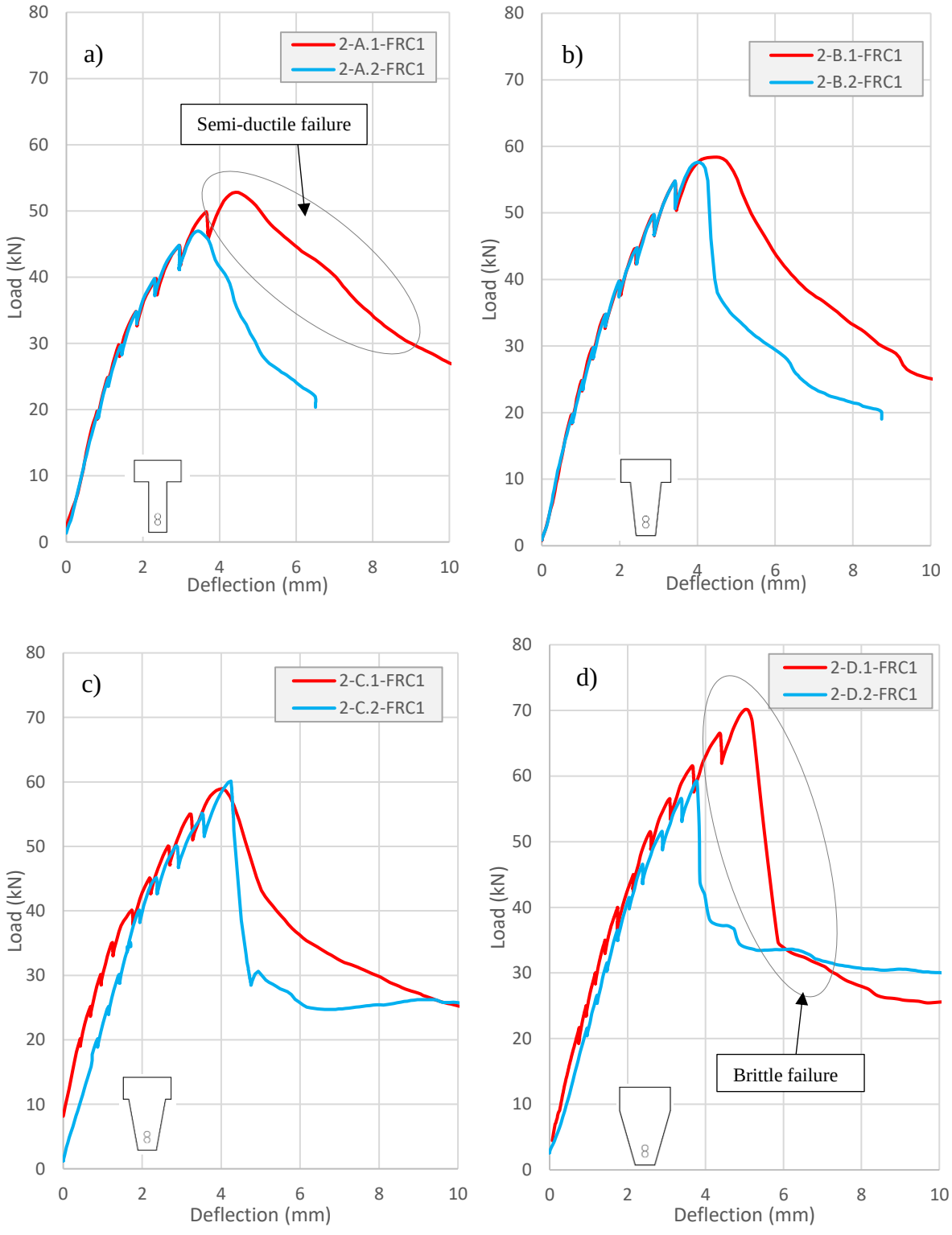

Figure 6.3: Load-deflection under point load for Set 2 containing 1% fibres: a) Beams A; b) Beams B; c) Beams C and d) Beams D.

The dips in the loading that are seen on the graphs results from the testing procedure, where the loading was applied at 5 kN intervals after which the load cell was kept in a stationary position for 3 minutes while the beam was inspected and the formation of cracks was identified. These dips in the load are indications of relaxation occurring in the beam as the load head is kept stationary.

In cases where beams contained fibres, both beams that were tested per beam type reached similar maximum loads. The most substantial difference occurred between beams 2-D.1-FRC1 and 2-D.2-FRC1, which differed by 16%. In the control set, where beams contained no fibres, the results were not that consistent. Maximum loads for beams CS-C.1-FRC0 and CS-C.2-FRC0, and beams CS-D.1-FRC1 and CS-D.2-FRC0 differed by 25% and 43%, respectively. This indicates that fibres result in more consistent failure loads and in cases where no fibres are used, the chances of a beam failing prematurely are higher.

Furthermore, the steep drop in load, which is observed in Beams C and Beams D of set 1 and 2, indicate a brittle failure after the beam had reached its maximum load. Similar results are observed for all beams in the control set. The other beams that displayed a gradual decrease in load after the maximum loading was reached indicates a semi-ductile behaviour (refer to Figure 6.3 a). Fibres change the failure mode from dangerous brittle failures to more desirable ductile failures. However, in cases where fibres increase the maximum loading significantly, brittle failures are still likely to occur. The ultimate shear force V_u and shear stresses v_u of the beams are tabulated in Table 6.1.

Table 6.1: Summary of the ultimate shear forces V_u and shear stresses v_u in all beams.

Control set			**Set 1 (0.6% fibres)**			**Set 2 (1%fibres)**		
Beam	**V_u (kN)**	**v_u (MPa)**	**Beam**	**V_u (kN)**	**v_u (MPa)**	**Beam**	**V_u (kN)**	**v_u (MPa)**
CS-A.1-FRC0	23.47	1.39	***1-A.1-FRC0.6***	26.35	1.56	***2-A.1-FRC1***	37.68	2.23
CS-A.2-FRC0	21.21	1.26	***1-A.2-FRC0.6***	23.24	1.38	***2-A.2-FRC1***	33.51	1.98
CS-B.1-FRC0	23.95	1.31	***1-B.1-FRC0.6***	32.90	1.80	***2-B.1-FRC1***	41.64	2.28
CS-B.2-FRC0	24.07	1.32	***1-B.2-FRC0.6***	38.92	2.13	***2-B.2-FRC1***	41.10	2.25
CS-C.1-FRC0	31.79	1.56	***1-C.1-FRC0.6***	37.42	1.83	***2-C.1-FRC1***	42.06	2.06
CS-C.2-FRC0	23.93	1.17	***1-C.2-FRC0.6***	34.17	1.67	***2-C.2-FRC1***	42.89	2.10
CS-D.1-FRC0	36.84	1.42	***1-D.1-FRC0.6***	41.07	1.58	***2-D.1-FRC1***	50.03	1.92
CS-D.2-FRC0	21.17	0.81	***1-D.2-FRC0.6***	45.68	1.76	***2-D.2-FRC1***	42.23	1.62

It is necessary to point out the unique result of beam 1-B.2-FRC0.6 (refer to Figure 6.2 b). The beam cracked horizontally along the length of the beam at the position where the longitudinal reinforcement is located and can be seen in Figure 6.4. This is referred to as rebar debonding. Another observation made from these beam results is that even though the fibres increased the ultimate loading of the beams, it did not affect the stiffness of the beam, because all beams had similar deflections at a specific load.

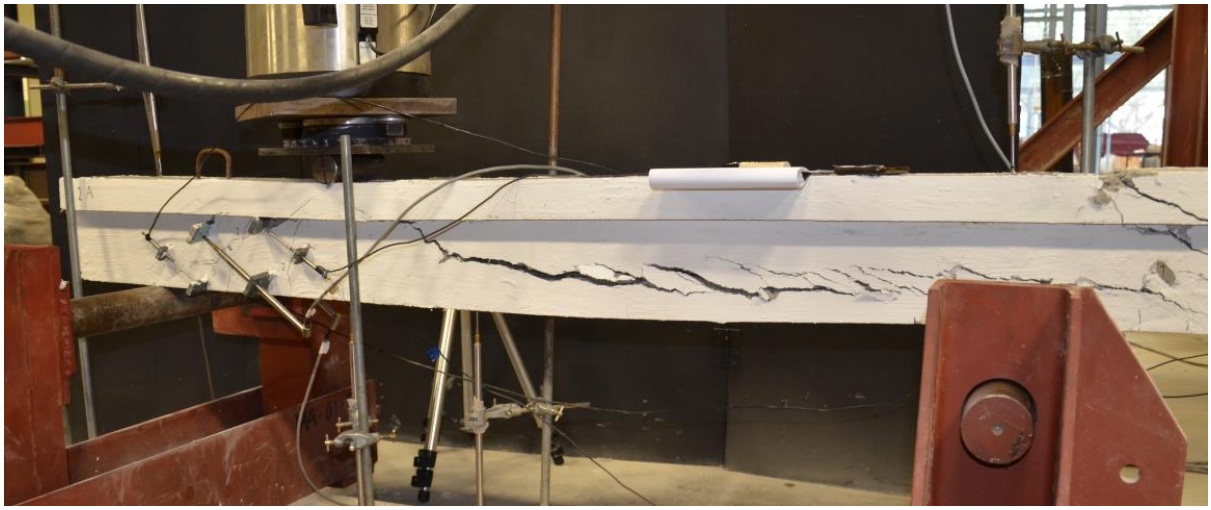

Figure 6.4: Failure mode of beam 1-B.2-FRC0.6.

6.1.2 Crack widths

The figures in this section show the data obtained from the asymmetric three-point bending tests where the width of the critical shear crack is measured using LVDTs as the beam is loaded. Every graph shows the crack width measurements on one side of the beam only (side labelled a), even though crack widths were measured on both sides at approximately mid-height of the web. The crack width measurements are similar on both sides of the beam, the complete sets of test results can be seen in Appendix A.

Figures 6.5 to 6.8, Figures 6.9 to 6.12 and Figures 6.13 to 6.16 show crack widths on beams in the control set, Set 1 and Set 2, respectively. The two curves on the graphs represent the crack width measurements of both beams tested of each beam type.

From the figures in this section, it is observed that in most beams, with only a few exceptions, the first diagonal crack formed at a load of approximately 25 ± 5 kN which is considered to be the load when local tensile stresses reached the maximum tensile stress of the concrete. The

variations in first diagonal crack loads are a result of slight variations in concrete strength and non-homogeneity of the material. In some cases, the first diagonal cracks formed just outside the range of the LVDT, and only at a later stage propagated through the measuring range of the LVDTs. Once again beam 1-B.2-FRC0.6 must be pointed out as the exception where the alternative failure mode resulted in anomalous results (refer to Figure 6.10).

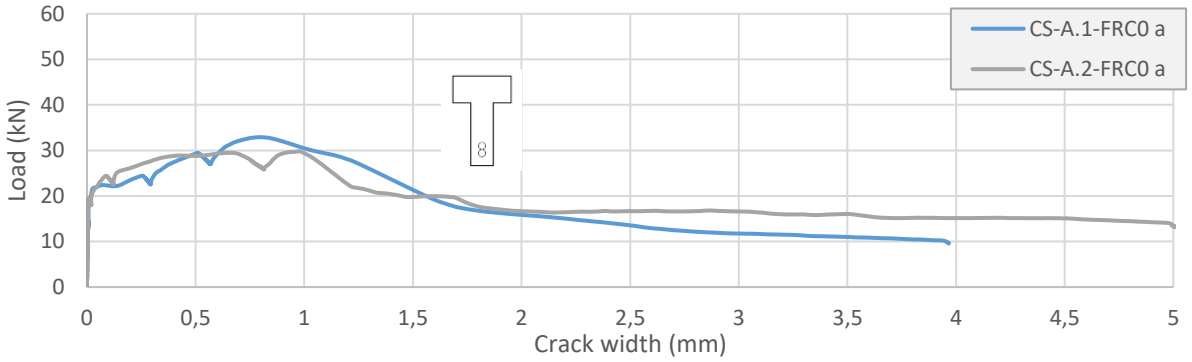

Figure 6.5: Critical shear crack width of Beams A in Control set containing no fibres.

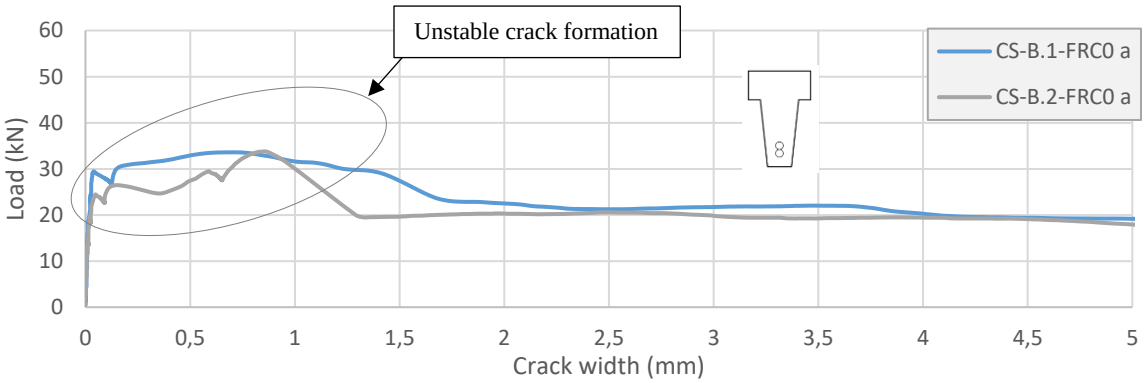

Figure 6.6: Critical shear crack width of Beams B in Control set containing no fibres.

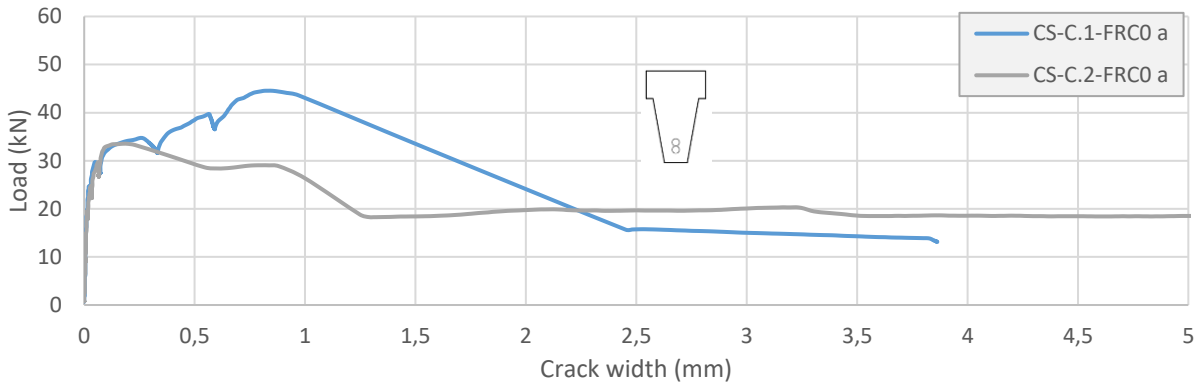

Figure 6.7: Critical shear crack width of Beams C in Control set containing no fibres.

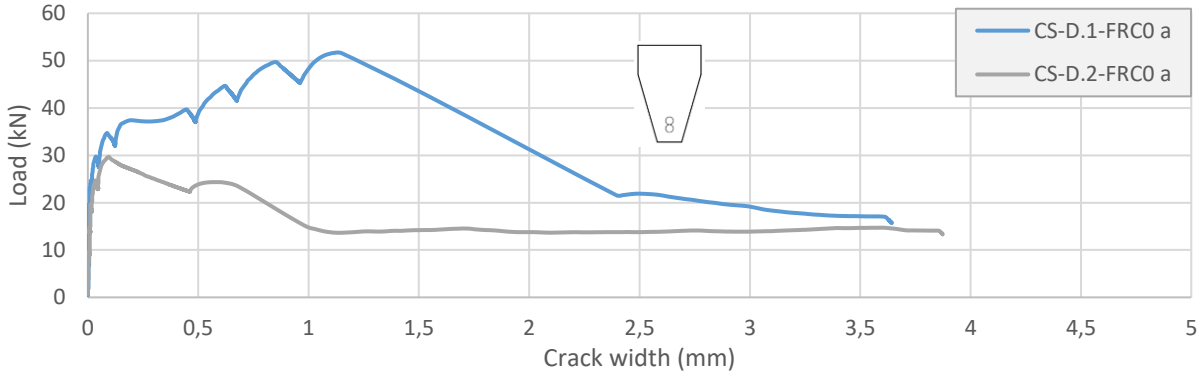

Figure 6.8: Critical shear crack width of Beams D in Control set containing no fibres.

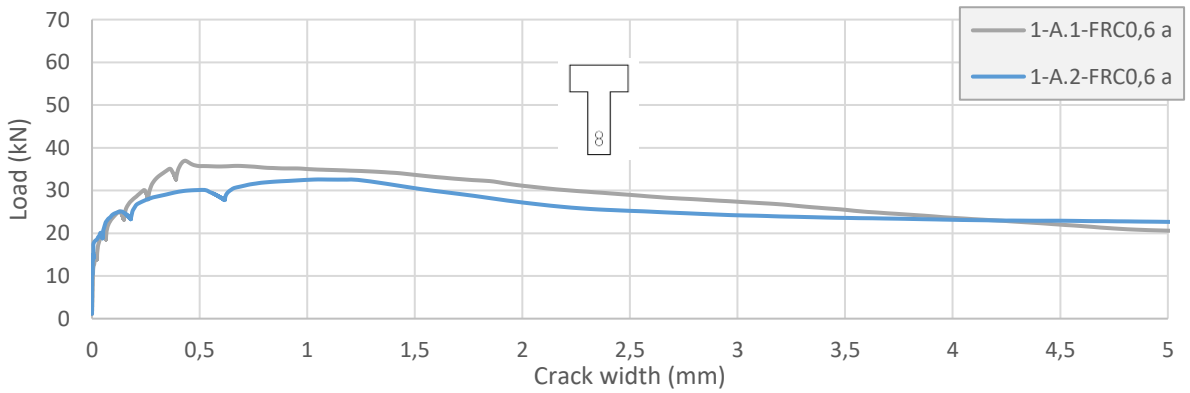

Figure 6.9: Critical shear crack width of Beams A in Set 1 containing 0.6% fibres.

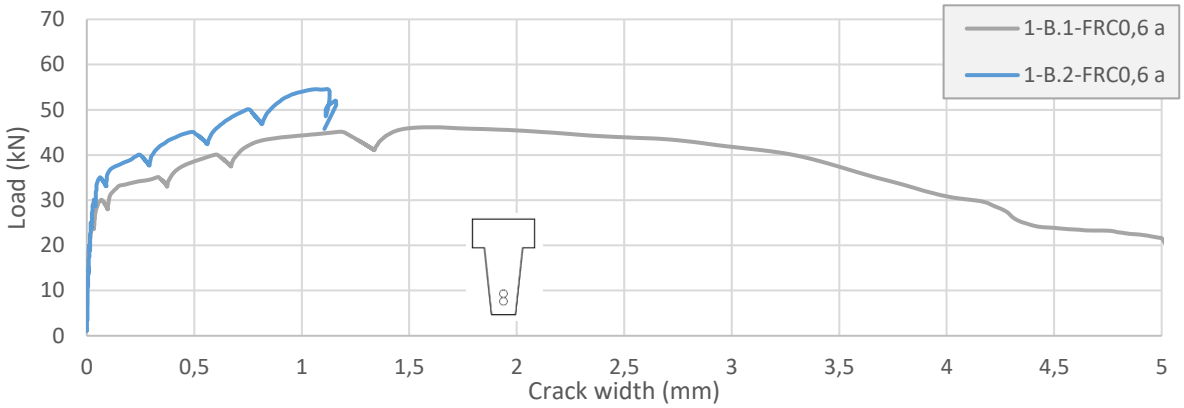

Figure 6.10: Critical shear crack width of Beams B in Set 1 containing 0.6% fibres.

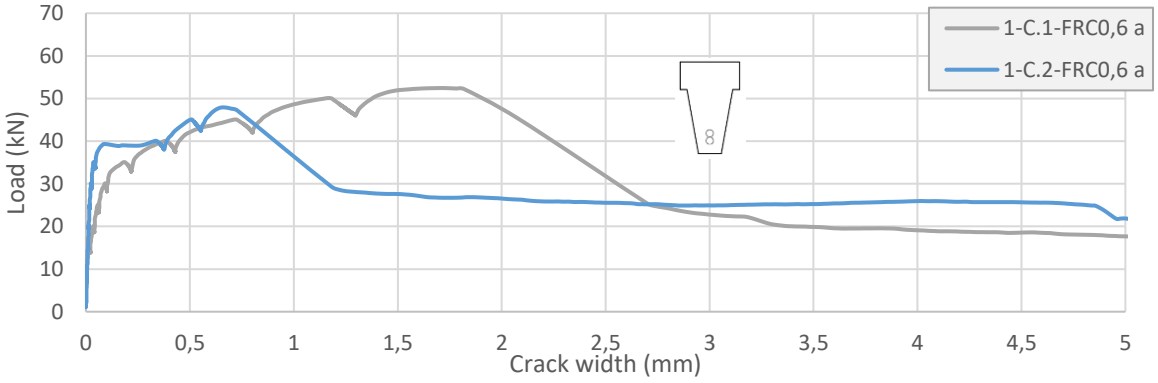

Figure 6.11: Critical shear crack width of Beams C in Set 1 containing 0.6% fibres.

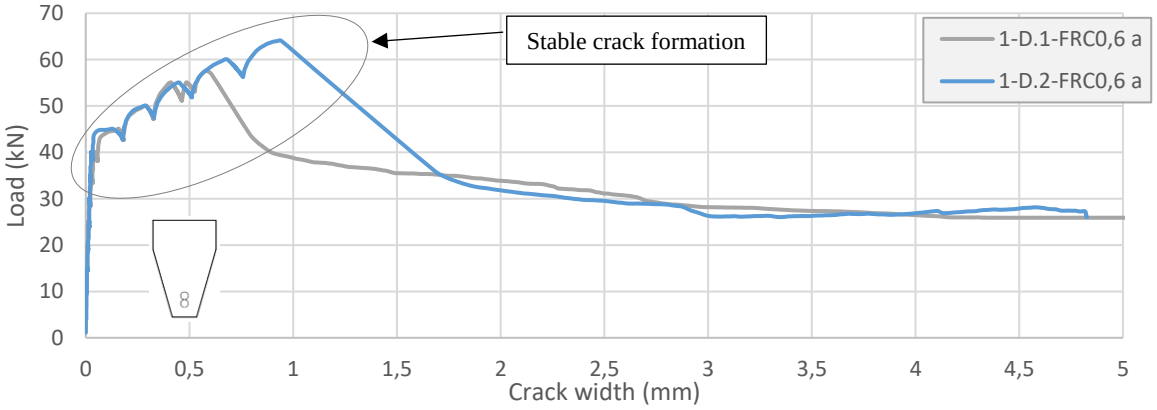

Figure 6.12: Critical shear crack width of Beams D in Set 1 containing 0.6% fibres.

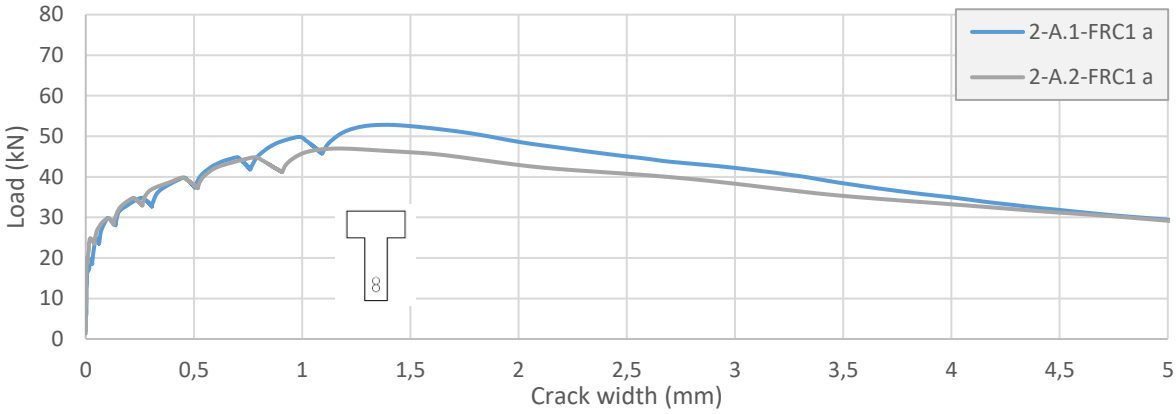

Figure 6.13: Critical shear crack width of Beams A in Set 2 containing 1% fibres.

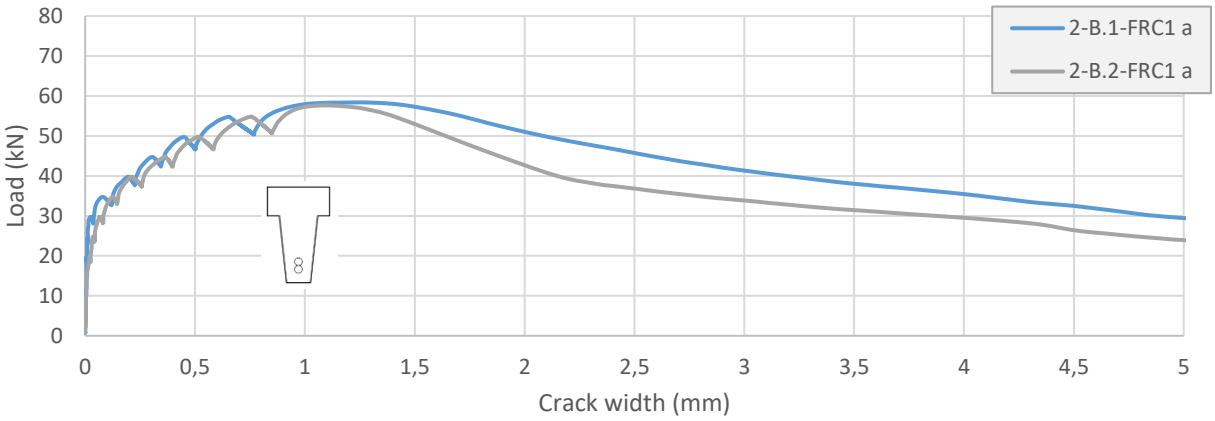

Figure 6.14: Critical shear crack width of Beams B in Set 2 containing 1% fibres.

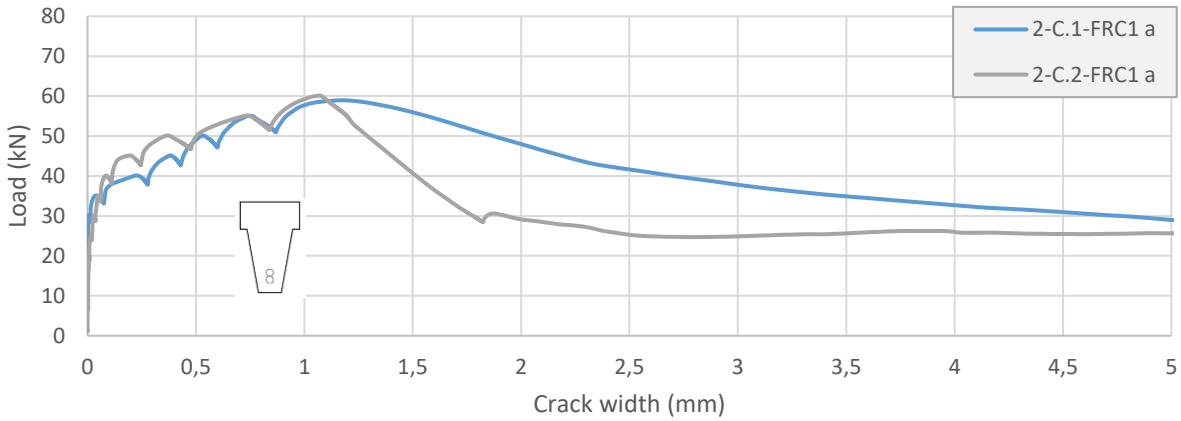

Figure 6.15: Critical shear crack width of Beams C in Set 2 containing 1% fibres.

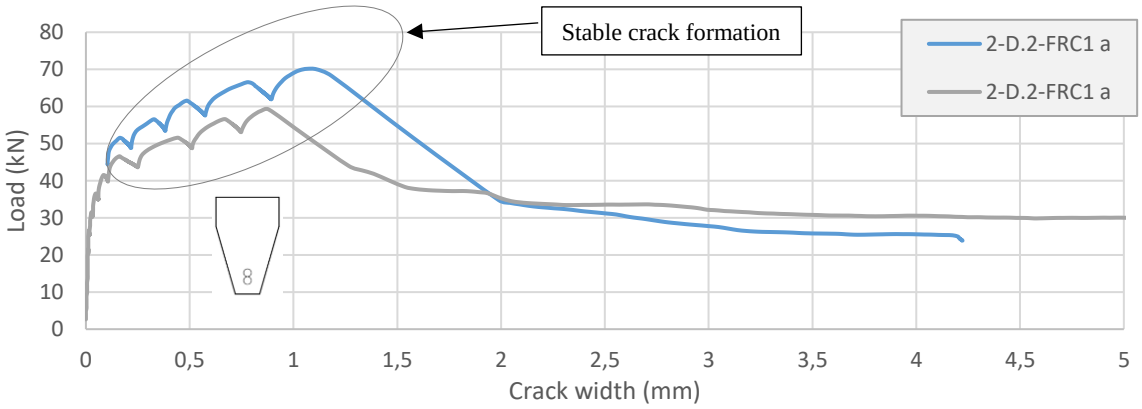

Figure 6.16: Critical shear crack width of Beams D in Set 2 containing 1% fibres.

Not only do fibres increase the load capacity after the formation of shear cracks, they also promote a more stable crack formation as the load increases. The crack growth rate in beams containing fibres is relatively constant, resulting in the stable crack formation, indicating that there is a steady load transfer across the cracks through the fibres that bridge the crack. The fibres bridging the cracks maintain material integrity, therefore allow for post-cracking tensile strength. Conversely, in beams containing no fibres, an unstable crack formation is observed with sudden increases of crack widths. This stable and unstable crack formation has been pointed out in Figure 6.6, 6.12 and 6.16.

Beams without fibres failed shortly after the formation of shear cracks, these cracks quickly widen to the point where no force is transferred across the crack resulting in failure. These failures happen suddenly with little or no warning prior to failure. On the other hand, since beams with fibres display increasing carrying capacity even after the shear cracks have formed, there are clear warning signs well before failure.

6.1.3 Angle of main diagonal shear crack

Table 6.2 presents a list of the main diagonal shear crack angles for every beam that was tested in this investigation. Crack angles were measured as explained in Section 5.3.5.3. The average inclination of diagonal shear angles were the same for all beam sets at 33°. Detailed discussions about the main diagonal shear crack angles follow in Chapter 7.

Table 6.2: Main diagonal shear crack angle.

Control Set		**Set 1**		**Set 2**	
Beam	***(°)***	***Beam***	***(°)***	***Beam***	***(°)***
CS-A.1-FRC0 a	31	1-A.1-FRC0.6 a	23	2-A.1-FRC1 a	35
CS-A.1-FRC0 b	36	1-A.1-FRC0.6 b	23	2-A.1-FRC1 b	29
CS-A.2-FRC0 a	32	1-A.2-FRC0.6 a	43	2-A.2-FRC1 a	40
CS-A.2-FRC0 b	32	1-A.2-FRC0.6 b	40	2-A.2-FRC1 b	34
CS-B.1-FRC0 a	25	1-B.1-FRC0.6 a	35	2-B.1-FRC1 a	37
CS-B.1-FRC0 b	36	1-B.1-FRC0.6 b	33	2-B.1-FRC1 b	31
CS-B.2-FRC0 a	28	1-B.2-FRC0.6 a	33	2-B.2-FRC1 a	36
CS-B.2-FRC0 b	32	1-B.2-FRC0.6 b	30	2-B.2-FRC1 b	31
CS-C.1-FRC0 a	33	1-C.1-FRC0.6 a	34	2-C.1-FRC1 a	33
CS-C.1-FRC0 b	36	1-C.1-FRC0.6 b	32	2-C.1-FRC1 b	32
CS-C.2-FRC0 a	33	1-C.2-FRC0.6 a	33	2-C.2-FRC1 a	29
CS-C.2-FRC0 b	31	1-C.2-FRC0.6 b	30	2-C.2-FRC1 b	35
CS-D.1-FRC0 a	36	1-D.1-FRC0.6 a	33	2-D.1-FRC1 a	30
CS-D.1-FRC0 b	33	1-D.1-FRC0.6 b	35	2-D.1-FRC1 b	34
CS-D.2-FRC0 a	34	1-D.2-FRC0.6 a	36	2-D.2-FRC1 a	32
CS-D.2-FRC0 b	32	1-D.2-FRC0.6 b	34	2-D.2-FRC1 b	34
Average	33	*Average*	33	*Average*	33

6.1.4 Final crack pattern and failure modes

Figures 6.17, 6.18 and 6.19 show the final crack patterns for all the beams tested in the control set, Set 1 and Set 2, respectively. The crack pattern of only one side of the beam is presented (the side labelled a). It was observed that for the beams in the control set, cracking was more developed at low loads when compared to beams containing fibres. In Table 6.3 the crack widths measured at an appropriate service load of 35 kN are recorded. It can be seen that most of the beams containing no fibres failed before the service load was reached. All beams containing fibres did not fail before the service load was reached. In beams with fibres, the cracks were narrower at low loads, which is a significant aspect in a durability point of view. Crack widths in beams containing 1% fibres were narrower than in beams containing 0.6% fibres. However, there was no noticeable difference between the crack development for beams with 0.6% and 1% fibres. Furthermore, multiple shear cracks formed in beams with fibres, this is particularly visible in Figure 6.19 (beams with 1% fibres). Even though multiple shear cracks formed during testing, there were always one or two critical cracks that eventually resulted in failure of the beam. Fewer cracks formed on the beams in the control set, generally only one shear crack formed which later resulted in the beam failing.

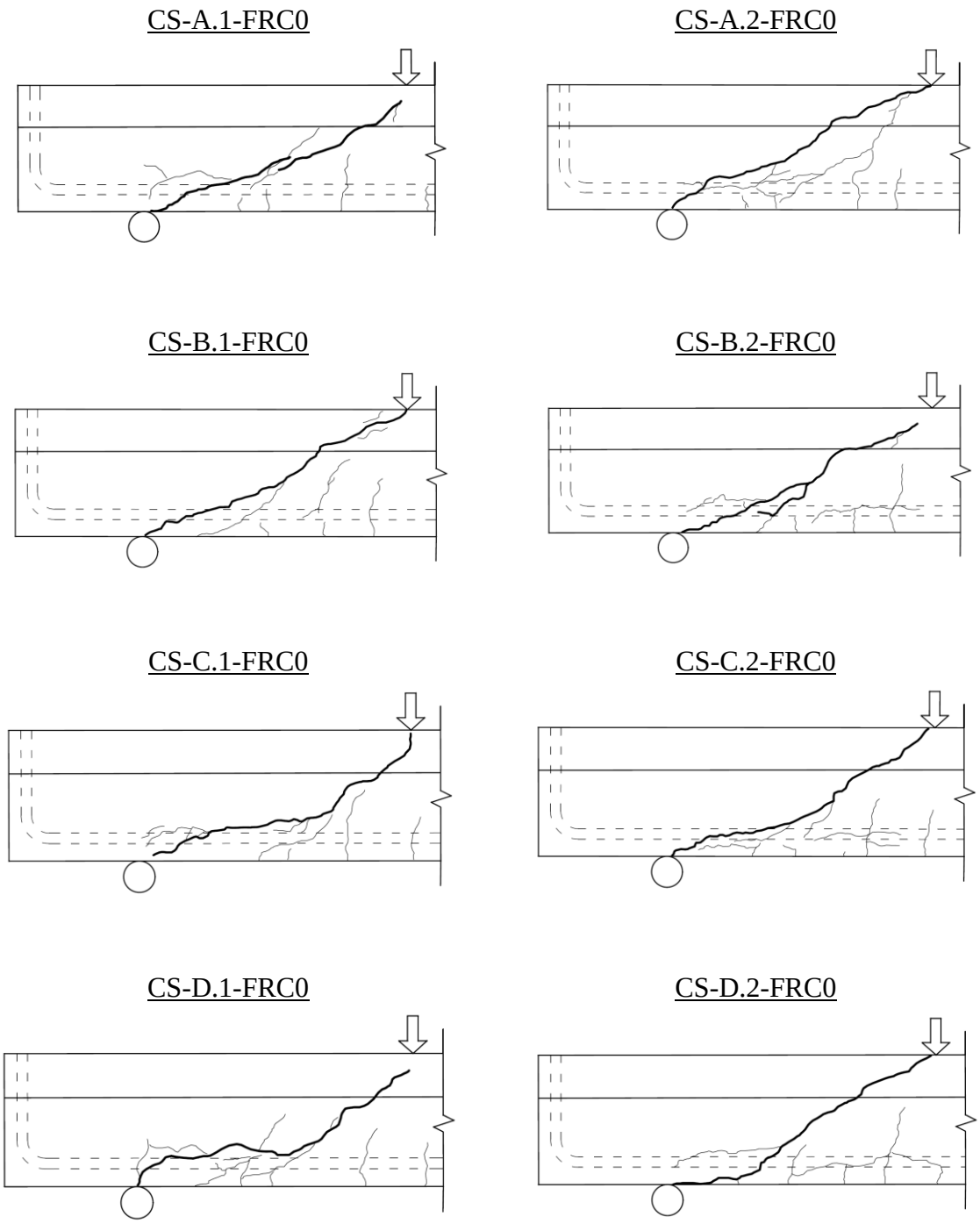

Figure 6.17: Final crack pattern of beams in the Control set containing no fibres.

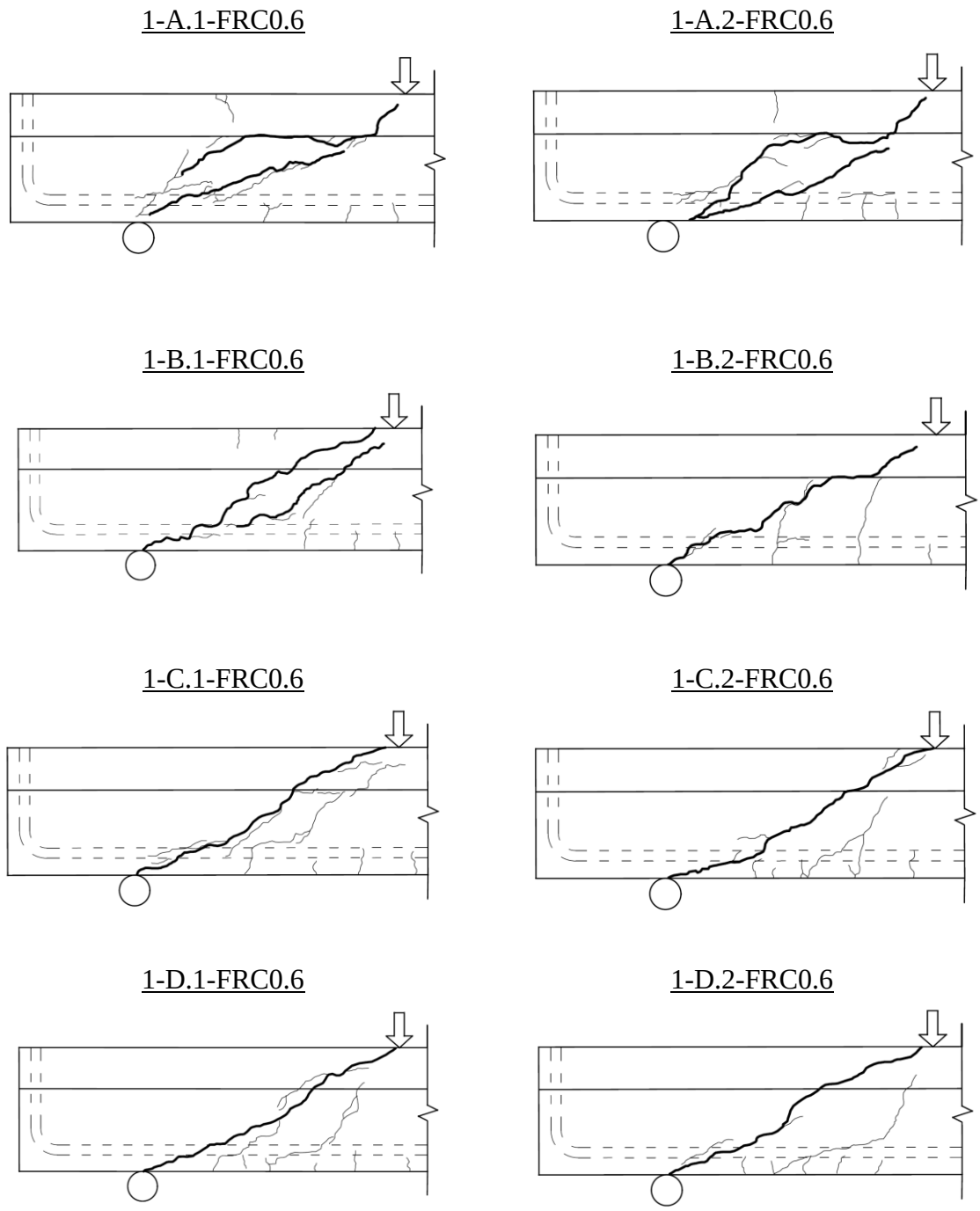

Figure 6.18: Final crack pattern of beams in Set 1 containing 0.6 % fibres.

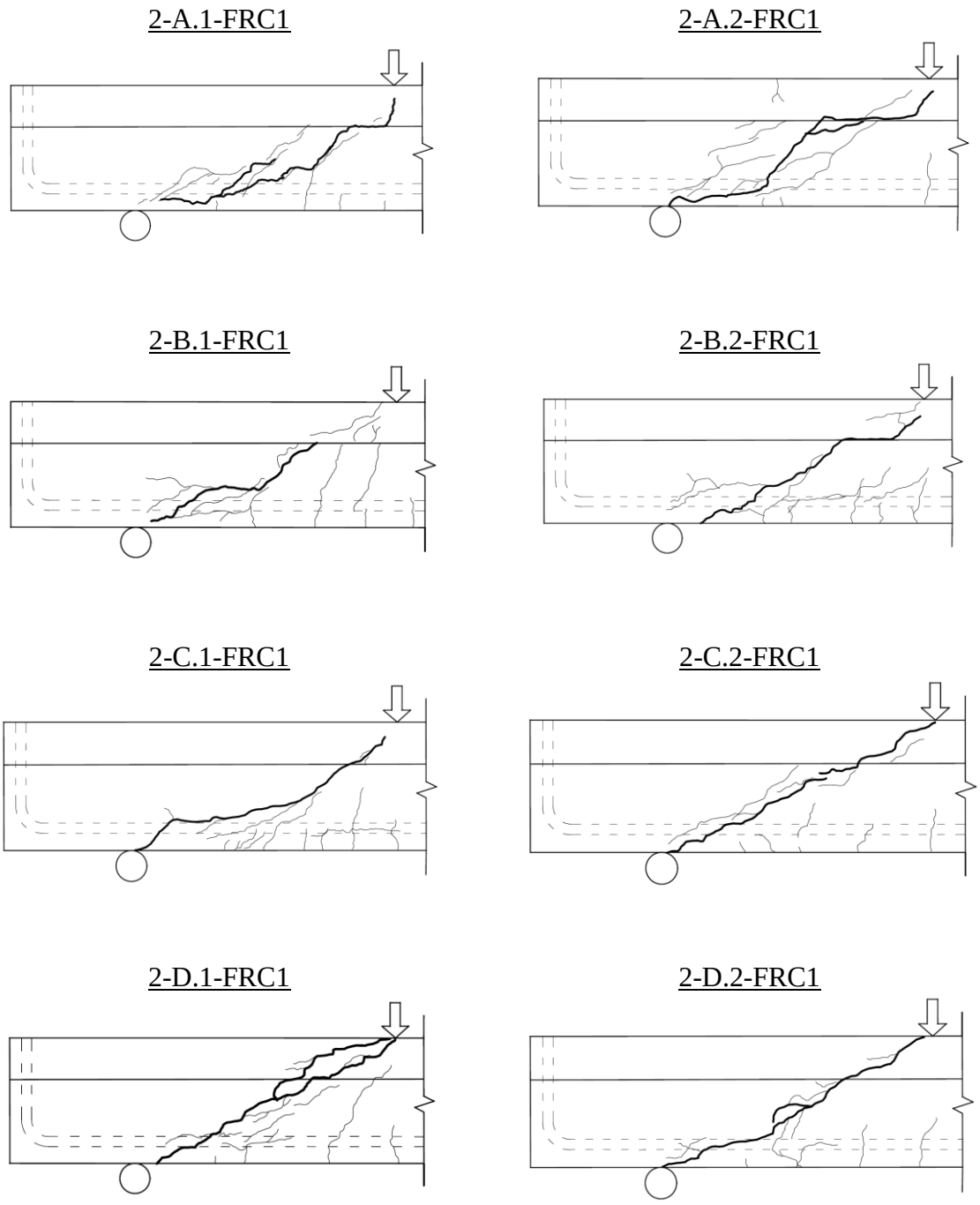

Figure 6.19: Final crack pattern of beams in Set 2 containing 1 % fibres.

Failure modes of the beams were distinguished between four typical failure modes. Most beams experienced more than one failure mode. However, the failure mode that was observed in all the beams is the mode referred to as Diagonal-tension (DT). This mode is indicated by a diagonal shear crack spanning almost directly from the support to the point of load application. This was the expected failure mode since beams with a shear span-to-effective depth ratio in the vicinity of 2.5, like in this investigation ($a_v/d = 2.6$), generally fails in this mode. The other

failure modes observed are Flexural-shear failure (FS), Shear-compression failure (SC) and Rebar debonding failure (RD). FS failure occurs when a flexural crack starts forming at the bottom of the beam and then propagates diagonally towards the point of load application. SC failure occurs at the point of load application where the concrete crashes due to the high local compressive stresses at that point. RD failure occurs when horizontal cracks form along the length of the beam at the height where the longitudinal reinforcement is situated, resulting from the doweling action of the reinforcement. The typical crack development procedure for the beams in this investigation is explained in more detail in Chapter 7.

Table 6.3 represents a summary of the results from the asymmetric three-point bending tests and amongst other things the average crack width at service load of 35 kN (w_{35}), the average crack width at ultimate resistance (w_u), average crack angle at failure (α_{avg}) and the failure modes observed in all the tested beams.

Table 6.3: Asymmetric three-point bending test results.

Beam	f'_c (MPa)	V_f (%)	V_u (kN)	v_u (MPa)	$v_u/f'_c{}^{0.5}$	w_{35} (mm)	w_u (mm)	α_{avg} (°)	Failure mode
CS-A.1-FRC0	27.0	0	23.47	1.39	0.27	failed	0.85	34	DT
CS-A.2-FRC0	27.0	0	21.21	1.26	0.24	failed	1.05	32	DT
CS-B.1-FRC0	27.7	0	23.95	1.31	0.25	failed	0.63	31	DT+SC
CS-B.2-FRC0	27.7	0	24.07	1.32	0.25	failed	0.70	30	DT+FS+RD
CS-C.1-FRC0	26.1	0	31.79	1.56	0.30	0.3	0.84	35	DT+SC
CS-C.2-FRC0	26.1	0	23.93	1.17	0.23	failed	0.15	32	DT+SC
CS-D.1-FRC0	27.8	0	36.84	1.42	0.27	0.45	1.04	35	DT+FS
CS-D.2-FRC0	27.8	0	21.17	0.81	0.15	failed	0.08	33	DT+FS
1-A.1-FRC0.6	26.6	0.6	26.35	1.56	0.30	0.7	0.42	23	DT+FS
1-A.2-FRC0.6	26.6	0.6	23.24	1.38	0.27	0.65	1.03	42	DT
1-B.1-FRC0.6	29.8	0.6	32.90	1.80	0.33	0.3	1.65	34	DT+FS
1-B.2-FRC0.6	29.8	0.6	38.92	2.13	0.39	0.05	1.14	32	RD+DT
1-C.1-FRC0.6	28.5	0.6	37.42	1.83	0.34	0.05	1.50	33	DT
1-C.2-FRC0.6	28.5	0.6	34.17	1.67	0.31	0.1	0.72	32	DT+SC
1-D.1-FRC0.6	26.6	0.6	41.07	1.58	0.31	0	0.70	34	DT+SC+FS
1-D.2-FRC0.6	26.6	0.6	45.68	1.76	0.34	0	0.84	35	DT+SC
2-A.1-FRC1	28.5	1	37.68	2.23	0.42	0.2	1.31	32	DT
2-A.2-FRC1	28.5	1	33.51	1.98	0.37	0.25	1.24	37	DT
2-B.1-FRC1	29.9	1	41.64	2.28	0.42	0.01	1.22	34	DT+SC+FS
2-B.2-FRC1	29.9	1	41.10	2.25	0.41	0.05	1.10	34	DT+SC+RD
2-C.1-FRC1	29.0	1	42.06	2.06	0.38	0.05	1.17	33	DT+FS
2-C.2-FRC1	29.0	1	42.89	2.10	0.39	0.01	1.00	32	DT+SC
2-D.1-FRC1	29.2	1	50.03	1.92	0.36	0	1.03	32	DT+FS
2-D.2-FRC1	29.2	1	42.23	1.62	0.30	0.01	0.75	33	DT+SC+FS

6.2 Application of modified shear models

Various shear models found in literature were adapted for the ISB tested in this investigation as explained in Section 4.1. The modified shear models were used to predict the shear capacity of the two sets of beams tested in this investigation as well as the results of an additional beam set of ISB that were tested previously. Detailed information on the additional beam set of which the results were used in this investigation can be found in Appendix B.

Since the shear prediction models are only applicable for FRC beams, the models were not used to predict the shear strength of the control set. Instead, the shear strengths of the control set was predicted using the method prescribed in EC 2 (EN 1992-1-1, 2004). Furthermore, it is essential to state that all partial factors in the shear models were used as 1, and the input parameters and material properties used are average measured values. For concrete compressive strength and residual flexural strength (according to EN 14651), six specimens were tested in each case and the average was used as input parameters in the models.

6.2.1 Shear predictions

Figure 6.20 represents the ultimate shear strength prediction of the beams in the control set. Only the method proposed in EC2 (refer to Section 3.5) was used to predict the shear strengths of the control set, to get an indication of whether the test results are relatively realistic. Figure 6.21 to 6.23 represent the shear strengths predicted by the investigated shear models of the various beams in Set 1, Set 2 and the additional beam set, respectively. The black dotted line on the graphs indicates the average of the measured shear strengths of the various beams obtained from the tests.

The majority of the shear models used in this investigation originally incorporates an effective cross-sectional area that contributes to the shear capacity of a beam, calculated as the narrowest part of the web (b_w) multiplied by the effective depth of the beam (d). Therefore, considering beams tested in this investigation, theoretically would have the same shear capacity since the effective area ($b_w \cdot d$) is the same for all four beams-types. However, this would result in over-conservative shear predictions. The shear models were modified to incorporate a larger effective area contributing to shear resistance by using the whole cross-sectional area of the web. For a detailed explanation on the modification of the shear models refer to Section 4.1.

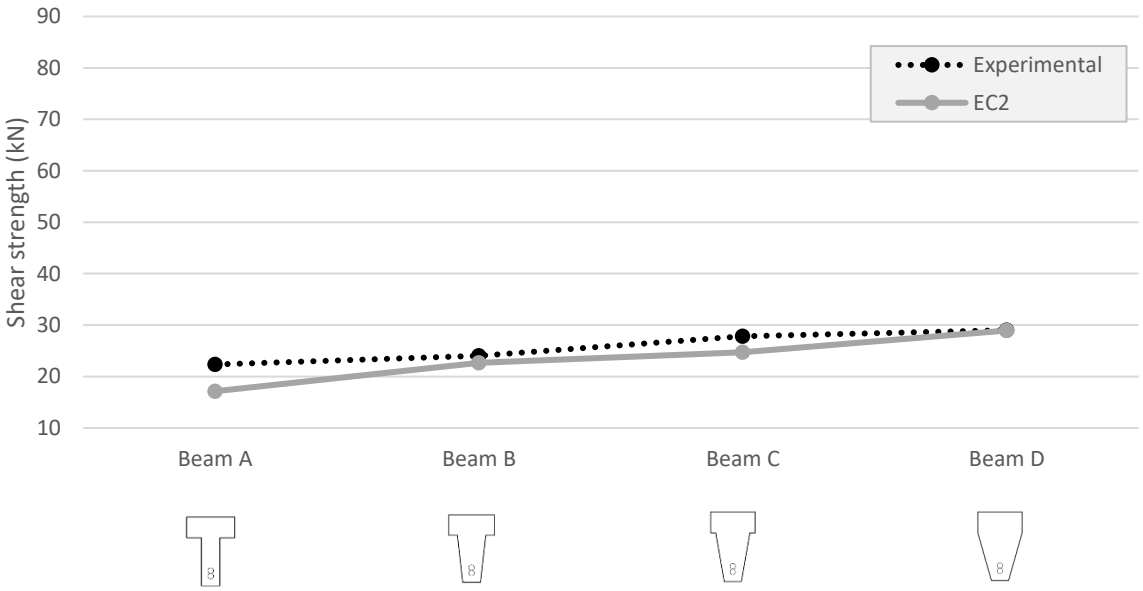

Figure 6.20: Predicted shear strengths of beams in the Control set containing no fibres.

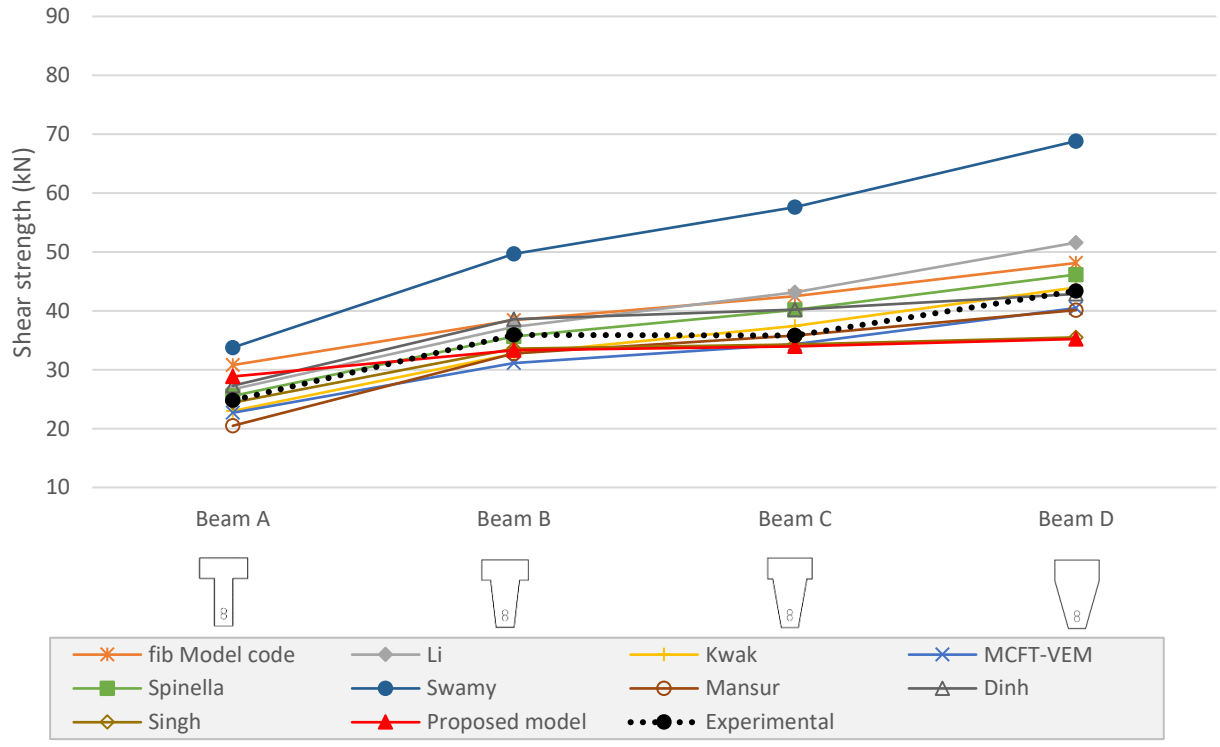

Figure 6.21: Predicted shear strengths of beams in Set 1 containing 0.6% fibres.

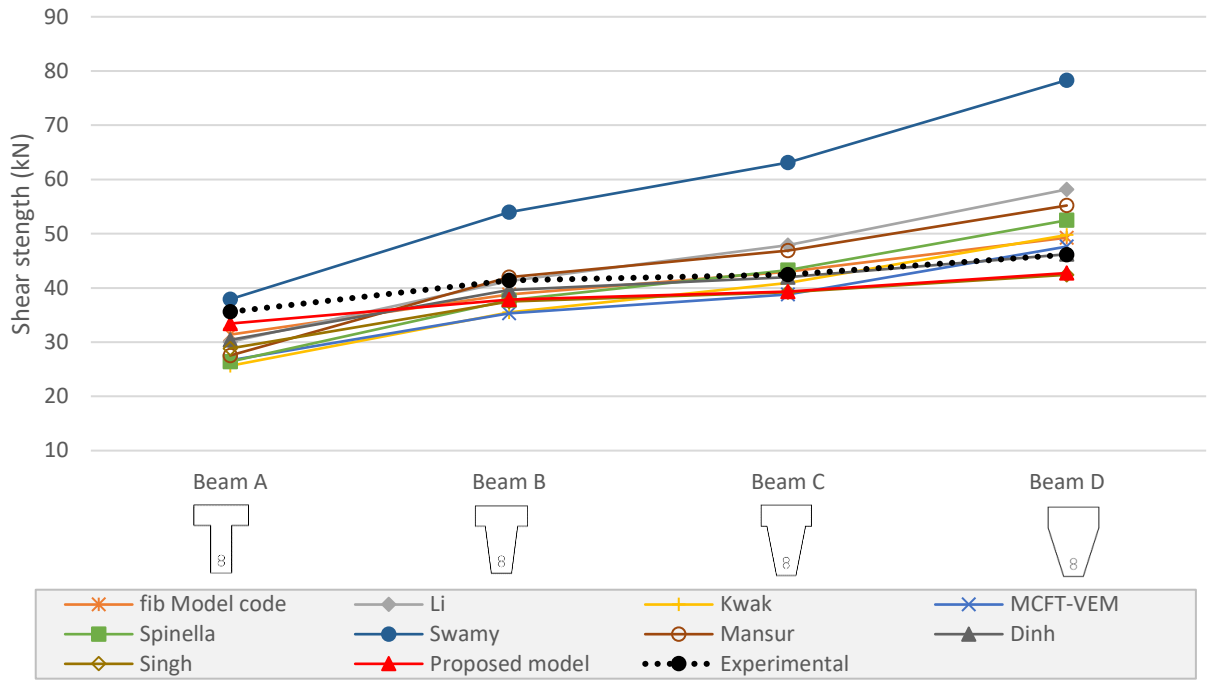

Figure 6.22: Predicted shear strengths of beams in Set 2 containing 1% fibres.

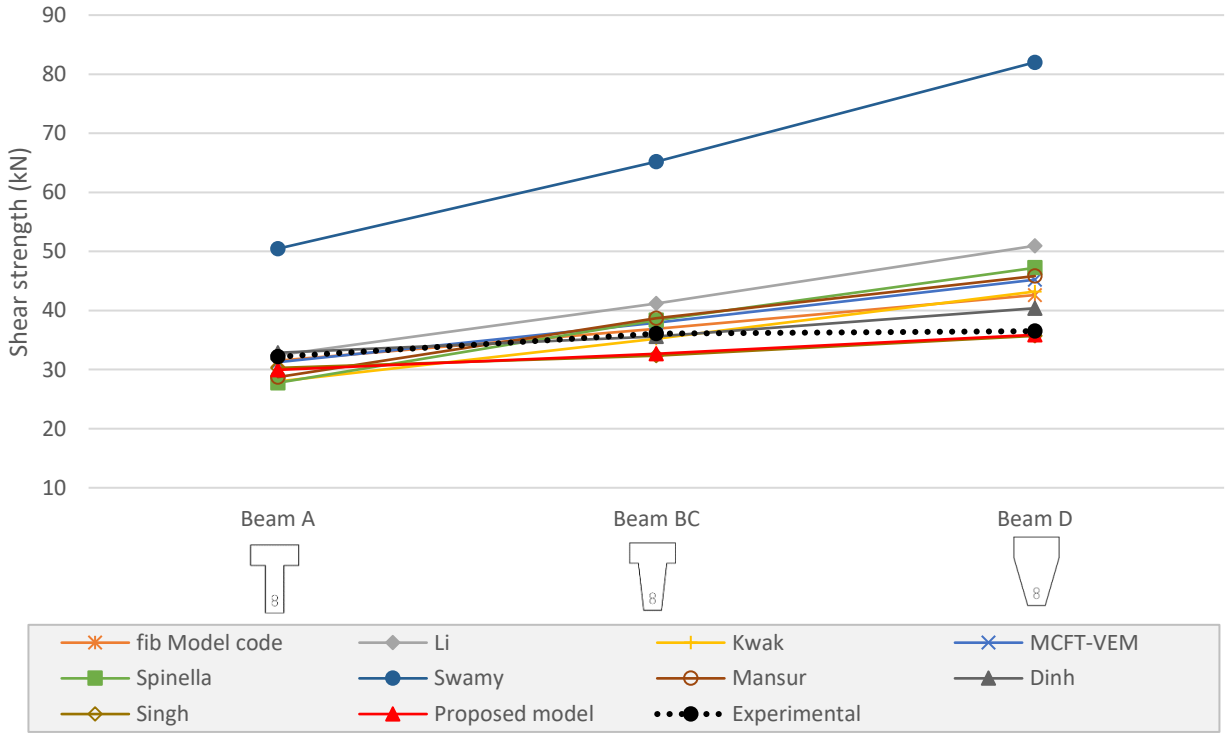

Figure 6.23: Predicted shear strengths of beams from additional beam set containing 0.6% fibres.

From Figure 6.21, Figure 6.22 and Figure 6.23 it can be seen that the shear strength predictions of the model proposed by Swamy *et al.* (1993) are significantly higher than the measured shear strengths for all the beam types and fibre contents. Looking into the formulation of this model it is found that a significantly high shear strength contribution by the concrete compression chord is estimated. This contributed is calculated as $V_c = 3.75\,\tau_R\,b_w\,d$. It is unclear how the constant of 3.75 was obtained, but it is considered to be the reason why this model predicts significantly high shear strengths. Furthermore, the term τ_R represents the shear strength of concrete, for the purpose of this investigation the shear strength was estimated according to the method in *fib* Model Code 2010 (FIB, 2010b) for Level I approximation since Swamy *et al.* (1993) does not propose a method to determine this value. Due to the reasons mentioned above, it is suggested that the model of Swamy *et al.* (1993) should not be used for ISB, since it will result in unconservative shear strength predictions.

However, most of the shear strength predictions by all other shear models are at least within 30% of the experimental shear strength. Table C.1 in Appendix C lists the specific ultimate shear strength results for all beams and the shear strength ratios for all the modified shear prediction models.

6.3 Concluding summary

The results of the primary tests and the shear predictions of the modified shear models are presented in this chapter. Test results of both beams per beam type that were tested are given on individual graphs. Furthermore, the main diagonal shear crack angles and final cracking pattern for every beam are given. Finally, the shear strength predictions of the modified shear models are presented graphically.

More detailed discussions on the test results and shear strength predictions by the shear models follow in Chapter 7.

CHAPTER 7

DISCUSSION OF EXPERIMENTAL RESULTS AND SHEAR PREDICTIONS

This chapter provides detailed discussions of the results presented in Chapter 6. These discussions are subdivided into two sections regarding the experimental tests performed on ISB and the results of the shear models used to predict the shear capacity of these beams.

7.1 Primary tests

This section discusses the effect that fibre volume and beam cross-sectional area, more specifically web area, has on the shear behaviour of longitudinally reinforced ISB containing steel fibres and no vertical shear reinforcement. To investigate the shear behaviour of the beams, the ultimate shear strengths and maximum shear stresses for the various types of beams and fibre volumes are compared. Furthermore, crack widths, crack angles and cracking patterns are also discussed.

7.1.1 Shear strengths comparison

Figure 7.1 presents the ultimate shear capacity and Figure 7.2 presents the normalised shear stresses obtained during testing for the various beam types with various fibre volumes. The average maximum shear capacity of the two beams per beam-type tested in this investigation was taken as the ultimate shear capacity for that specific beam-type. The shear stress is calculated by dividing the ultimate shear capacity by the beam cross-sectional area and is then normalised by dividing it with the square root of the cylinder compressive strength of the concrete. In Figure 7.1 and 7.2 the dashed lines indicate linear trendlines for the various fibre volumes.

7.1.1.1 Comparison of beam-types

From the results, it can be seen that there is a significant increase in shear strength from beam-type A to D. The web cross-sectional area has a significant influence on the shear capacity of the beams. As the web area increases the shear capacity increases as well. An increase in shear strength from beams A to beams D of 6.7 kN, 18.6 kN and 10.5 kN was obtained for the control set, Set 1 and Set 2, respectively. This is an average increase of 11.9 kN.

These results are expected for beams containing fibres, since the fibres allow for increasing carrying capacity after diagonal cracking. As the diagonal shear cracks forms in the web, fibres bridging the crack allow stress transfer and increase the carrying capacity of the beam. Therefore, as the web area increases, the area of the crack face over which fibres transfer stresses increases, resulting in higher shear capacity.

Similar results are observed from the control set where the beams contain no fibres. This finding is contradictory to what has been observed in the investigation of Thamrin *et al.* (2016). In a study performed by Thamrin *et al.* (2016), it was found that the shear capacity of flanged beams is affected considerably more by the flange and that the effect of the web on shear capacity is insignificant and can be ignored in T-beams. It is argued by Kotsovos *et al.* (1987) that in beams containing no fibres, mechanisms that contribute to shear strength such as aggregate interlock in the web diminishes as the crack widens and the shear contribution of this mechanism after diagonal cracking in the web is questionable. From what was observed in this investigation one should not ignore the shear contribution of the web in ISB beams when predicting the shear strength as this increases the shear capacity significantly.

In Figure 7.2 it can be seen that the normalised shear stresses at failure for the various beam-types are relatively constant. This indicates that the shear capacity of ISB has a direct proportional relationship to its cross-sectional area.

A slight decrease in normalised shear stresses for no fibres and 1% fibre volume is observed, yet a slight increase in normalised shear stresses is observed for 0.6% fibre volume. The differences in the slopes of the trendlines between the various fibre volumes in both Figure 7.1 and 7.2 are assumed to be a consequence of the small sample size of the beams tested per beam-type since only two beams per beam-type were tested. As more such beams get tested and more test results are available the trendlines will presumably have the same slope.

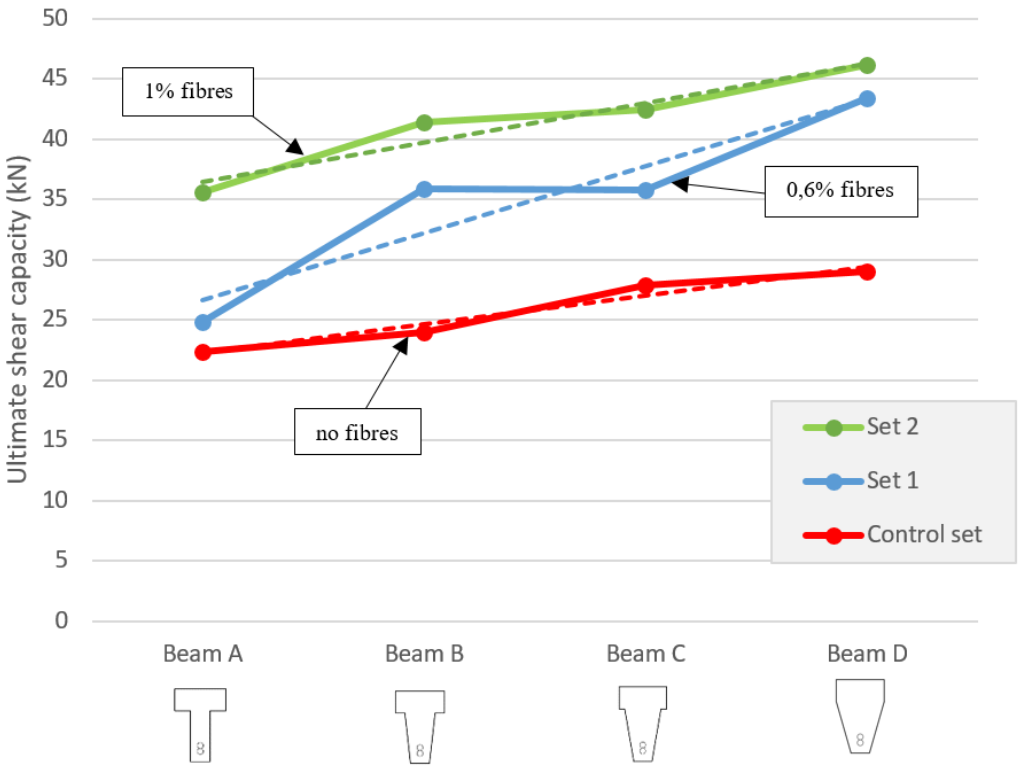

Figure 7.1: Maximum shear capacity for various types of beams and fibre volumes with linear trendlines indicated by dashed lines.

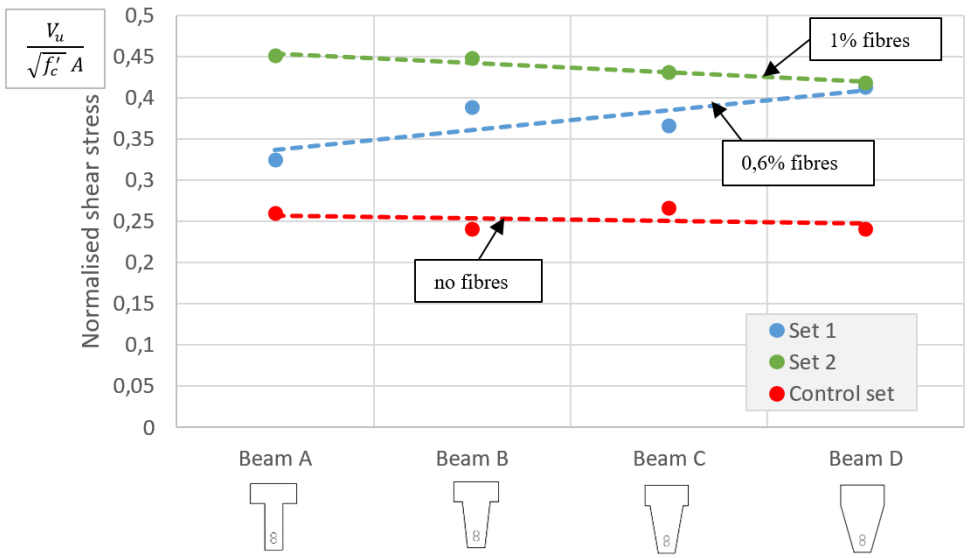

Figure 7.2: Normalised shear stresses for various beam types and fibre volumes with linear trendlines indicated by dashed lines.

7.1.1.2 Comparison of fibre volume

Figures 7.1 and 7.2 show a significant increase in shear capacity, for all beam-types, as the fibre volume increases. The average normalised shear stress at failure for the control set, Set 1 and Set 2 are 0.25, 0.37 and 0.44, respectively. On average, there is an increase of 49% in normalised shear stress at failure for all beam types containing 0.6% fibres and an increase of 74% for beams containing 1% fibres compared to the beams containing no fibres.

Figure 7.3 shows the relationship between fibre volume and shear stresses in the beam at failure. The regression analyses based on the average normalised shear stress for various fibre contents indicates that the normalised shear stress increases as the fibre content increases and results in a R^2 value of 0.996. This means that the normalised shear stress at failure, on average increases approximately by 0.02 per 0.1% fibre volume increase. However, this is not sufficient to conclude that the relationship between normalised shear stress and fibre content is linear and proportional, and further research is required.

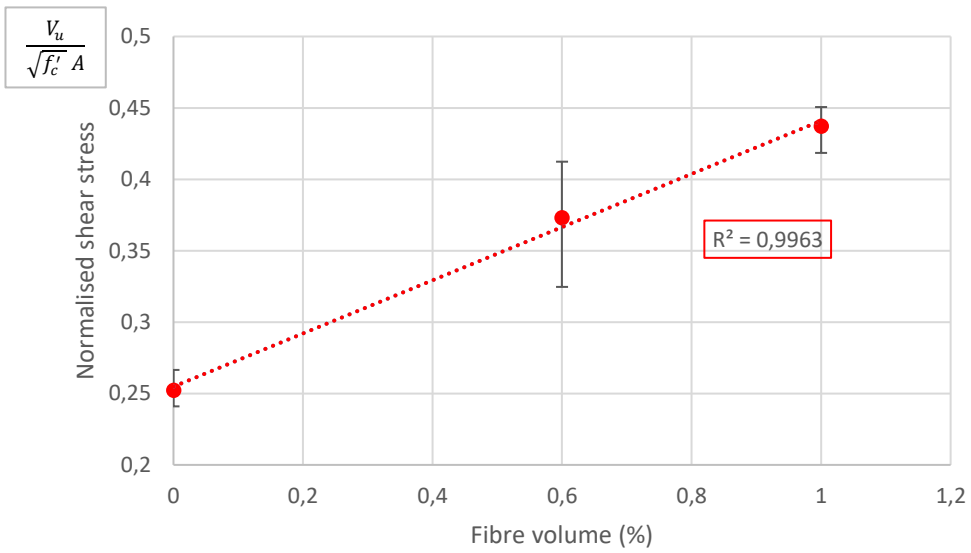

Figure 7.3: Normalised shear stress versus Fibre volume.

7.1.2 Steel fibres as minimum shear reinforcement

According to the criteria of ACI Committee 318 (2005), minimum shear reinforcement must be provided for beams with factored loads that induce normalised shear stresses in the range of 0.085 to 0.17. Moreover, Parra-Montesinos (2006) proposed a conservative lower bound normalised shear stress limit where minimum shear reinforcement is required of 0.3. This is to prevent brittle shear failure that occurs with little or no warning signs prior to failure. Figure 7.4 represents the normalised shear stresses at failure obtained by the beams with various fibre contents tested in this investigation. The minimum shear reinforcement limits proposed by ACI Committee 318 (2005) and Parra-Montesinos (2006) are indicated on the figure as well.

It has been justified that steel fibres can potentially replace stirrup reinforcement in RC beams when minimum shear reinforcement is required (Greenough and Nehdi, 2008). Similar results are obtained in this investigation and are presented in Figure 7.4, where the normalised shear stresses obtained in all beams with 0.6% and 1% fibres are greater than the proposed limit of 0.3 by Parra-Montesinos (2006). The average normalised shear stresses at failure were of 0.37 and 0.44 for 0.6% and 1% fibres, respectively. Conversely, all the control beams with no fibres reached a normalised shear stress below the limit proposed by Parra-Montesinos (2006), with

an average normalised shear stress of only 0.25. However all results fall above the ACI Committee 318 (2005) range of 0.085 to 0.17 where minimum stirrups are required.

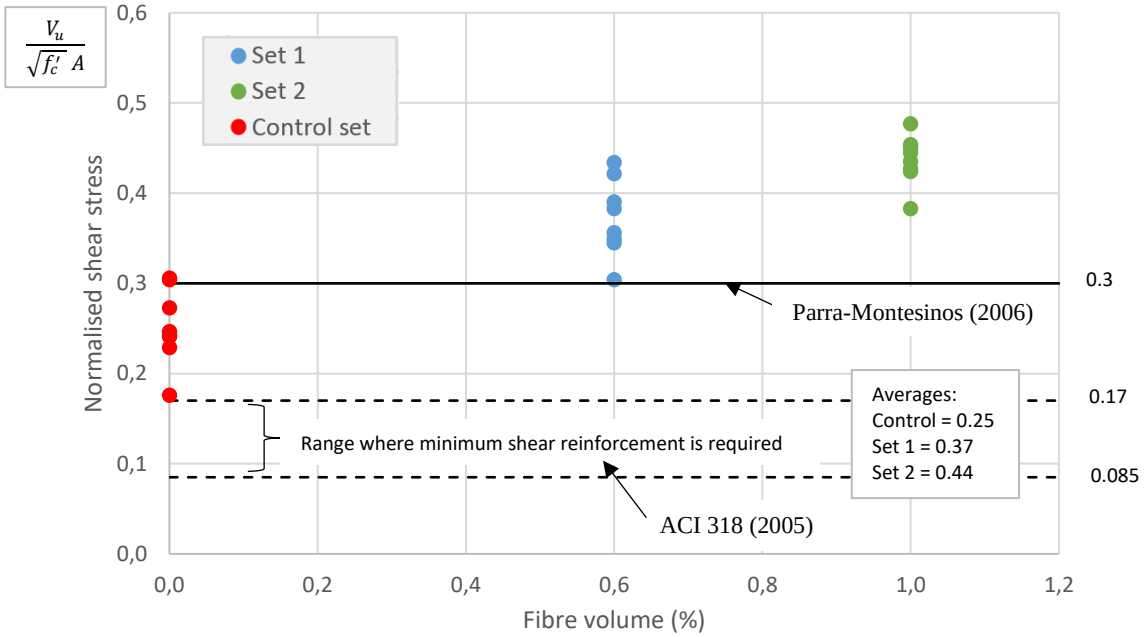

Figure 7.4: Fibres as minimum shear reinforcement.

Although the average normalised shear stresses of beams with 0.6% fibres are higher than the limit proposed by Parra-Montesinos (2006), some beams failed at normalised shear stresses relatively close to the limit of 0.3. It is assumed that if the beam sample size increases some might fail at normalised shear stresses below 0.3. Therefore, the results obtained in this investigation support the suggestion of by Parra-Montesinos (2006) and Greenough & Nehdi, (2008) that 0.75% fibres are sufficient for minimum shear reinforcement. However, this is a bold statement since the shear reinforcement is highly dependent on the type of fibre used and physical properties of the fibres. From the results of this investigation, it is suggested that 0.75% of steel fibres with hooked ends are sufficient for minimum shear reinforcement.

7.1.3 Crack widths

Figure 7.5 presents the average crack widths of all beam-types with various fibre contents. The markers indicate the average crack width values and the dashed lines indicate the best fit linear regression line.

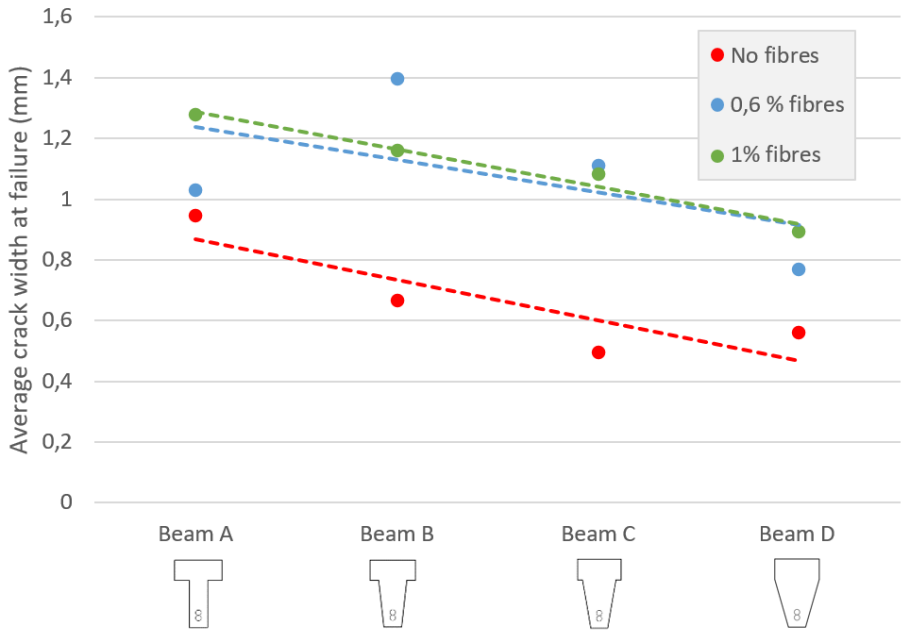

Figure 7.5: Average diagonal crack width at ultimate resistance of various beam types and fibre content with dashed lines indicating linear regression line.

7.1.3.1 Comparison of beam-types

From Figure 7.5 it is noted that the average crack width at ultimate resistance decreases significantly as the web area and, therefore, the cross-sectional area of the beam increases for both beams with and without fibres. From the test results, a decrease crack width from beam-type A to beam-type D of approximately 30% and 45% is observed for beams with and without fibres, respectively. It is assumed that in beams containing fibres, the crack widths at ultimate resistance for larger cross-sectional areas are smaller since more fibres bridge the crack and therefore confine the cracks to some extent. However, similar results are seen in beams containing no fibres. It is reasoned that beams with larger cross-sectional areas are stiffer, therefore, deflect less at a specific load compared to beams with smaller cross-sections. Consequently, cracks are not as wide at the ultimate shear stress in beams with larger cross-sectional areas compared to beams with smaller cross-sectional areas and, therefore, fail at smaller crack widths.

It must be stated that during testing, in some cases with beams containing fibres, additional smaller shear cracks formed within the measuring range of the LVDT. With measurements of

the crack widths using LVDTs, it is impossible to estimate the amount that these additional smaller cracks add to the crack width measurement from the LVDT readings. This suggests that additional research can be done to investigate this phenomenon. The use of Digital Image Correlation (DIC) can give more accurate results.

7.1.3.2 Comparison of fibre volume

Figure 7.5 shows that the average crack widths at the point of maximum resistance is significantly larger in beams with fibres, for all beams types, compared to the reference beams containing no fibres. However, there is no significant difference between beams with 0.6% and 1% fibres, where the regression lines indicate almost identical results. For beam types and beams containing fibres, the average crack width at ultimate resistance is approximately 0.4 mm larger compared to the reference beams. This is a significant increase in crack width of about 40% for beam-type A and 90% for beam-type D. In Chapter 6, it was stated that at lower loads, cracking was more developed in beams without fibres and that fibres enable additional post-cracking strength. In Figure 7.5 it is evident that fibres not only enhance shear capacity but it also enables the beam to carry load at greater crack widths, which points out the ability of fibres to bridge cracks and act as stress transfer bridges.

7.1.4 Crack angles

Figure 7.6 presents the average crack angles for the beams with various fibre volumes that were tested in this investigation. Crack angles on both sides of the beams were measured from photographs that were taken during the testing, as described in Section 5.3.5.3, and the average of both angles was taken as the crack angle of the relevant beam.

No significant difference in crack angle was observed for the various beam-types or the various fibre contents. Even though it has been found in previous investigations that fibres decrease the angle of the critical diagonal crack (Minelli *et al.*, 2014), the diagonal crack angles in this investigation are found to be relatively constant for all fibre volumes and can be seen in Figure 7.6. The different trends in diagonal crack angle of this investigation and the investigation of Minelli *et al.* (2014) is considered to be a consequence of the different beam heights in the relevant investigations. The height of the beams tested by Minelli *et al.* (2014) were significantly larger and ranged between 500 mm and 1500 mm, and the beam heights of this investigation is only 200 mm. Furthermore, beam size effect would have influenced the

results of Minelli *et al.*, (2014), which would not be the case in this investigation due to the small beam height.

The inclination of the critical shear crack for all beams was measured in the range of 30° to 37°, except for beams 1-A.1-FRC0.6 and 1-A.2-FRC0.6, which had crack angles of 41 and 23, respectively. These were considered to be exceptions as all other crack angles were relatively similar. This is comparable to the results obtained from Singh and Jain (2014), which crack angles were measured in the range of 25° to 36°. The average diagonal crack angle for all beams tested in this investigation is approximately 33° to the horizontal.

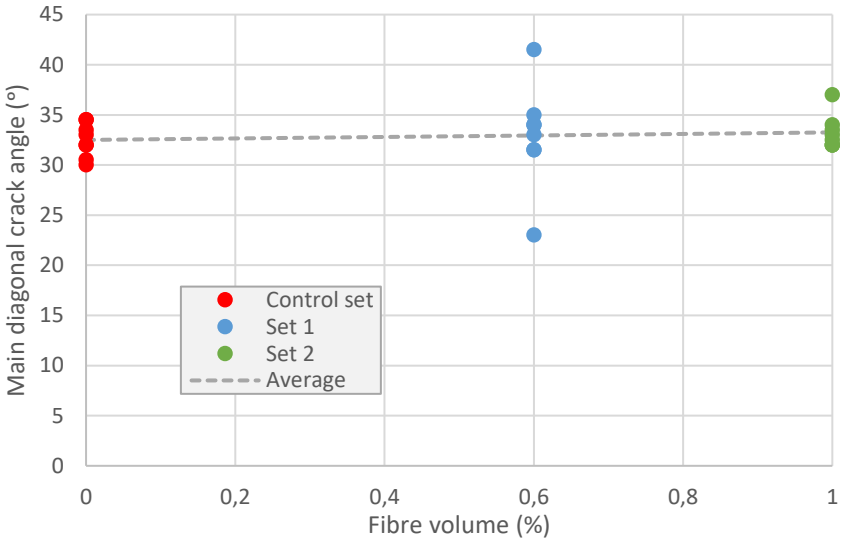

Figure 7.6: Average diagonal crack angles for various fibre volumes.

7.1.5 Crack development

In terms of crack development, there were no significant differences observed for the various beam-types. However, slight variations in final cracking pattern were noted for beams with and without fibres. The typical crack development procedure is explained in Table 7.1 with the aid of images that were taken during testing and the slight differences resulting from fibres are pointed out.

Table 7.1: Typical crack development procedure.

1. The first cracks to appear are flexural cracks that form at the bottom of the beam under or in the close vicinity of the point of load application.	
2. Shortly after, the shear cracks start to appear at approximately mid-height of the web. Bending cracks do not develop much further before the shear cracks appear.	
3. As the load gets increased multiple shear cracks as well as bending cracks form.	
4. Shear cracks develop relatively quickly and propagate from the mid-height of the beam towards the support and point load, spanning almost the whole depth of the beam.	
5. Prior to failure, additional shear cracks form, indicating redistribution of stresses due to fibres. This was not the case in the reference beams containing no fibres.	

All beams failed in shear, where the failure was indicated by rapid propagation and increase in size of shear cracks, followed by a sudden collapse and decrease in load-carrying capacity. In

some cases where beams contained fibres, semi-ductile failure occurred where the drop in load resistance was slightly more gradual compared to beams with no fibres. In some instances bending cracks propagated to become diagonal shear cracks that lead to failure and in other cases initial shear cracks resulted in failure. However, mostly failure was trigger by crushing of the concrete at the point of load application.

The main differences in crack development procedure between the beams containing fibres and the reference beams containing no fibres was firstly, the rate at which shear cracks developed and failure occurred after the first shear cracks appeared and, secondly, the amount of shear cracks that formed during testing. Generally the reference beams failed shortly after the first shear cracks had formed. Shear cracks rapidly increased in size and propagated towards the support and point load with little increase in load. In beams with fibres, crack development was much more stable and failure only occurred at a much later stage and higher loads. This depicts the ability of fibre reinforced beams to support increasing load after diagonal shear cracking due to the stress transfer of fibres bridging over cracks.

Furthermore, in the reference beams fewer shear cracks had formed, typically only one critical shear crack. In beams with fibres multiple shear cracks formed and redistribution occurred prior to failure. Crack development was similar for beams with 0.6% and 1% fibres, no significant differences were observed.

7.2 Application of Shear Models

The experimental results obtained from the tests performed in this investigation are compared to the shear strength predictions of proposed models reported in literature. These models are, however, developed for either webbed T-beams or rectangular beams and have been modified to accommodate the irregular cross-sectional shape of the beams tested in this investigation.

7.2.1 Comparison of Experimental and Predicted results

Table 7.2 represents the mean of the shear strength (MSS) ratios, which is defined as the ratio of the predicted shear strength V_{pr} to the experimental shear strength V_{exp} of the various beams, the standard deviation on the mean strength ratios (SD) and coefficient of variation (COV) for the nine shear models investigated as well as the proposed model of this study. These models

have further been grouped into three groups according to the bases on which they have been developed. These groups include complex, empirical and analytical models. A more detailed version of Table 7.2 can be seen in Appendix C containing all experimental shear strengths measured in this investigation, shear predictions and strength ratios.

Table 7.2: Comparison of predictions of shear models with experimental results.

Model type	***Model proposer***	V_{pr}/V_{exp}		
		MSS	***SD***	***COV***
Complex	MCFT-VEM	0.97	0.15	15.71%
	Spinella *et al.* (2010)	1.03	0.17	16.60%
Empirical	fib Model code 2010 (2010)	1.07	0.13	12.32%
	Li *et al.* (1992)	1.13	0.17	15.39%
	Kwak *et al.* (2002)	0.97	0.15	15.02%
Analytical	Swamy *et al.* (1993)	1.60	0.35	21.57%
	Mansur *et al.* (1987)	1.01	0.17	16.85%
	Dinh *et al.* (2011)	1.03	0.11	10.36%
	Singh and Jain (2014)	0.92	0.09	9.37%
	Proposed model	0.95	0.10	10.97%

Table 7.2 shows that an overwhelming majority of the proposed models predict relatively accurate shear strengths with considerably small standard deviations although these models had to be slightly modified for this investigation. The model proposed by Swamy *et al.* (1993) is the only exception, which predictions are significantly higher than the measured shear strengths with MSS ratio of 1.60 and SD of 0.35 resulting in COV of 21.57%. Another model that slightly predicts unconservative shear strengths is the model proposed by Li *et al.* (1992), with a MSS ratio of 1.13 and SD of 0.17. However, since this model is based on an empirical approach, variations in materials used in the various investigation could lead to these results.

The MSS ratios of the other models are in the range of 0.92 to 1.07 with SD ranging only between 0.09 and 0.17. Since the majority of the models performed relatively well in terms of predicting the strength of the tested beams, it is difficult to point out any specific model as being the best. However, the model proposed by Dinh *et al.* (2011), the model proposed in the fib Model code 2010 (FIB, 2010b) and the dated model of Mansur *et al.* (1987) are considered to be the preferred models according to the performance in this investigation in predicting the shear strengths. The model of Dinh *et al.* (2011) has a good MSS ratio of 1.03 and SD of 0.11.

The model proposed in the fib Model code 2010 (FIB, 2010b) predicts slightly higher shear strengths with MSS ratio of 1.07 but has SD of 0.13. The model of Mansur *et al.* (1987) has MSS ratio of 1.01 but has a slightly higher SD of 0.17. Similar to the model of fib Model code 2010 (FIB, 2010b), the model proposed by Singh and Jain (2014) has a low SD of 0.09 but does predict conservative shear strengths with MSS ratio of 0.92. The complex models performed similarly with slightly larger SD. The model proposed by Spinella *et al.* (2010) had MSS ratio of 1.03 and SD of 0.17. The MCFT-VEM model and the model proposed by Kwak *et al.* (2002) had MSS ratios of 0.97 and SD of 0.15.

The model proposed in this investigation performed considerably well, predicting slightly conservative shear strengths, which is favourable, with a MSS ratio of 0.95 and a low SD of 0.10. Comparing the proposed model to all other models, it is one of the more accurate shear prediction models.

A comparison of the experimental shear strengths with the predictions of the various shear models compiled in Table 7.2 is presented graphically in Figure 7.7 to 7.10. It must be mentioned that these results are based only on the experimental results from this investigation. As the database with results of ISB tested in shear increases, the accuracy in shear predictions associated with each model may change considerably.

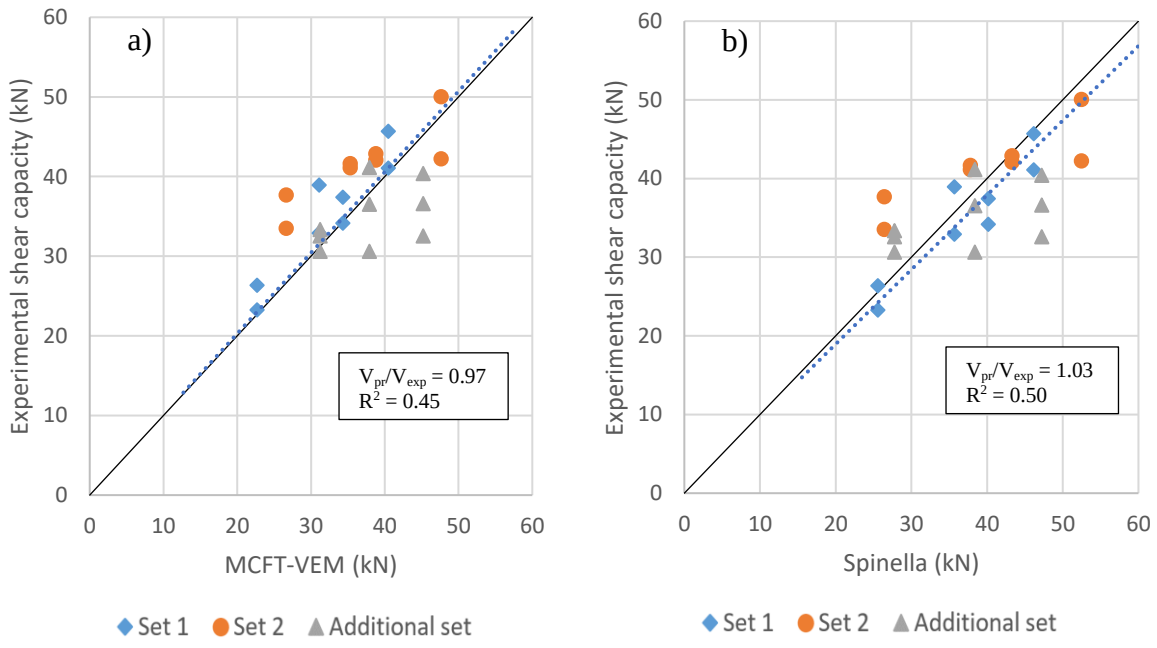

Figure 7.7: Comparison of experimental and predicted results by complex models.

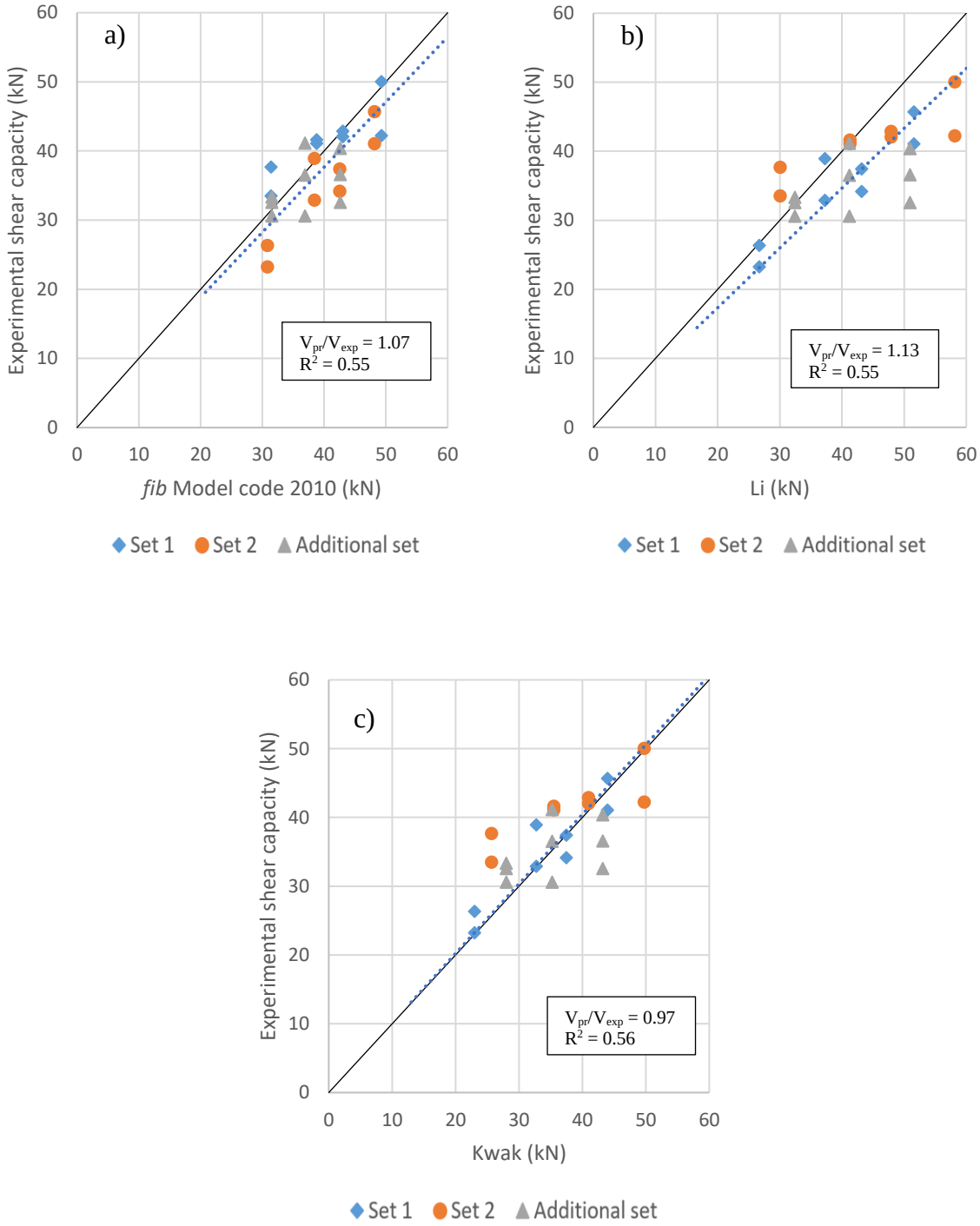

Figure 7.8: Comparison of experimental and predicted results by empirical models.

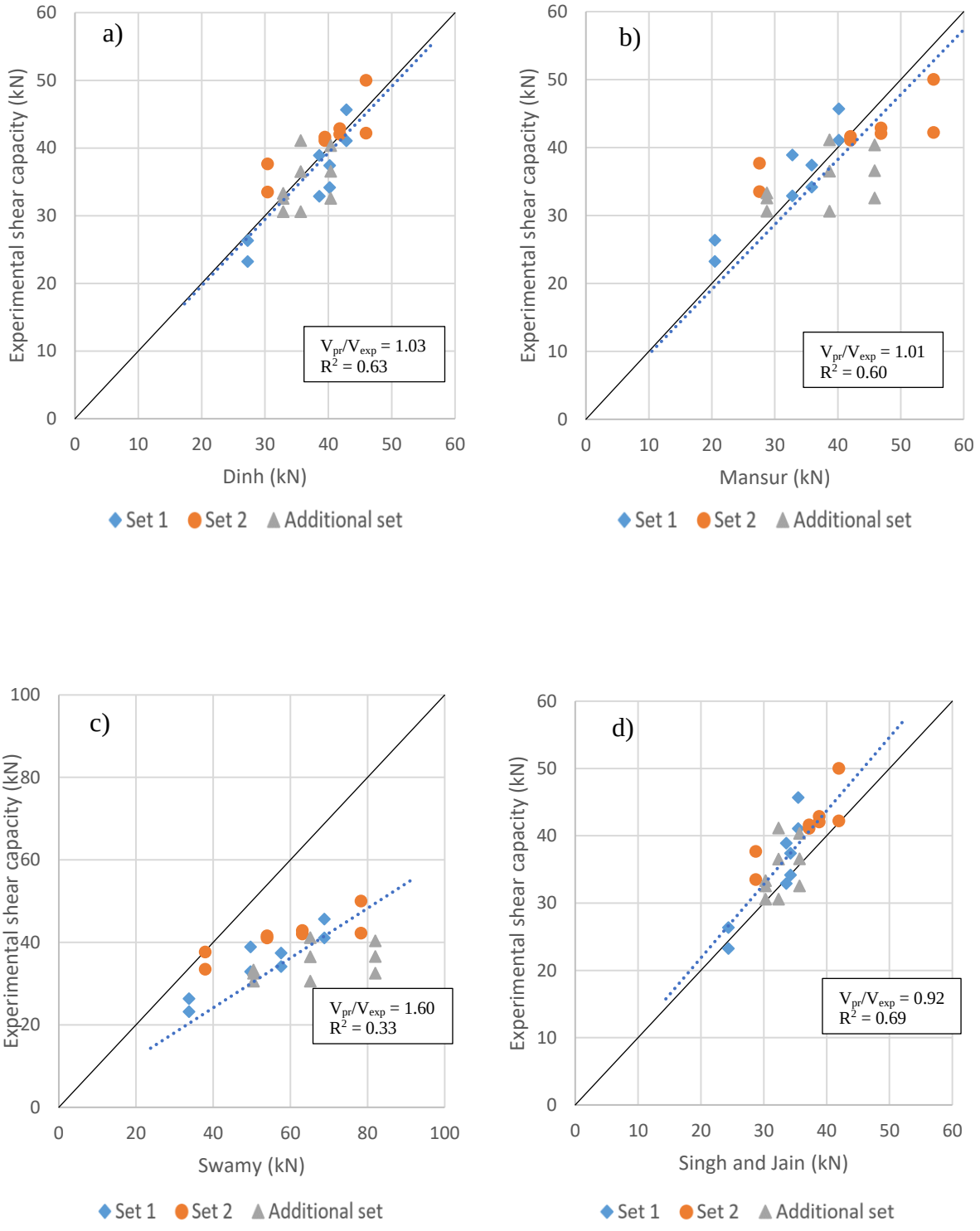

Figure 7.9: Comparison of experimental and predicted results by analytical models.

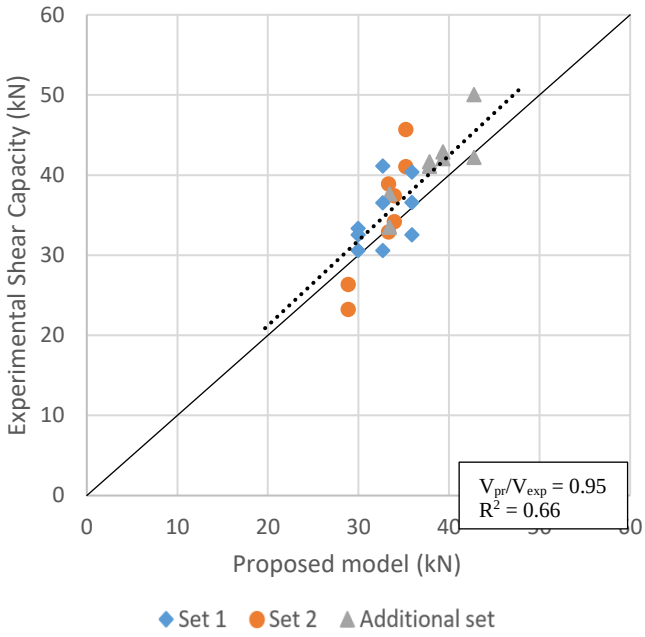

Figure 7.10: Comparison of experimental and predicted results of the proposed model.

Figure 7.7 to 7.10 the experimental measured shear strengths from 25 beam tests performed on various ISB with fibre volumes of either 0.6% or 1% are compared to the shear strength predictions of nine various shear models reported in the literature and a model proposed in this investigation. Strength ratios and coefficients of determination R^2 are presented on the figures to indicate the precision of the investigated shear models.

The coefficients of determination for the shear models range between 0.33 and 0.69. The model proposed by Swamy *et al.* (1993) has a significantly low R^2 –value of 0.33. The highest R^2 –value was obtained by the model proposed by Singh and Jain (2014) of 0.69. The majority of the models have R^2 –values ranging between 0.5 and 0.6. The model proposed in this investigation obtained an R^2 –value of 0.66, which is the second highest of all the models. Therefore, this model is considered as a relatively accurate shear strength prediction model.

Figure 7.11 represents a summary of the comparisons of the predicted and experimental shear strengths indicating the accuracy and precision of the shear models. From this figure an accurate and precise model can easily be identified, in which the mean strength ratio and R^2 –value are close or equal to 1 (black line), and the COV is as low as possible. Following these

guidelines, the favoured models are fib Model code 2010 (FIB, 2010b), Mansur *et al.* (1987), Dinh *et al.* (2011) and the proposed model.

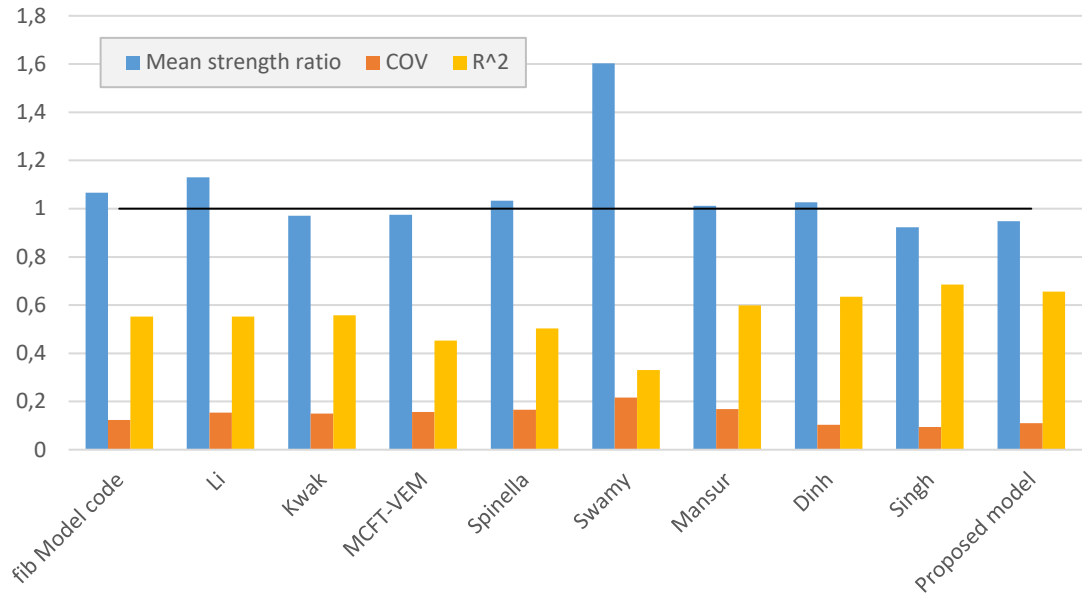

Figure 7.11: Summary of comparison of predicted and experimental results for various shear strength models.

7.2.2 Shear predictions of conventional shear models

As previously mentioned, shear failure is always a non-desired failure mode due to its brittle and sudden formation and thus, existing shear models were often proposed with an over-conservative formulation by assuming that shear is resisted only by the web or by an effective cross-sectional area calculated as $b_w \cdot d$. The MSS ratios of conventional shear models for simplified rectangular sections are presented in Figure 7.12 for the various beam-types tested in this investigation (beam set 1 & 2). The original shear models, considering the simplified rectangular cross section, were used to predict the shear strength of the various beam-types.

It is clear that as the area of the web increases the shear predictions of the conventional shear models are significantly over-conservative, and certain models predicted a shear strength of just over half the experimental shear strength for beams of type D when considering the simplified rectangular section. This proves that considering the whole cross sectional area of

the web leads to more accurate shear predictions and when considering only the simplified rectangular section, shear strengths are

Comparing the MSS ratios of the conventional shear models to the MSS ratios of the proposed model it can be seen that in beams where conventional shear models predict over-conservative shear strengths, the proposed model predicts accurate shear strengths. From Figure 7.12 it can be seen that the shear models predict relatively accurate shear strengths for beam-type A, however, the shear predictions get more conservative as the beam cross-section increases. Since the proposed model uses the full web cross-sectional area in predicting the shear strength, the predictions are accurate for all beam-types.

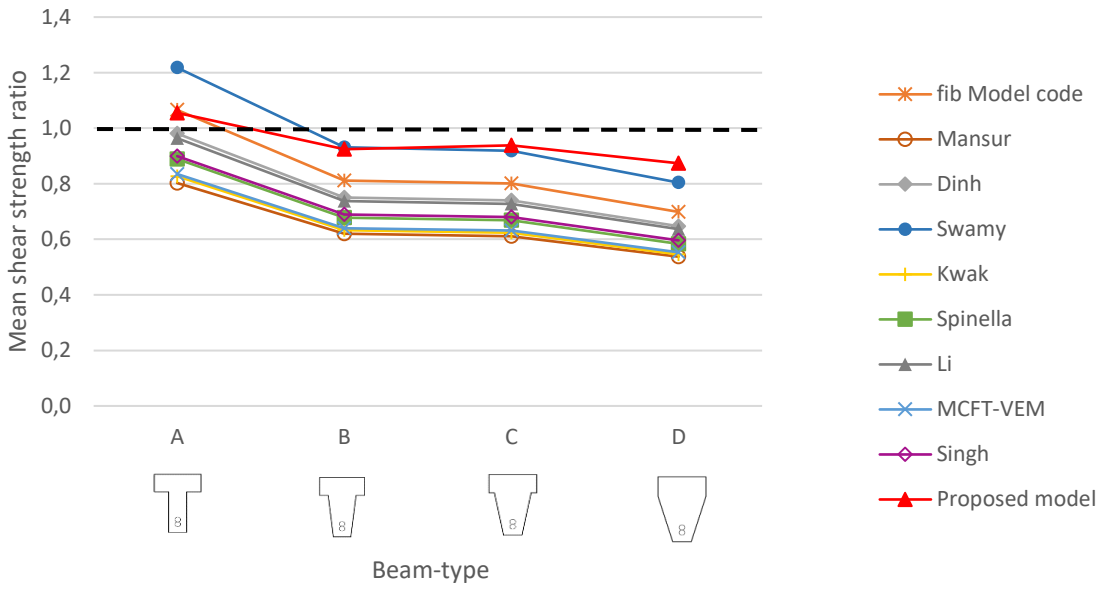

Figure 7.12: Shear predictions of conventional shear prediction models

7.2.3 Parameter study of the diagonal crack inclination

One of the input parameters required in the shear model that is proposed in this investigation is the inclination of the main diagonal shear crack α. This angle determines the cross-sectional area over which fibres bridge cracks and transfer tensile stresses over the crack face. Consequently, this angle has a major influence on the shear strength prediction of a particular beam. For the application of the proposed model in this investigation, the exact crack angle was measured for every individual beam that was tested and was then used as input parameter

to obtain accurate shear strength predictions. However, when this model is to be applied by a structural designer in practice, the diagonal shear crack angle will be unknown and the designer will be responsible to use engineering judgement in order to choose an appropriate angle for the application of this model.

A parameter study is performed on the inclination of the main diagonal shear crack to determine the influence that this angle has on the shear strength prediction for the various beam types tested in this investigation. For the purpose of this study, an assumption is made that the inclination of the compression strut in a particular beam corresponds to the angle of the diagonal shear crack. Limits on the angle between the concrete compression strut and the beam's axis perpendicular to the shear force *(θ),* proposed in EN1992-1-1, of $1 \leq \cot(\theta) \leq 2.5$ is used as a guide for the diagonal shear crack angles used in the parameter study. These limits result in α ranging from 22° to 45°. The input parameters used for the parameter study are listed in Table 7.3, and the results are presented graphically in Figure 7.13.

Table 7.3: Input parameters used in parameter study.

Concrete properties		
Cylinder compressive strength (f'_c)	28	MPa
Fibre properties		
Volume fraction (V_f)	1	%
Diameter (d)	1.05	mm
Length (L)	50	mm
Modulus of elasticity (E)	200	GPa
Ultimate tensile strength (σ_u)	1115	MPa
Longitudinal reinforcing details		
Yield stress (f_y)	500	MPa
Reinforcing area (A_s)	402	mm^2
Modulus of elasticity (E)	200	GPa

The normalised shear stresses for diagonal shear crack angles in the range of $22° \leq \alpha \leq 45°$ for the various beam-types obtained from the prediction of the proposed shear model are shown in Figure 7.13. An indication of the influence of the diagonal crack angle on predicted shear strength of a beam is given. The black dashed line represents the minimum shear stress limit for a beam proposed by ACI Committee 318 (2008).

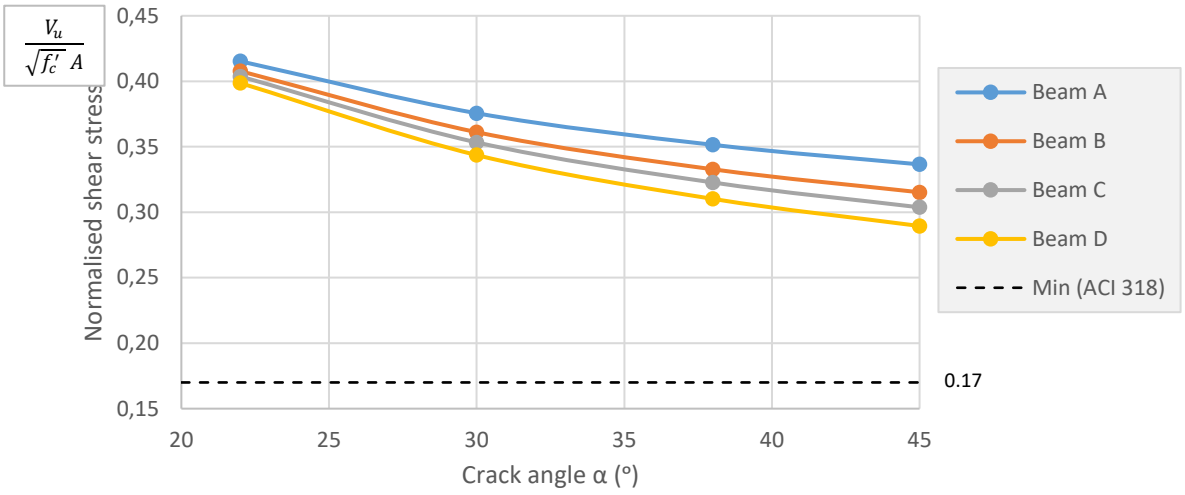

Figure 7.13: Parameter study on the influence of the diagonal shear crack inclination of the prediction of shear strength.

There is a significant decrease in shear strength prediction as the assumed diagonal crack angle increases from 22° to 45° for all types of beams. However, in Figure 7.13 it can be seen that the cross-sectional area of the web also influences the shear strength. Shear strength decreases at a higher rate as the shear crack angle increases for beams with larger web cross-sectional area. From a diagonal crack angle of 22° to 45° the shear strength decreases by 19% for beam-type A with a web area of 7000 mm^2 and it decreases by 27% for beam-type D with a web area of 12 600 mm^2. The cross-sectional area in the plane of the diagonal crack, over which the fibres transfer stresses, is influenced more in beams with larger web cross-sectional areas as the inclination of the diagonal crack changes.

However, to facilitate the prediction of shear strength of a beam using the proposed model (Eq 4.12), it is recommended that α is to be chosen in the range of $30^o \leq \alpha \leq 35^o$ which corresponds to the average diagonal crack angle obtained in this investigation of 33°. This value of α is comparable to the average diagonal shear crack inclination obtained in the investigations of Dinh *et al.* (2011) and Singh and Jain (2014) of 29° and 30°, respectively.

7.3 Concluding summary

This chapter describes the influences that the various beam-types and fibre contents have on the shear behaviour of ISB and the shear prediction models are evaluated by comparing the predicted and experimental shear capacities of the various beams.

It was found that fibre volume significantly increases the shear capacity of all types of beams and the normalised shear stresses for the various beam-types are relatively constant but increase as fibre volume increases. It is suggested that 0.75% of hooked-end steel fibres are sufficient for minimum shear reinforcement requirements. Furthermore, fibres increase the crack width at ultimate resistance, however, crack width decreases as cross-sectional area increases. No significant influence was observed in the inclination of the diagonal shear crack.

The modified shear prediction models predict relatively accurate results with the exception of the model proposed by Swamy *et al.* (1993). The proposed model also predicts relative accurate results with MSS of 0.95 and SD of 0.10.

The conclusions drawn from the results in this chapter are strictly applicable to V-beams with simply supported end conditions. Considering the efficiency of these V-beams with continuous support conditions raises some concern. In such a case, hogging moments form at the locations of supports resulting in a shift of the compression zone. This would potentially influence the individual contributions of the various shear mechanisms and ultimately affect the shear behaviour of V-beams. Further research should be conducted to investigate this matter.

CHAPTER 8

CONCLUSIONS AND RECOMMENDATIONS

8.1 Conclusions

This research investigated the shear behaviour of irregular shaped beams (ISB) containing various fibre volumes and to propose a shear model that can accurately predict the shear strength of such beams containing only longitudinal reinforcement and steel fibres. The irregular shapes of the beams are inspired by the shape of an optimised simply supported beam formed with fabric formwork. This research consists of three main parts, namely the development of steel fibre reinforced self-compacting concrete (SFR-SCC) that is suitable for the use of ISB, the physical testing of beams to investigate the effect on shear behaviour of irregular sections and various fibre contents, and the investigation of various existing FRC shear models and the proposal of a shear model for ISB.

The following conclusions can be drawn from investigating the influence of irregular sections on the shear behaviour of beams:

- The normalised shear stresses at failure for beam-type A (T-beam with constant web thickness throughout the depth of the beam) to beam-type D (V-shape webbed beam

with increasing web thickness from the bottom to the top of the web) were relatively constant. All beam-types failed at the same shear stresses, indicating that the shear strength of an ISB is proportional to the cross-sectional area.

- Larger cross-sectional areas due to increased web areas significantly increase the shear strength of the beams. This indicates that the web area significantly influences the carrying capacity of the beam and should not be ignored when predicting the shear strength of ISB with V-shaped webs.
- Crack widths at ultimate resistance area significantly influenced by the cross-sectional area of the beam. A linear reduction in crack width at ultimate resistance is observed as the cross-sectional area of the beams increases, i.e. crack widths at ultimate resistance decrease from beam-type A (T-beams) to beam-type D (V-shape webbed beams).
- Diagonal shear crack angles are not influenced by the beam-type and are similar for all beams. An average diagonal shear crack angle of 33° was measured for all beams.

The conclusions drawn for the influence of fibre content on the shear behaviour of ISB are:

- Fibres increase the shear strength of ISB. There is an average increase in maximum shear stresses, for the various beam types of 49% for beams with 0.6% fibre content and 74% for beams with 1% fibre content compared to beams with no fibres.
- Normalised shear stress increases as fibre content increases and a regression analyses on the average normalised shear stress at ultimate resistance and fibre content resulted in a R^2-value of 0.996. However, further research is required to conclude that the relationship is linear and proportional.
- Fibres have the potential to change the failure mode from a dangerous brittle failure to a more desirable semi-ductile failure. However, in beams where fibres significantly increase the ultimate load, brittle failures are still likely to occur.
- Similar to Parra-Montesinos (2006) and Greenough & Nehdi, (2008), it is proposed that 0.75% of hooked-end steel fibres are sufficient for minimum shear reinforcement.
- Fibres increase the crack width at ultimate resistance. An increase of approximately 0.4 mm is observed in beams containing fibres compared to beams with no fibres. However, no significant difference was seen in beams containing 0.6% and 1% fibres. This depicts the ability of fibres to enhance the load carrying capacity after diagonal cracking has occurred. This is due to fibres bridging the cracks and allowing for stress transfer resulting in increased shear capacity.

- From the final cracking pattern, it was observed that fibres increase the amount of cracks formed during testing. In beams containing fibres, multiple smaller shear cracks form alongside the main diagonal shear crack during testing prior to failure. In beams with no fibres, fewer shear crack formed where mostly one dominant shear crack formed which eventually caused shear failure. However, there was no noticeable difference in shear cracking between beams containing 0.6% and 1% fibres.
- In this investigation, the angle of the main diagonal shear crack was not significantly affected by the addition of fibres. An average diagonal shear crack angle of 33° to the horizontal was measured for all beams tested in this investigation. This finding is contradictory to other investigations reported in literature in which fibres content significantly reduces the angle at which the diagonal shear crack forms.
- Fibres significantly influence the rate at which shear cracks form in beams. Fibres reduce the rate at which shear cracks propagate towards the support and point of load application, after they have formed at approximately mid-height of the web. In beams with no fibres, failure occurs shortly after the first shear cracks appear. In beams containing fibres, cracks propagate steadily with a significant increase in load-carrying capacity. Therefore, members containing fibres display sufficient warning signs before failure.

The following conclusions can be drawn from the investigation of the existing shear models that have been modified for ISB and the model proposed in this investigation:

- Most of the existing shear models used in this investigation predicted accurate shear strengths for the tested ISB by modifying them as described in Section 4.1 with the exception of the model proposed by Swamy *et al.* (1993). This method of modifying the models incorporates the whole cross-sectional area of the web and the part of the flange above the web with the same width as the top of the web. Without considering the results predicted by the model proposed by Swamy *et al.* (1993) the mean shear strength (MSS) ratio of all other shear models is 1.01 with an average standard deviation (SD) on the mean shear strength ratio of 0.14 and average coefficient of variation (COV) of 13.62%.
- The empirical model proposed by Li *et al.* (1992) predicted slightly higher shear strengths than the measured shear strengths obtained from the experiments. Therefore

using this model to predict shear strengths for ISB will result in unconservative shear strength predictions.

- The widely used semi-empirical shear prediction formula proposed by the *fib* Model code (2010) predicts relatively accurate shear strengths for ISB when the term $(b_w \cdot d)$ is replaced by an alternative effective area proposed in Section 4.1. The MSS ratio for the model proposed in *fib* Model code (2010) is 1.07 with a SD of 0.13 and COV of 12.32%.
- The simple mechanics-based analytical shear prediction model proposed in this investigation predicts accurate and slightly conservative shear strengths for ISB with MSS ratio of 0.95, a SD of 0.10 and a COV of 10.97%. The proposed model considers only the shear contribution of the concrete compression block and the contribution of the tensile resistance of steel fibres. The model is based on the characteristics of deformed steel fibres and the mechanical properties of concrete and is only applicable to longitudinal reinforced beams containing steel fibres and no transverse reinforcement. The proposed model is simple and can easily be used by designers in practice.
- The shear predictions of the proposed model are highly dependent on the diagonal shear crack angle α chosen by the designer using the model. It is recommended that the diagonal shear crack angle is chosen in the range of $30^o \leq \alpha \leq 35^o$ for design purposes with larger angles resulting in slightly more conservative predictions.

8.2 Recommendations for future research

The following recommendations for future research can be considered:

- The methodology of this investigation could be repeated to obtain more test result which can be used to set up an established database with test results of ISB tested in shear. In future investigations, it should be considered to change various parameters for testing such as:
    - Fibre length, aspect ratio and volumes
    - Concrete compressive strength
    - Shear span-to-effective depth ratio
    - Beam dimensions

- Since this investigation focuses mainly on the irregularity if the beam sections inspired by beams formed in fabric formwork, more research could be done to investigate the effect that varying section depth along the length of the beam has on shear behaviour by casting beams using fabric formwork. This can eventually be used to understand the shear behaviour of FFB.
- Although the proposed model gave accurate predictions compared to the experimental results it is suggested that more similar tests are performed and a larger test database is used to verify the proposed model further. More research is required to study the reliability of this model, and design values need to be established taking into account material variability and model variability.
- It is suggested that DIC is used in future investigations to obtain more accurate measurements, especially when measuring crack widths and investigating cracking pattern.
- Further research is required to investigate the shear contribution of the flange as this investigation focuses mainly on varying web parameters.
- Significant research has been conducted to investigate the various parameters that contribute to shear resistance. However, it is suggested that further research is conducted to study the synergetic effect of these various shear mechanisms. Most shear models superimpose the shear contribution of individual shear parameters even though it plausible that specific shear mechanisms are interdependent, especially when using fibres.
- The pouring procedure used to pour the ISB in this investigation was adopted from BS EN 14651-A1, however, this procedure ensures optimum fibre orientation for beams tested in bending. In the case where beams are testd in shear an alternative pouring procedure might result in optimum fibre orientation for beams tested in shear. It could be more suitable to start pouring the beams from the sides in order tio guarentee a correct fibre orientation in the shear span.

CHAPTER 9

REFERENCES

Abdelgader, H., West, M. & Górski, J. 2008. State-of-the-Art Report on Fabric Formwork. *International Conference on Construction and Building Technology*. 08:93-106.

ACI Committee 318. 2008. *Building code and commentary*. ACI 318-08/318R-08. Farmington Hills. American Concrete Institute.

ASTM C1609. 2019. *Standard Test Method for Flexural Performance of Fiber-Reinforced Concrete (Using Beam With Third-Point Loading)*. West Conshohocken. ASTM International.

ASTM C1621. 2017. *Standard Test Method for Passing Ability of Self-Consolidating Concrete by J-Ring*. West Conshohocken. ASTM International.

Bazant, Z. P. & Kim, J. 1984. Size Effect in Shear Failure of Longitudinally Reinforced Beams. *ACI Journal*. 81:456-468

Bentz, E. C. 2005. Empirical Modeling of Reinforced Concrete Shear Strength Size Effect for Members without Stirrups. *ACI Journal.* 102:232-241.

Bentz, E. C., Vecchio, F. J. & Collins, M. P. 2006. Simplified Compression Field Theory for Calculating Shear Strength of Reinforced Concrete Elements. *ACI Structural Journal*. 103(4):614–624.

Bresler, B. & Pister, K. S. 1958. Strength of concrete under combined stress. *Cement and Concrete Research*. 55(9):321–345.

Buratti, N., Mazzotti, C. and Savoia, M., 2011. *Post-cracking behaviour of steel and macro-synthetic fibre-reinforced concretes.*

Chandler, A. & Pedreschi, R. 2007. Fabric Formwork. London: RIBA Publishing.

Dinh, H. H., Parra-Montesinos, G. J. & Wight, J. K., 2011. Shear strength model for steel fiber reinforced concrete beams without stirrup reinforcement. ASCE Journal of Structural Engineering. October. 137(10):1039-1051.

EFNARC, 2002. *Specification and Guidelines for Self-Compacting Concrete.* February 2002, www.efnarc.org.

EN 14651-A1:2007. Test method for metallic fibered concrete - Measuring the flexural tensile strength (limit of proportionality (LOP), residual). *BSI Standards Publication.*

EN 14889-2, 2006. *Fibres for Concrete: Part 2: 2006. Polymer Fibres: Definitions, specifications and conformity.*

EN 1992-1-1:2004. Eurocode 2: Design of concrete structures. Part 1-1: General rules and rules for buildings. Brussels. European Committee for Standardization: 2004.

EN 206-1:2000. Concrete - Part 1: Specifications, performance, productionand conformity. *BSI Standards Publication.*

EN 8110-1:1997. Structural use of concrete - Part 1: Code of practice for design and construction. *BSI Standards Publication.*

FIB. 2010a. *Model Code 2010*. Bulletin 65. Laussanne, Switzerland.

FIB. 2010b. *Model Code 2010*. Bulletin 66. Laussanne, Switzerland.

FIB. 2010c. *Shear and punching shear in RC and FRC elements*. Bulletin 57. Laussanne, Switzerland.

Firth, I. 2018. *Bridges should be beautiful* [Online]. Available: https://www.ted.com/talks/ian_firth_bridges_should_be_beautiful?language=en. [2018, June 25].

Foster, S. J., Voo, Y. L. & Chong, K. T. 2006. FE Analysis of Steel Fiber Reinforced Concrete Beams Failing in Shear: Variable Engagement Model. *ACI Special Publications*. 237: 55-70.

Frosch, R. J. 2001. Behavior of Large-Scale Reinforced Concrete Beams with Minimum Shear Reinforcement. *ACI Structural Journal*. 97:814–820.

Gao, T., Shen, L., Shen, M., Chen, F., Liu, L. & Gao, L. 2015. Analysis on differences of carbon dioxide emission from cement production and their major determinants. *Journal of Cleaner Production*. 103:160–170.

Greenough, T. & Nehdi, M. 2009. Shear Behavior of Fiber-Reinforced Self-Consolidating Concrete Slender Beams. *ACI Structural Journal*. 105:468-477.

Illstone, J.M. & Domone, P.L.J. (eds). 2001. Construction Materials: their nature and behaviour. 3rd ed. New York: Spon Press.

Kong, F. K. & Evans, R. H., 1987. Reinforced and pre-stressed concrete. 3rd ed. Wokingham, England: Van Nostrand Reinhold

Kotsovos, M. D., Bobrowski, J. & Eibl, J. 1987. Behaviour of reinforced concrete T-beams in shear. *The Structural Engineer*. March. 65:1-10.

Kwak, Y., Eberhard, M. O., Kim, W. & Kim, J., 2002. Shear strength of steel fiber-reinforced concrete beams without stirrups. *ACI Structural Journal*, 99(4):530-538.

Lee, D. S. H. 2010. Study of construction methodology and structural behaviour of fabric formed form-efficient reinforced concrete beam. PhD Thesis, School of Architecture and Landscape Architecture, 2010.

Li, V. C., Ward, R. & Hamza, A. M. 1992. Steel and Synthetic Fibres as Shear Reinforcement. *ACI Structural Journal. 89(5):499–508.*

Mansur, M. A., Ong, K. C. G. & Paramasivam, P., 1987. Shear strength of fibrous concrete beams without stirrups. *ASCE Journal of Structural Engineering*, September. 112(9):2066-2079.

Martín-Pérez, B., Zibara, H., Hooton, R. D. & Thomas, M. D. A. 2000. A study of the effect of chloride binding on service life predictions. *Cement and Concrete Research*. 30(8):1215–1223.

Minelli, F., Conforti, A., Cuenca, E. & Plizzari, G., 2014. Are steel fibres able to mitigate or eliminate size effect in shear? *Materials and Structures*, April, 47:459–473.

Mohammadi, Y., Singh, S. P. & Kaushik, S. K. 2008. Properties of steel fibrous concrete containing mixed fibres in fresh and hardened state. *Construction and Building Materials* 22:956–965.

Okamura, H., Ouchi, M., 1999. Self-Compacting Concrete. Development, Present Use and Future. *First Int. Symposium on SCC*. Stockholm, Edited by Skarendahl and Petersson, RILEM publications PRO 7, Cachan, pp. 3-14.

Orr, J., Darby, A., Ibell, T., Evernden, M., & Otlet, M. 2011. Concrete structures using fabric formwork. *Structural Engineer*, 89(8):20-26.

Orr, J. J., Ibell, T. J., Darby, A. P. & Evernden, M. 2013. Durability enhancements using fabric formwork. *Magazine of Concrete Research*, 65(20):1236–1245.

Orr, J. J., Ibell, T. J., Darby, A. P. & Evernden, M. 2014. Shear behaviour of non-prismatic steel reinforced concrete beams. *Engineering Structures*. 71:48–59.

Pajak, M. & Ponikiewski, T. 2017. Experimental Investigation on Hybrid Steel Fibers Reinforced Self-compacting Concrete under Flexure. *Procedia Engineering*. 193:218–225.

Parra-Montesinos, G. J., 2006. Shear strength of beams with deformed steel fibers - Evaluating an alternative to minimum transverse reinforcement. *Concrete International*, November. pp. 57-66.

Ponikiewski, T. & Golaszewski, J. 2013. Properties of steel fibre reinforced self-compacting concrete for optimal rheological and mechanical properties in precast beams. *Procedia Engineering*. 65:290–295.

SANS. 2000. SANS 10100-1. *The structural use of concrete Part 1: Design.*South Africa

SANS. 2006a. SANS 5863 *Concrete tests- Compressive strength of hardened concrete.* South Africa.

SANS. 2006b. SANS 5862-1. *Concrete tests- Consistence of freshly mixed concrete- Slump test.* South Africa

SANS. 2010. SANS 68921-1. *Metallic materials - Tensile Testing, Part 1: Method of test at room temperature.* South Africa

SANS 50450-1:2014: *Fly ash for concrete, Part 1: Definition, specifications and conformity criteria*. Pretoria: South African Bureau of Standards.

SCCEP Group, 2005. *The European Guidelines for Self-Compacting Concrete: Specification, Production and Use.* May 2005, www.efca.info or www.efnarc.org.

Shi, C., Wu, Z., Lv, K. & Wu, L. 2015. A review on mixture design methods for self-compacting concrete. *Construction and Building Materials.* 88:387-398.

Singh, B. & Jain, K. 2014. Appraisal of steel fibers as minimum shear reinforcement in concrete beams. *ACI Structural Journal*. 111(5):1191–1202.

Spinella, N., Colajanni, P. and Recupero, A. 2010. Simple Plastic Model for Shear Critical SFRC Beams. *ASCE Journal of Structural Engineering*, April. 136(4):390–400.

Steffens, A., Dinkler, D. & Ahrens, H. 2002. Modeling carbonation for corrosion risk prediction of concrete structures. *Cement and Concrete Research.* 32(6):935–941.

Su, N., Hsu, K. & Chai, H. 2001. A simple mix design method for self-compacting concrete. *Cement and Concrete Research.* 31:1799-1807.

Suryavanshi, A. K. & Swamy, R. N. 1997. An Evaluation of Controlled Permeability Formwork fro long-term durability of structural concrete elements. *Cement and Concrete Composites*. 27(7):1047–1060.

Swamy, R. N. & Mangat, P. S. 1976. The Interfacial bond stress in Steel Fiber Cement Composites. *ACI Structural Journal.* 6:641–649.

Swamy, R. N., Jones, R. & Chiam, A. T. P. 1993. Influence of Steel Fibres on the Shear Resistance of Lightweight Concrete I-beams. *ACI Structural Journal.* 90:103–114.

Thamrin, R., Tanjung, J., Aryanti, R., Nur, O. F. & Devinus, A. 2016. Shear strength of reinforced concrete T-beams without stirrups. *Journal of Engineering Science and Technology*. 11(4):548-562.

Tung, N. D. & Tue, N. V. 2016. A new approach to shear design of slender reinforced concrete members without transverse reinforcement. *Engineering Structures*. 107:180–194.

Tung, N. D. & Tue, N. V. 2018. Shear resistance of steel fiber-reinforced concrete beams without conventional shear reinforcement on the basis of the critical shear band concept. *Engineering Structures*. 168: 698–707.

Vandewalle, L., Heirman, G. & Van Rickstal, F. 2008. Fibre Reinforced Concrete: Design and Application. *Fibre orientationin self-compacting fibre reinforced concrete.* Chennai. RILEM Publications SARL, Bagneux, pp. 719-728.

Voo, J. Y. L. & Foster, S. J. S. J. 2003. Variable Engagement Model for the Fibre Reinforced Concrete in Tension. *Advanced Materials for Construction of Bridges, Buildings, and Other Structures III*. 86:1-10.

West, M. 2016. *The Fabric Formwork Book - Methods for Building New Architectural and Structural Forms in Concrete.* Abingdon: Routledge.

Yehia, S., Douba, A., Abdullahi, O. & Farrag, S. 2016. Mechanical and durability evaluation of fiber-reinforced self-compacting concrete. *Construction and Building Materials*. 121:120–133.

Zararis, I. P., Karaveziroglou, M. K. & Zararis, P. D. 2006. Shear Strength of Reinforced Concrete T-Beams. *ACI Structural Journal*. 103:693-700.

Zeranka, S. 2017. Steel Fibre-Reinforced Concrete : Multi-scale Characterisation towards Numerical Modelling. PhD Thesis, University of Stellenbosch, 2017.

Zhang, F., Ding, Y., Xu, J., Zhang, Y., Zhu, W. & Shi, Y. 2016. Shear strength prediction for steel fibre reinforced concrete beams without stirrups. *Engineering Structures.* 127:101-116.

Zsutty, T. 1971. Shear Strength Prediction for Separate Categories of Simple Beam Tests. *ACI Journal Proceedings*. 68(2):138–143.

APPENDIX A

CRITICAL SHEAR CRACK WIDTHS

Figures A.1 to A.12 represent the critical shear crack widths measured while the beam was tested. Every figure represents the both beams that were tested per beam-type. Crack measurements of both sides of the beams (labelled side a and b) are presented on each graph.

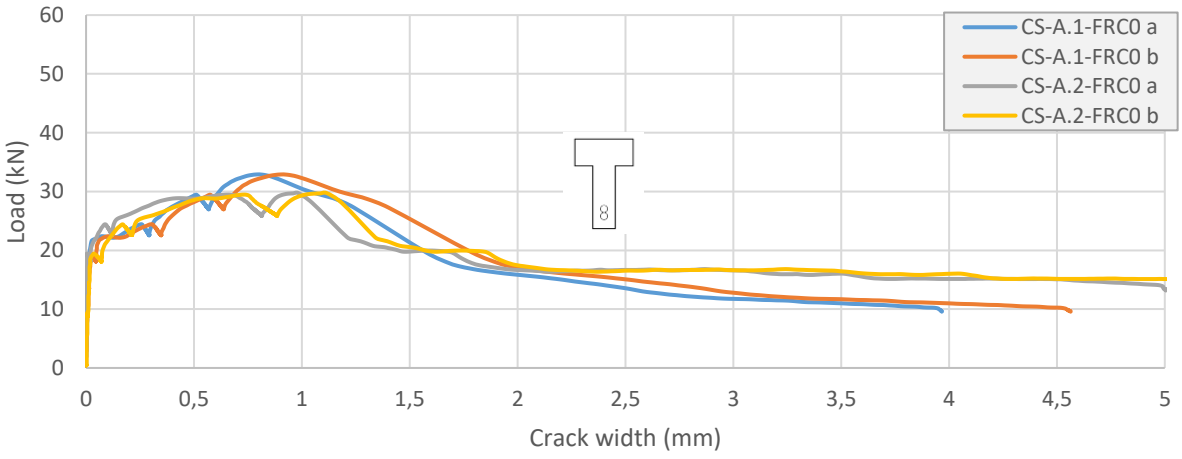

Figure A.1: Critical shear crack width of beam-type A in Control set containing no fibres.

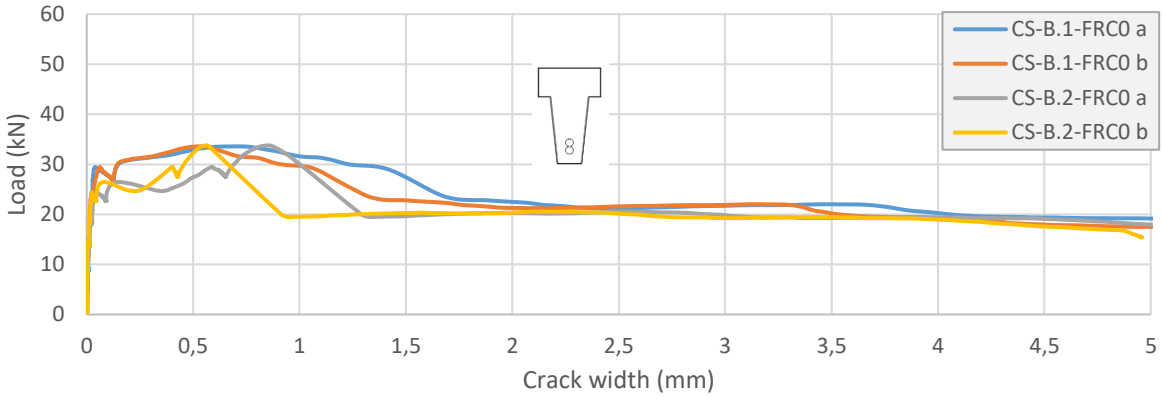

Figure A.2: Critical shear crack width of beam-type B in Control set containing no fibres.

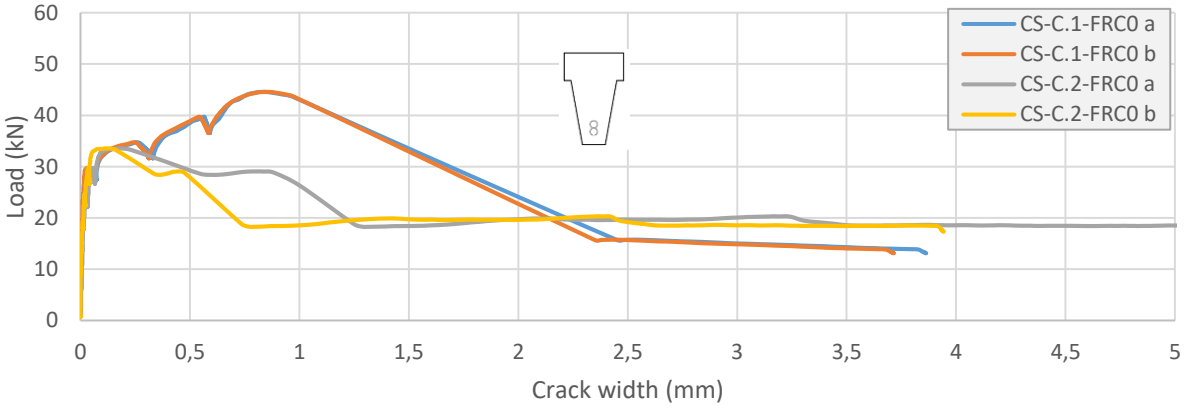

Figure A.3: Critical shear crack width of beam-type C in Control set containing no fibres.

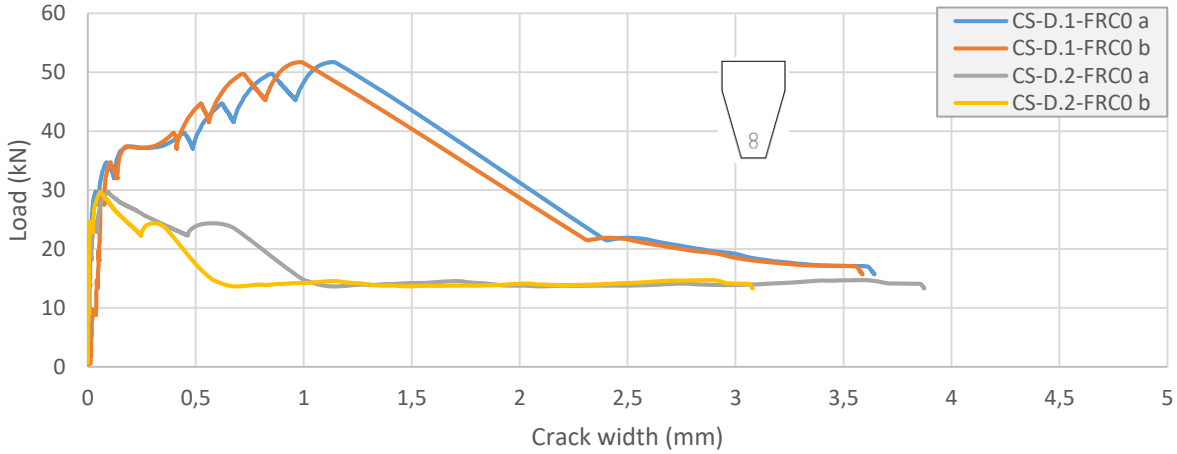

Figure A.4: Critical shear crack width of beam-type D in Control set containing no fibres.

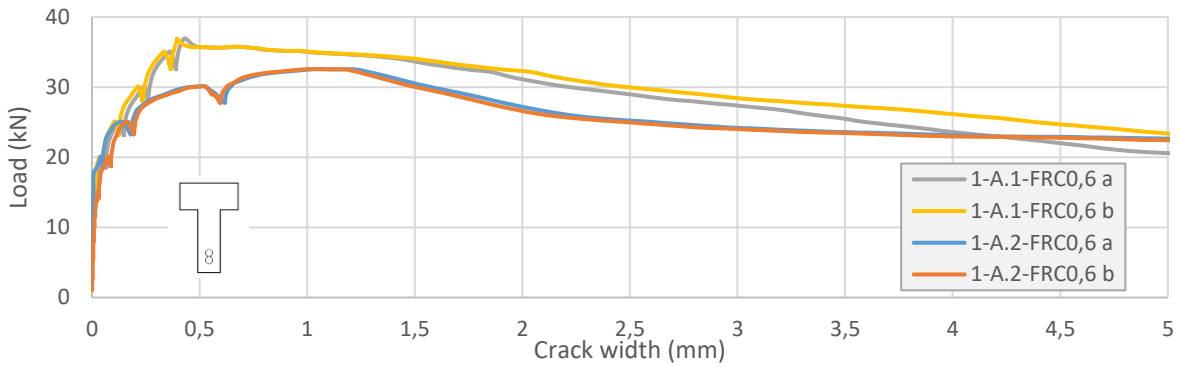

Figure A.5: Critical shear crack width of beam-type A in Set 1 containing 0.6% fibres.

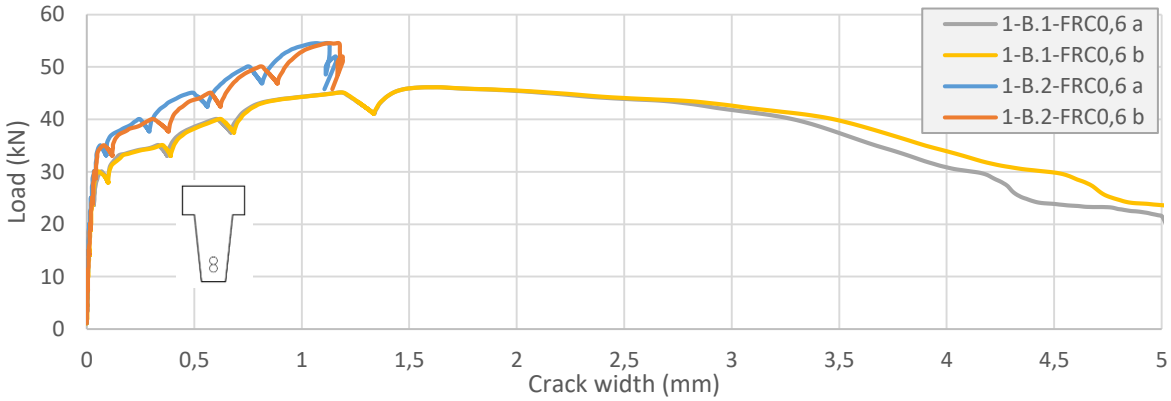

Figure A.6: Critical shear crack width of beam-type B in Set 1 containing 0.6% fibres.

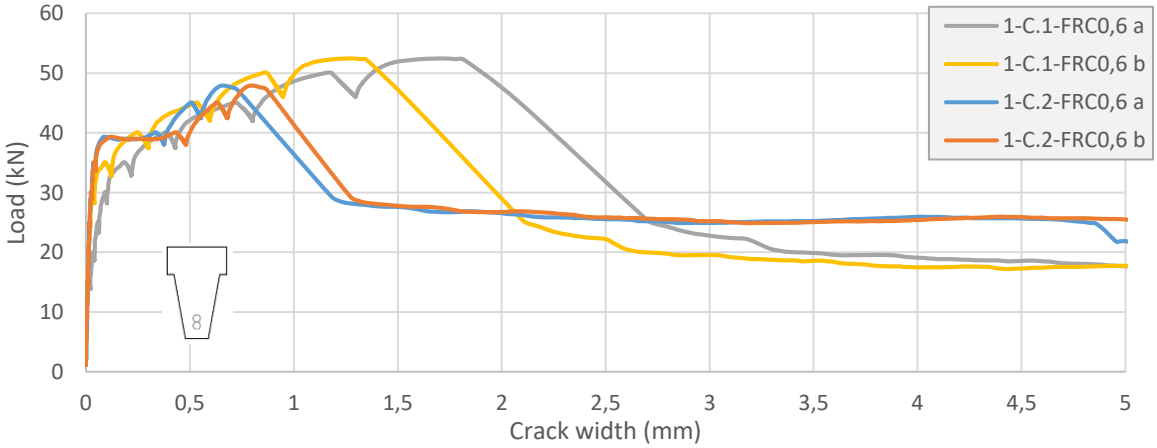

Figure A.7: Critical shear crack width of beam-type C in Set 1 containing 0.6% fibres.

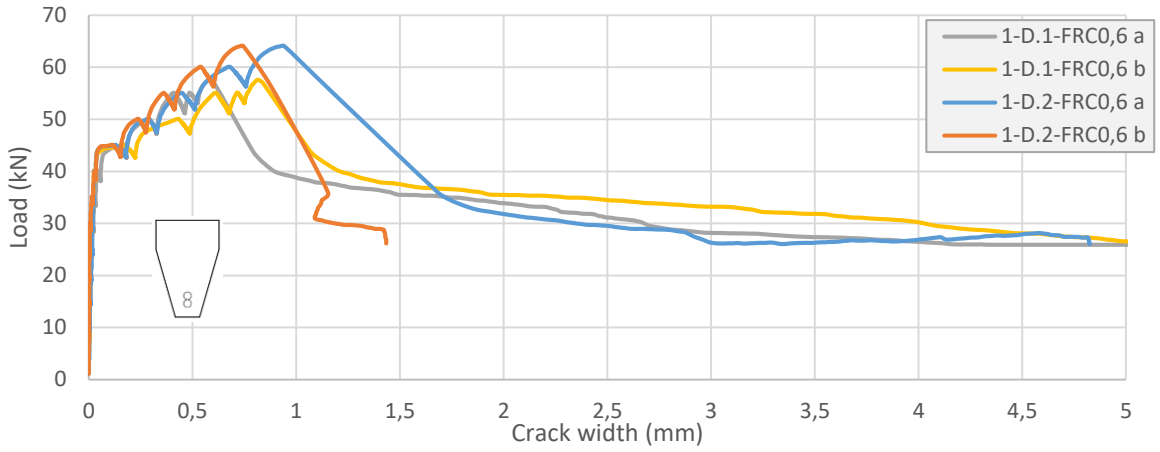

Figure A.8: Critical shear crack width of beam-type D in Set 1 containing 0.6% fibres.

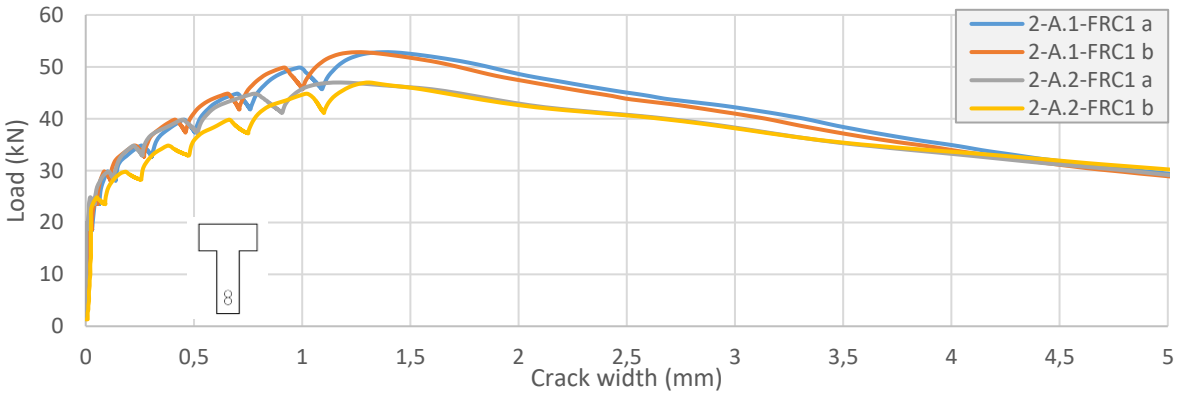

Figure A.9: Critical shear crack width of beam-type A in Set 2 containing 1% fibres.

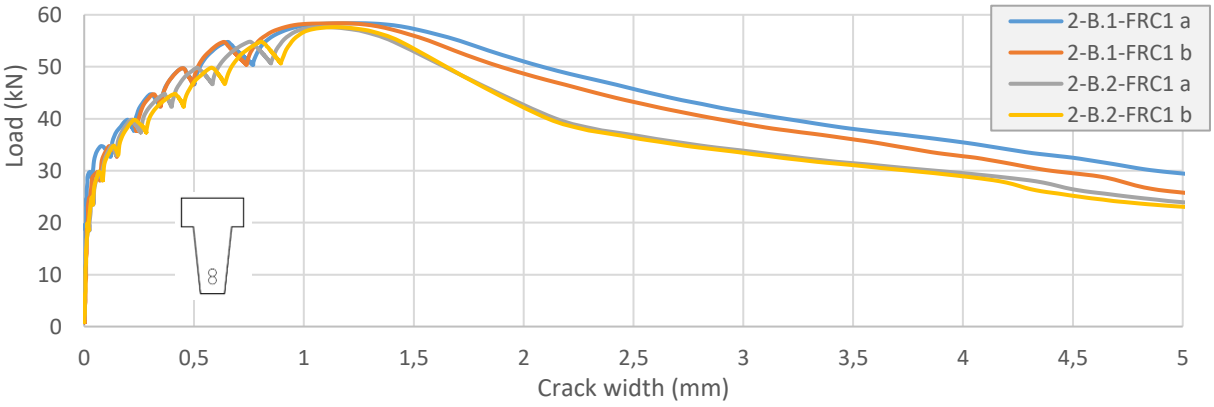

Figure A.10: Critical shear crack width of beam-type B in Set 2 containing 1% fibres.

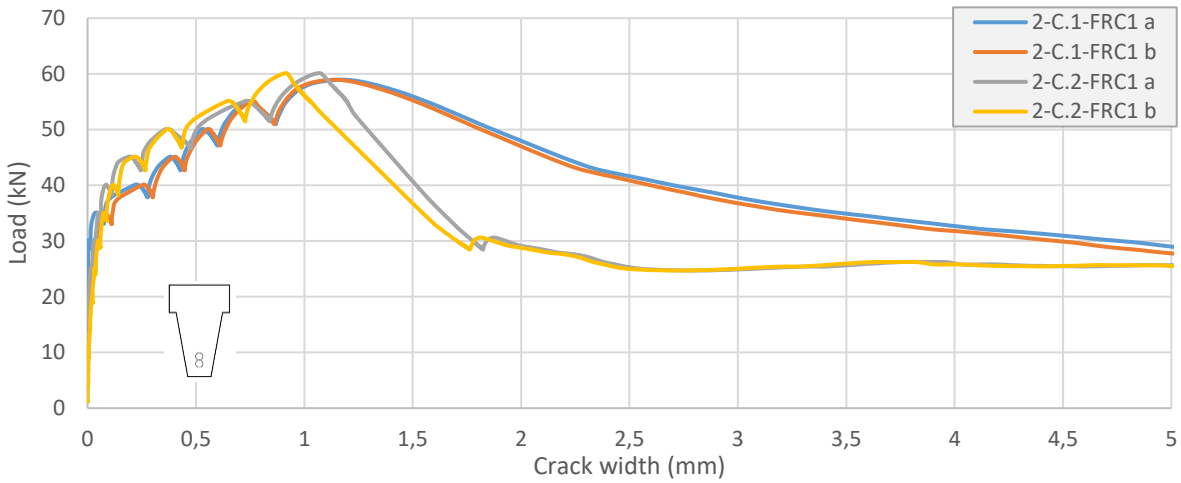

Figure A.11: Critical shear crack width of beam-type C in Set 2 containing 1% fibres.

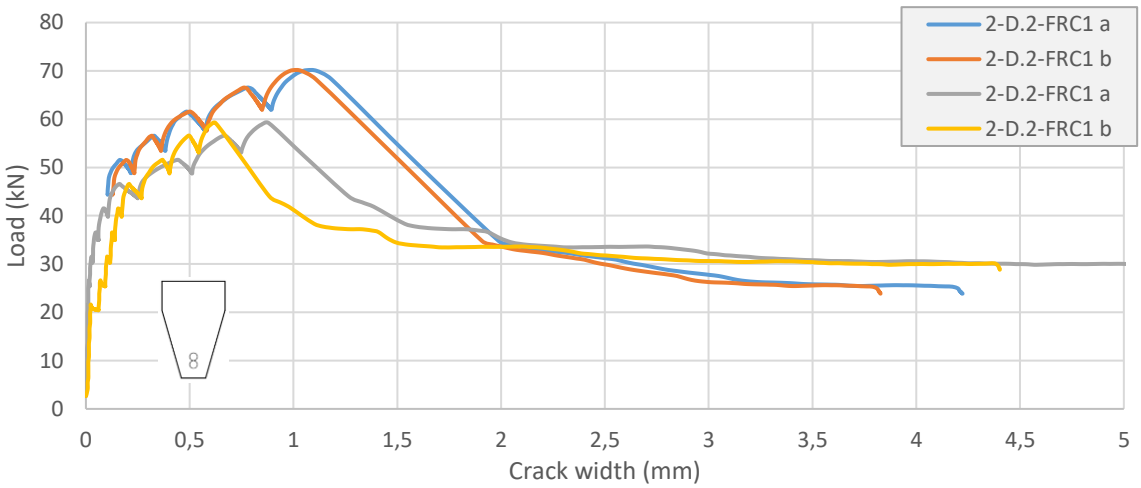

Figure A.12: Critical shear crack width of beam-type D in Set 2 containing 1% fibres.

APPENDIX B

ADDITIONAL BEAM SET DETAILS

Details on the additional set of ISB which results were used in this investigation are presented in this section. Additional beam test results were used to increase the test results to which the predictions of the shear models are compared to. Similar tests as the asymmetrical three-point bending tests performed in this investigation were done on the additional beam set.

Table B.1: Details of additional beam set

Beam	Beams tested	f'_c [MPa]	f_y [MPa]	A_c [mm^2]	A_s [mm^2]	V_f [%] ‡	L [mm]	a_v/d
3-A-FRC0.6	3	33.5	500*	18750	314	0.6	1500	2.9
3-BC-FRC0.6	3	34.8	500*	21375	314	0.6	1500	2.9
3-D-FRC0.6	3	33.9	500*	24375	314	0.6	1500	2.9
* Yield stress of reinforcement was unknown, the tested yield stress of reinforcement used in this investigation of 500 MPa was used. ‡ The same type of fibres were used for additional beam set as for other beam sets in this investigation.								

Figure B.1 and B.2 represent the dimensions of the additional beam set and the CMOD test results, respectively.

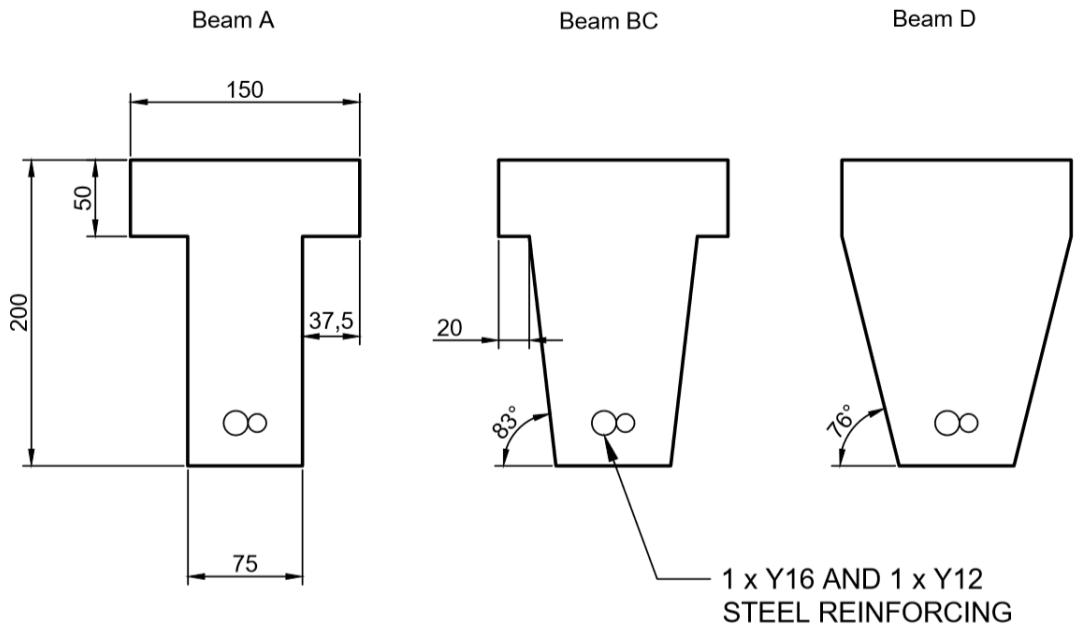

Figure B.1: Beam dimensions of additional beam set.

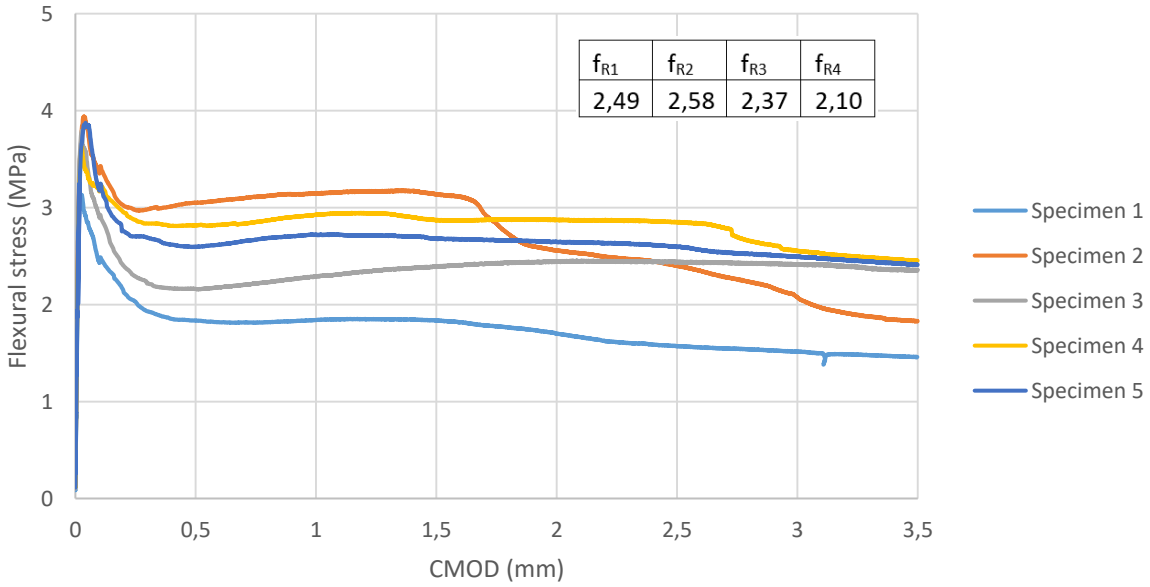

Figure B.2: CMOD test results performed on concrete mix of additional beam set.

APPENDIX C

ULTIMATE SHEAR STRENGTHS AND SHEAR STRENGTH RATIOS

Table C.1 represents the experimental shear strengths and the shear strength ratios of the 16 beams containing fibres that we tested in this investigation. The shear strengths and shear strength ratios of the additional beam set are listed in the table as well. The shear strength ratios of the nine modified shear models obtained from literature and the proposed model for all beams containing fibres are listed in Table C.1

Table C.1: Comparison of experimental results and predicted shear strengths of shear model

Beam	Experimental	fib Model code		Li		Kwak		MCFT-VEM		Spinella		Swamy		Mansur		Dinh		Singh		Proposed model	
	V_u (kN)	V_u (kN)	V_{pr}/V_{exp}	V_u (kN)	V_{pr}/V_{exp}	V_u (kN)	V_{pr}/V_{exp}	V_u (kN)	V_{pr}/V_{exp}	V_u (kN)	V_{pr}/V_{exp}	V_u (kN)	V_{pr}/V_{exp}	V_u (kN)	V_{pr}/V_{exp}	V_u (kN)	V_{pr}/V_{exp}	V_u (kN)	V_{pr}/V_{exp}	V_u (kN)	V_{pr}/V_{exp}
1-A.1-FRC0.6	26.35	30.79	1.17	26.68	1.01	22.99	0.87	22.69	0.86	25.54	0.97	33.76	1.28	20.47	0.78	27.28	1.04	24.42	0.93	28.84	1.09
1-A.2-FRC0.6	23.24	30.79	1.32	26.68	1.15	22.99	0.99	22.69	0.98	25.54	1.10	33.76	1.45	20.47	0.88	27.28	1.17	24.42	1.05	28.84	1.24
1-B.1-FRC0.6	32.90	38.43	1.17	37.26	1.13	32.72	0.99	31.11	0.95	35.64	1.08	49.67	1.51	32.77	1.00	38.59	1.17	33.59	1.02	33.30	1.01
1-B.2-FRC0.6	38.92	38.43	0.99	37.26	0.96	32.72	0.84	31.11	0.80	35.64	0.92	49.67	1.28	32.77	0.84	38.59	0.99	33.59	0.86	33.30	0.86
1-C.1-FRC0.6	37.42	42.50	1.14	43.15	1.15	37.46	1.00	34.31	0.92	40.15	1.07	57.63	1.54	35.83	0.96	40.22	1.07	34.27	0.92	33.95	0.91
1-C.2-FRC0.6	34.17	42.50	1.24	43.15	1.26	37.46	1.10	34.31	1.00	40.15	1.17	57.63	1.69	35.83	1.05	40.22	1.18	34.27	1.00	33.95	0.99
1-D.1-FRC0.6	41.07	48.12	1.17	51.58	1.26	43.96	1.07	40.47	0.99	46.16	1.12	68.82	1.68	40.12	0.98	42.86	1.04	35.49	0.86	35.21	0.86
1-D.2-FRC0.6	45.68	48.12	1.05	51.58	1.13	43.96	0.96	40.47	0.89	46.16	1.01	68.82	1.51	40.12	0.88	42.86	0.94	35.49	0.78	35.21	0.77
2-A.1-FRC1	37.68	31.39	0.83	30.07	0.80	25.64	0.68	26.65	0.71	26.41	0.70	37.92	1.01	27.54	0.73	30.42	0.81	28.85	0.77	33.43	0.89
2-A.2-FRC1	33.51	31.39	0.94	30.07	0.90	25.64	0.77	26.65	0.80	26.41	0.79	37.92	1.13	27.54	0.82	30.42	0.91	28.85	0.86	33.43	1.00
2-B.1-FRC1	41.64	38.77	0.93	41.27	0.99	35.48	0.85	35.32	0.85	37.76	0.91	53.98	1.30	41.99	1.01	39.63	0.95	37.52	0.90	37.84	0.91
2-B.2-FRC1	41.10	38.77	0.94	41.27	1.00	35.48	0.86	35.32	0.86	37.76	0.92	53.98	1.31	41.99	1.02	39.63	0.96	37.52	0.91	37.84	0.92
2-C.1-FRC1	42.06	42.99	1.02	47.90	1.14	40.95	0.97	38.81	0.92	43.26	1.03	63.11	1.50	46.86	1.11	41.98	1.00	39.18	0.93	39.30	0.93
2-C.2-FRC1	42.89	42.99	1.00	47.90	1.12	40.95	0.95	38.81	0.90	43.26	1.01	63.11	1.47	46.86	1.09	41.98	0.98	39.18	0.91	39.30	0.92
2-D.1-FRC1	50.03	49.27	0.98	58.16	1.16	49.75	0.99	47.63	0.95	52.47	1.05	78.31	1.57	55.20	1.10	46.21	0.92	42.42	0.85	42.74	0.85
2-D.2-FRC1	42.23	49.27	1.17	58.16	1.38	49.75	1.18	47.63	1.13	52.47	1.24	78.31	1.85	55.20	1.31	46.21	1.09	42.42	1.00	42.74	1.01
3-A.1-FRC0.6	33.33	31.51	0.95	32.44	0.97	27.99	0.84	31.25	0.94	27.77	0.83	50.47	1.51	28.73	0.86	32.85	0.99	30.29	0.91	29.96	0.90
3-A.2-FRC0.6	30.60	31.51	1.03	32.44	1.06	27.99	0.91	31.25	1.02	27.77	0.91	50.47	1.65	28.73	0.94	32.85	1.07	30.29	0.99	29.96	0.98
3-A.3-FRC0.6	32.56	31.51	0.97	32.44	1.00	27.99	0.86	31.25	0.96	27.77	0.85	50.47	1.55	28.73	0.88	32.85	1.01	30.29	0.93	29.96	0.92
3-BC.1-FRC0.6	30.60	36.90	1.21	41.19	1.35	35.24	1.15	37.94	1.24	38.36	1.25	65.19	2.13	38.67	1.26	35.63	1.16	32.37	1.06	32.68	1.07
3-BC.2-FRC0.6	36.53	36.90	1.01	41.19	1.13	35.24	0.96	37.94	1.04	38.36	1.05	65.19	1.78	38.67	1.06	35.63	0.98	32.37	0.89	32.68	0.89
3-BC.3-FRC0.6	41.14	36.90	0.90	41.19	1.00	35.24	0.86	37.94	0.92	38.36	0.93	65.19	1.58	38.67	0.94	35.63	0.87	32.37	0.79	32.68	0.79
3-D.1-FRC0.6	32.56	42.62	1.31	50.95	1.56	43.21	1.33	45.21	1.39	47.23	1.45	82.01	2.52	45.83	1.41	40.39	1.24	35.71	1.10	35.89	1.10
3-D.2-FRC0.6	40.37	42.62	1.06	50.95	1.26	43.21	1.07	45.21	1.12	47.23	1.17	82.01	2.03	45.83	1.14	40.39	1.00	35.71	0.88	35.89	0.89
3-D.3-FRC0.6	36.59	42.62	1.16	50.95	1.39	43.21	1.18	45.21	1.24	47.23	1.29	82.01	2.24	45.83	1.25	40.39	1.10	35.71	0.98	35.89	0.98
Mean			1.07	-	1.13	-	0.97	-	0.97	-	1.03	-	1.60	-	1.01	-	1.03	-	0.92	-	0.95
SD			0.13	-	0.17	-	0.15	-	0.15	-	0.17	-	0.35	-	0.17	-	0.11	-	0.09	-	0.10
COV			0.12	-	0.15	-	0.15	-	0.16	-	0.17	-	0.22	-	0.17	-	0.10	-	0.09	-	0.11

APPENDIX D

TENSILE TESTS ON REINFORCEMENT STEEL

Figure D.1 to D.3 represent the tests performed on the reinforcement steel to obtain the actual yield stress of the steel for the application of the modified shear prediction models.

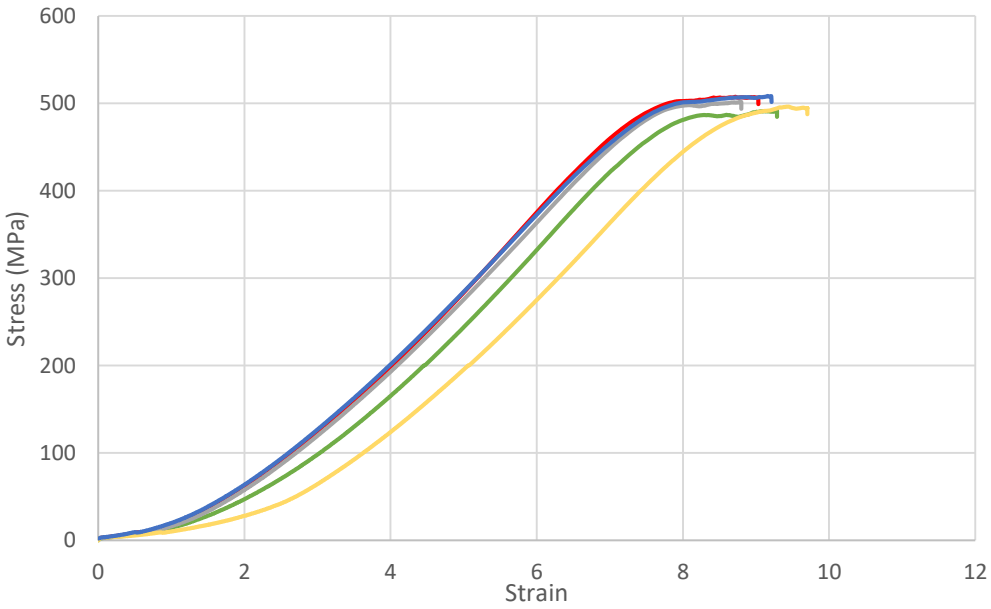

Figure D.1: Tensile test results of reinforcement steel used in the control set.

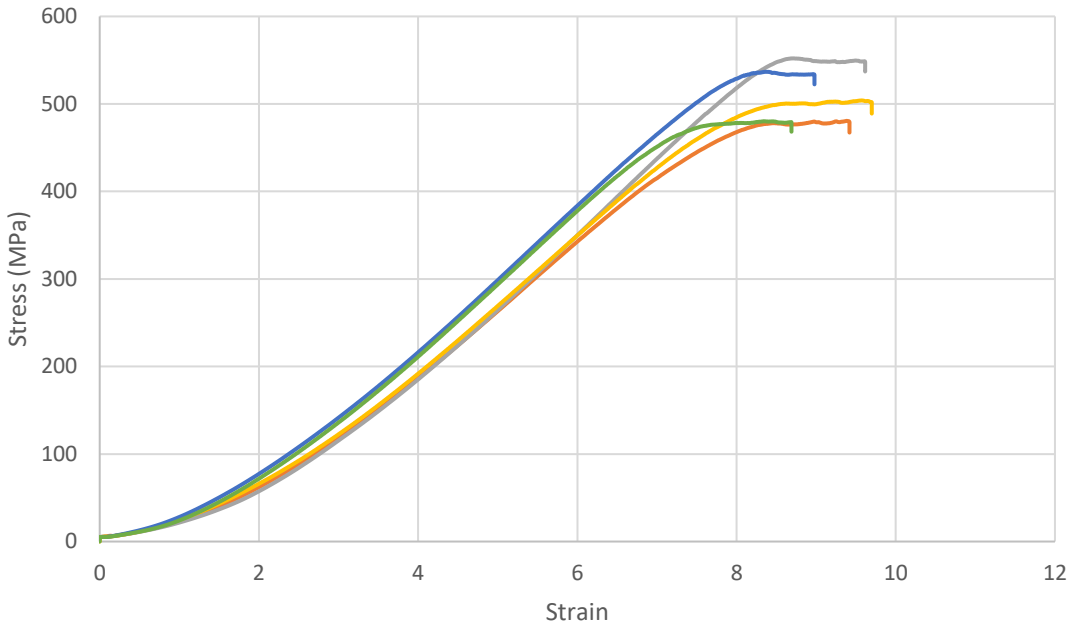

Figure D.2: Tensile test results of reinforcement steel used in Set 1.

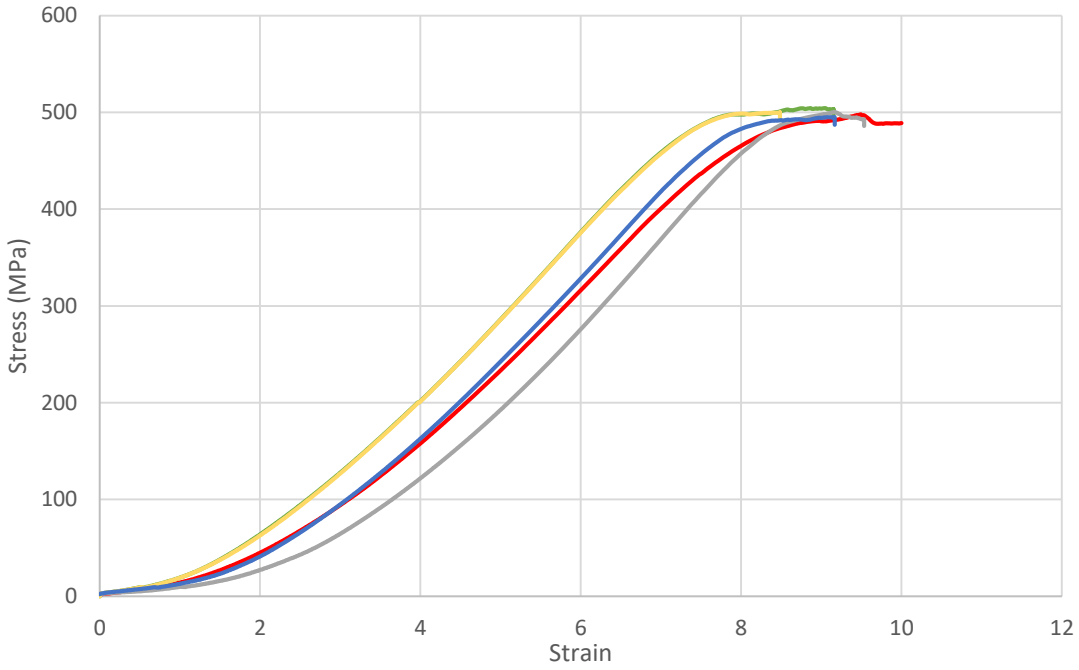

Figure D.3: Tensile test results of reinforcement steel used in Set 2.